MULTI-SCALE OPTIMIZATION OF HYBRID SODIUM SULFATE-ACTIVATED BINDERS

Chloé Monin

Thesis submitted to the University of Ottawa
in partial Fulfillment of the requirements for the
MASTER OF APPLIED SCIENCE

Department of Civil Engineering
Faculty of Engineering
University of Ottawa

Abstract

Civil engineering plays a crucial role in addressing pressing societal concerns, from ensuring safety to promoting sustainability. With the ongoing challenge of climate change, there is an increasing need to mitigate carbon emissions, which can be achieved by driving innovation in construction materials and methods. Concrete, essential for modern infrastructure, is environmentally impactful mainly due to its dependence on Portland cement in production, and the large volumes that are being consumed to fulfill societal needs.

This thesis investigates hybrid alkali-activated materials (AAMs) as a viable alternative to traditional concrete formulations. By substituting a significant portion of Portland cement with supplementary cementitious materials (SCMs), hybrid AAMs offer a pathway towards reducing environmental footprint while maintaining performance. The focus of this work is on optimizing sodium sulfate-activated hybrid AAMs comprising metakaolin, limestone, and Portland cement, along with an alkali-activator, in this case sodium sulfate.

Through a systematic approach using factorial design of experiments (DOE) and multi-scale testing, this research aims to tailor the performance of hybrid AAMs to meet both early-age strength requirements and long-term performance. Initial findings indicate that the addition of sodium sulfate enhances the reactivity of metakaolin, allowing for a reduction in Portland cement content without compromising early-age performance. However, challenges have been identified through this work concerning the long-term strength of hybrid AAMs, which are tentatively attributed to phase instability and higher porosity (as inferred from the decreased electrical resistivity). Recommendations emphasize a nuanced approach to binder composition, balancing alkali content with Portland cement and metakaolin content to ensure optimal strength development.

The proposed framework proposes the following steps in designing hybrid AAMs activated with sodium sulfate:

(1) Determining binder composition: Identify optimal ratios of metakaolin, limestone, and Portland cement to achieve the desired later age performance and reduce carbon footprint.
(2) Achieving sulfate balance: Evaluate the adequate sulfate content to achieve sulfate balance in the system.

(3) Optimizing alkali content: Evaluate the minimal alkali content needed to achieve the required early-age strength.

(4) Re-evaluating binder composition: If the selected alkali content compromises later-age strength, reassess binder composition. Replacing metakaolin by limestone increases the tolerance of the system to high alkali content and increasing Portland cement content may help reduce the amount of alkalis needed.

Acknowledgements

The journey which has preceded this master's thesis started 9 years ago, when I first discovered geopolymers and decided to make one for a high school science fair project. At the time, I sent dozens of emails to the University of Ottawa, hoping that I could access batching equipment and materials. One of the administrators I had contacted, Mrs. Margaret McKenna, put me in contact with Professors Leandro Sanchez and Martin Noel who accepted to meet with me. They listened to my ideas and accepted to start a project with an undergraduate student and myself. This first opportunity brought me here, in materials civil engineering and research. Therefore, I want to start by acknowledging the support of the University of Ottawa, and particularly of Mrs. McKenna, and Professors Sanchez and Noel. Without these incredible individuals, this thesis would not be.

Throughout my undergrad, here, at the University of Ottawa, I had the immense privilege of learning from many of the graduate students of Professor Sanchez's group. The mentorship provided by the uStructure group was key in helping me develop the research skills I needed to start this master's project. I would like to particularly thank Leah Kristufek, Derick Asirvatham, Diego Jesus de Souza, Mayra T. de Grazia, Cassandra Trottier, Agnes Bezerra and Rennan Medeiros. Many thanks to all of you for answering so many of my questions, giving me feedback on presentations, posters and papers, listening to my concerns and lending me a helping hand every time. Professor Sanchez, thank you for being my supervisor and a source of inspiration, and for always believing in my potential all these years. Your passion for concrete shows in everything that you do, and I am beyond thankful for your excellent mentorship and for all the opportunities you have given me.

I am very much indebted to Professor Susan Bernal for her great support and invaluable guidance over the past two years. Thank you, Professor Bernal, for being such a wonderful co-supervisor. You have been my role model for many years now, and I cannot express how grateful I am that I had the chance to work under your supervision.

Finally, I would like to thank my family, my two brothers, my father and my mother, for their unconditional love and faith in me. They gave me the strength I needed to keep moving forward every day. Thank you, Maman, for believing in me and being my greatest pillar on this research journey for the past 9 years. I dedicate this thesis to you.

Table of Contents

List of Figures

List of Tables

List of Abbreviations

AAMs	Alkali-activated materials
C-A-S-H	Calcium aluminum silicate hydrate
C-S-H	Calcium silicate hydrate
DOE	Design of experiment
LS	Limestone ($CaCO_3$)
N-A-S-(H)	Sodium aluminum silicate gel
NMR	Nuclear magnetic resonance
NS	Sodium sulfate (Na_2SO_4)
PC	Portland cement
RSM	Response surface analysis
SCMs	Supplementary cementitious materials
SSA	Specific surface area
TGA	Thermogravimetric analysis
XRD	X-Ray diffraction
XRF	X-Ray fluorescence

Chapter 1 Introduction

1.1 Background

The field of civil engineering is at the intersection of many other fields and at the heart of many societal concerns. Civil engineers must notably consider in their design the safety, durability, functionality, environmental impact, social impact, cost-effectiveness and aesthetic of everyday infrastructure. Safety and cost-effectiveness have long been the most important considerations of civil engineers from every country. Nevertheless, the growing concerns around climate change and carbon dioxide emissions have started decades ago to cause a shift in construction practices and civil engineering research. Today, the sustainability of construction materials is a very important topic for the industry, and an active field of research in many countries.

Amongst all construction materials, concrete is by far the most produced and therefore, the one which is causing the largest environmental impact. The popularity of concrete as a construction material largely stems from its versatility, cost-effectiveness, low embodied CO_2 footprint per mass, as well as the large-scale availability of its raw materials, the simplicity of its quality control processes and the possibility for low-skilled workers to easily manufacture concrete and use it in the field. Making concrete is rather simple: it requires mixing around 70% of crushed rocks, or aggregates, to a paste of Portland cement and water. Depending on many factors such as the grading of the aggregates, the type of Portland cement or the water-to-cement ratio used, the performance of concrete may be tailored to the physical element that will be built, its placement requirements, exposure conditions, life expectancy and more.

Determining Portland cement content is a crucial aspect of mix-design due to the relationship between cement content, and strength and permeability. However, of all concrete components, cement has by far the largest environmental impact. Despite being only a small percentage of total concrete volume and mass, Portland cement typically generates about 96% of the CO_2 emission of a "standard" concrete (i.e., cement content of 350 kg/m^3 and clinker factor of 80%) [1]. It should be added that little improvement may be done on the production of Portland cement to decrease its emissions since a large portion of the CO_2 is generated from the chemical decomposition of limestone ($CaCO_3$) in the clinker to form lime (CaO) and carbon dioxide (CO_2). Reducing the cement content in concrete is a possibility, but unless performed with advanced mix-design

techniques and particle packing, it usually results in a loss of durability and strength, particularly at early age. In addition, due to the loss of compressive strength, more concrete is needed to sustain a given load, which negates any gain from the cement reduction.

Therefore, to reduce the carbon footprint of concrete while enhancing its mechanical properties and durability, the cement industry has significantly shifted in the past decades towards higher cement replacement by using supplementary cementitious materials (SCMs) instead of plain Portland cement. Despite the established reduction in CO_2 emissions that have been achieved through this shift, the industry is limited in its ability to further increase cement replacement with SCMs due to the losses it may cause in early age mechanical performance related to the slower reaction kinetics of SCMs compared to PC or the lack of available portlandite [2]. This is particularly true in the case of low calcium SCMs, such as metakaolin or fly ash. Nonetheless, decades of research in the field of alkali-activation have shown that SCMs may react and form strong binders at early ages in the presence of alkalis and with added calcium [3–5]. In attempts to reach a similar behavior, research has been conducted by various authors [6–8] on the addition of small amounts of alkalis to binders containing Portland cement. The subject at the heart of this thesis is thus at the intersection of two major fields in civil engineering and material science. The first is the topic of hybrid alkali-activated materials, which are formed by mixing an alkaline solution to about 70 wt.% of aluminosilicate precursors or SCMs, and about 30% of Portland cement. The second is the topic of blended Portland cement binders, which are formed mainly of Portland cement, with moderate amounts of SCMs incorporated. A particularly known subset of this binder type are the limestone calcined clay cements (LC_3), which typically consist of 50% of Portland cement, 35% of calcined clay and 15% of limestone.

It is interesting to observe that hybrid AAMs, LC_3 cements and Portland cements boosted with small amounts of alkalis all face a common challenge. Both alkalis and high specific surface area particles such as those of calcined clays and limestone accelerate the early reaction kinetics, which tends to negatively affect the final extent of reaction of the binder, and therefore lower strength at 7 days and onwards [2,9–11]. However, in the absence of this acceleration, early age strength is significantly impaired. It is therefore possible to observe that binders with high levels of PC replacement by SCMs will generally either suffer from low early strength or reduced later ages strength. There is thus a need to combine the knowledge gained from the fields of hybrid alkali-

activation and Portland cement chemistry to shed light on how to accelerate kinetics without altering later ages performance.

1.1.1 Rationale for the choice of materials in this thesis

This thesis will be focused on hybrid sodium sulfate activated AAMs binders made from metakaolin, limestone and Portland cement. The rationale behind the choice of the raw materials is presented shortly in this section.

Many studies have focused on the use of fly ash and blast furnace slag as precursor materials for AAMs or as SCMs for Portland cement mixes. However, the depletion of these SCMs in some locations, due to changes in global industrial production are expected to raise issues on their future availability [12]. To achieve high levels of substitution of Portland cement, it is thus necessary to investigate other types of precursors that are globally available. In this regard, calcined clays have emerged as a promising option [12,13]. Metakaolin originates from the calcination of kaolinitic clays at around 650°C. It is the most studied calcined clay, both as a SCMs in Portland cement binders and as a precursor for AAMs [12]. In this research, metakaolin was chosen as a model system for calcined clays due to its high purity and reactivity.

Pure metakaolin AAMs experience significant issues with poor flowability and early age strength [14]. They also require strong alkaline solutions for the alkali-activation of the metakaolin to take place. Activators such as sodium hydroxide and sodium silicate have traditionally been used, but are problematic due to their high corrosivity, cost and environmental impacts on noncarbon categories [15]. The addition of small amounts of Portland cement to metakaolin raises the pH of the system, which enables the use of near-neutral salts such as sodium carbonate and sodium sulfate [16]. For this thesis, sodium sulfate was selected because, it is a by-product from other industries but can also be found naturally in the environment [17]. It is also a low-cost and substantially eco-friendlier option to traditional activators. Finally, studies on the addition of small amounts of $NaSO_4$ and NaOH to Portland cement pastes and alite pastes have reported negative impacts on long term strength of NaOH [18]. From these findings, it is hypothesized that sodium sulfate might be more compatible with a hybrid Portland cement – metakaolin blend.

Many researchers have identified promising synergic behavior when incorporating moderate amounts of limestone to metakaolin-Portland cement binders [19,20], as well as in metakaolin

AAMs [21–23]. Perez-Cortes & Escalante-Garcia (2020) [23] showed that the addition of limestone to metakaolin AAMs helped refining the pore structure and improved microstructural features by allowing the incorporation of calcium products in the main reaction phases. Since limestone is an affordable, low embodied CO_2 and widely available raw material, it is a promising addition to hybrid metakaolin-Portland cement binders.

1.2 Research objectives

The objectives of this thesis are two-fold. The first goal is to try to optimize the strength of hybrid sodium sulfate-activated metakaolin AAMs containing moderate additions of limestone and Portland cement with the use of a factorial design of experiment (DOE). The second goal of this thesis is to investigate how sodium sulfate alone affects the early kinetics and the microscopic phases of these same binders.

The first goal will be addressed through two sets of experiments, the first of which being conducted on a simpler sodium sulfate-activated mix containing only metakaolin and Portland cement. In this preliminary experiment, the Portland cement (PC) and sodium sulfate (NS) contents were varied over a large range of values (i.e., 0 to 5% NS and 10 to 50% PC) to easily evaluate the strength response at early ages (i.e., 1 and 6 days). To further understand the impact of the binder compositions on the performance of the cement pastes, Vicat needle, thermogravimetric analysis (TGA) and X-Ray diffraction (XRD) testing were conducted. Based on the results of this preliminary experiment, the lowest optimal PC is determined, as well as a refined range of optimal NS contents. In a second experiment, a factorial DOE was conducted on ternary NS-activated metakaolin AAMs now also containing limestone (LS). For these binders, LS will be varied from 5 to 25% of binder composition and NS is added to the total binder mass between 0.5 to 2.5%, while PC content is fixed at 30% of binder composition. The early kinetics of these samples was investigated through isothermal calorimetry testing, while their hardened state's properties was evaluated through compressive strength and bulk resistivity testing at 3, 7 and 28 days. After 90 days of curing, XRD and TGA were performed on the samples to help relate macroscale performance to microscale semi-quantitative features. A statistical analysis on compressive strength values at all ages was also performed to relate LS and NS dosages to changes in strength between the binders.

The second goal will be addressed in a third experiment. Based on the second experiment, an optimal binder composition to maximize early age strength was determined. For the third experiment, the optimal early strength binder, and a water-activated binder of equal (MK-PC-LS) composition were compared. For both binders, isothermal calorimetry was used to assess the early kinetics. TGA and XRD were also conducted to follow the development of crystalline phases, as well as amorphous ones. TGA was used in a semi-quantitative manner to estimate hydrate water, portlandite and calcite contents at various ages. The aim of this experimental program is to shed light on how microscale features are evolving during the hydration/alkali-activation of optimized early strength NS-activated binders.

1.3 Thesis outline

This thesis is divided into five chapters, including the present one. While this chapter focuses on introducing the literature and objectives supporting this thesis, the second chapter provides a more in-depth background. The background first includes a section on alkali-activation and the various types of gel forming in low calcium, high calcium, and hybrid AAMs. The following section is centered around the properties of binders containing metakaolin and other calcined clays, with subsections on clay particles, fresh state of calcined clay binders and porosity evolution in calcined clay binders.

The third chapter consists of the preliminary investigation on metakaolin hybrid AAMs. This work resulted in a conference paper presented at the 16th International Congress on the Chemistry of Cement and Concrete (ICCC) in Bangkok in 2023. In this chapter, the impact of PC and NS contents on setting time, compressive strength, as well as TGA and XRD profiles are studied. The strength results are treated statistically in Appendix A – *Factorial design* rationale so that an optimal minimal PC amount and an optimal NS range of values are determined for the next set of experiments.

The fourth chapter is reported in a journal paper format centered on the optimization of NS-activated hybrid AAMs composed of metakaolin, limestone and Portland cement. This chapter also investigates the impact of NS on early kinetics and microscale features. The performance of binders of various composition was evaluated by means of fresh state (i.e., setting time and isothermal calorimetry), macroscale (i.e., compressive strength and bulk resistivity), and

microscale (i.e., XRD and TGA) evaluation. More insight is also gained on how the binder composition affect the optimal NS content with regards to early strength. The study of the evolution of microscale features for a water-activated versus NS-activated hybrid binder further sheds light on the microscale changes induced by NS addition.

Finally, the fifth chapter summarizes the main conclusions of the work, as well as recommendations for future work.

1.4 References

[1] F. Zunino, A two-fold strategy towards low-carbon concrete, RILEM Technical Letters 8 (2023) 45–58. https://doi.org/10.21809/rilemtechlett.2023.179.

[2] F. Zunino, K. Scrivener, The reaction between metakaolin and limestone and its effect in porosity refinement and mechanical properties, Cem Concr Res 140 (2021) 106307. https://doi.org/10.1016/j.cemconres.2020.106307.

[3] F. Puertas, S. Martínez-Ramírez, S. Alonso, T. Vázquez, Alkali-activated fly ash/slag cements. Strength behaviour and hydration products, Cem Concr Res 30 (2000) 1625–1632. https://doi.org/10.1016/S0008-8846(00)00298-2.

[4] H. Ye, A. Radlińska, Fly ash-slag interaction during alkaline activation: Influence of activators on phase assemblage and microstructure formation, Constr Build Mater 122 (2016) 594–606. https://doi.org/10.1016/j.conbuildmat.2016.06.099.

[5] I. García-Lodeiro, A. Fernández-Jiménez, A. Palomo, Variation in hybrid cements over time. Alkaline activation of fly ash-portland cement blends, Cem Concr Res 52 (2013) 112–122. https://doi.org/10.1016/j.cemconres.2013.03.022.

[6] B. Mota, T. Matschei, K. Scrivener, The influence of sodium salts and gypsum on alite hydration, Cem Concr Res 75 (2015) 53–65. https://doi.org/10.1016/J.CEMCONRES.2015.04.015.

[7] B. Mota, T. Matschei, K. Scrivener, Impact of NaOH and Na2SO4 on the kinetics and microstructural development of white cement hydration, Cem Concr Res 108 (2018) 172–185. https://doi.org/10.1016/j.cemconres.2018.03.017.

[8] N. Smaoui, M.A. Bérubé, B. Fournier, B. Bissonnette, B. Durand, Effects of alkali addition on the mechanical properties and durability of concrete, Cem Concr Res 35 (2005) 203–212. https://doi.org/10.1016/j.cemconres.2004.05.007.

[9] Y. Briki, F. Avet, M. Zajac, P. Bowen, M. Ben Haha, K. Scrivener, Understanding of the factors slowing down metakaolin reaction in limestone calcined clay cement (LC3) at late

ages, Cem Concr Res 146 (2021) 106477. https://doi.org/10.1016/J.CEMCONRES.2021.106477.

[10] J. Fu, M.W. Bligh, I. Shikhov, A.M. Jones, C. Holt, L.M. Keyte, F. Moghaddam, C.H. Arns, S.J. Foster, T.D. Waite, A microstructural investigation of a Na2SO4 activated cement-slag blend, Cem Concr Res 150 (2021) 106609. https://doi.org/10.1016/j.cemconres.2021.106609.

[11] J. Fu, A.M. Jones, M.W. Bligh, C. Holt, L.M. Keyte, F. Moghaddam, S.J. Foster, T.D. Waite, Mechanisms of enhancement in early hydration by sodium sulfate in a slag-cement blend – Insights from pore solution chemistry, Cem Concr Res 135 (2020) 106110. https://doi.org/10.1016/j.cemconres.2020.106110.

[12] A.Z. Khalifa, Ö. Cizer, Y. Pontikes, A. Heath, P. Patureau, S.A. Bernal, A.T.M. Marsh, Advances in alkali-activation of clay minerals, Cem Concr Res 132 (2020) 106050. https://doi.org/10.1016/j.cemconres.2020.106050.

[13] N.R. Rakhimova, A review of calcined clays and ceramic wastes as sources for alkali-activated materials, Geosystem Engineering 23 (2020) 287–298. https://doi.org/10.1080/12269328.2020.1768154.

[14] T. Hanein, K.T. Franco, A.T.M. Marsh, M. Maier, B. Wang, M. Canut, M.C.G. Juenger, M. Ben, H. Franc, A. Karen, L.S. Susan, M.A. Alujas-diaz, A. Rossetti, A. Tagnit-hamou, A. Castel, C. White, F. Kanavaris, F. Zunino, G. Geng, H. Ez-zaki, H. Beltagui, J. Ivan, Clay calcination technology: state-of-the-art review by the RILEM TC 282-CCL, 6 (2022) https://doi.org/10.1617/s11527-021-01807-6.

[15] G. Habert, J.B. D'Espinose De Lacaillerie, N. Roussel, An environmental evaluation of geopolymer based concrete production: Reviewing current research trends, J Clean Prod 19 (2011) 1229–1238. https://doi.org/10.1016/j.jclepro.2011.03.012.

[16] I. García-Lodeiro, A. Fernández-Jiménez, A. Palomo, Variation in hybrid cements over time. Alkaline activation of fly ash-portland cement blends, Cem Concr Res 52 (2013) 112–122. https://doi.org/10.1016/j.cemconres.2013.03.022.

[17] S.A. Bernal, Advances in near-neutral salts activation of blast furnace slags, RILEM Technical Letters 1 (2016) 39. https://doi.org/10.21809/rilemtechlett.v1.8.

[18] B. Mota, T. Matschei, K. Scrivener, The influence of sodium salts and gypsum on alite hydration, Cem Concr Res 75 (2015) 53–65. https://doi.org/10.1016/J.CEMCONRES.2015.04.015.

[19] M. Sharma, S. Bishnoi, F. Martirena, K. Scrivener, Limestone calcined clay cement and concrete: A state-of-the-art review, Cem Concr Res 149 (2021) 106564. https://doi.org/10.1016/J.CEMCONRES.2021.106564.

[20] M. Antoni, J. Rossen, F. Martirena, K. Scrivener, Cement substitution by a combination of metakaolin and limestone, Cem Concr Res 42 (2012) 1579–1589. https://doi.org/10.1016/J.CEMCONRES.2012.09.006.

[21] P. Perez-Cortes, J.I. Escalante-Garcia, Design and optimization of alkaline binders of limestone-metakaolin – A comparison of strength, microstructure and sustainability with portland cement and geopolymers, J Clean Prod 273 (2020). https://doi.org/10.1016/j.jclepro.2020.123118.

[22] P. Perez-Cortes, J.I. Escalante-Garcia, Alkali activated metakaolin with high limestone contents – Statistical modeling of strength and environmental and cost analyses, Cem Concr Compos 106 (2020) 103450. https://doi.org/10.1016/j.cemconcomp.2019.103450.

[23] P. Perez-Cortes, J.I. Escalante-Garcia, Gel composition and molecular structure of alkali-activated metakaolin-limestone cements, Cem Concr Res 137 (2020) 106211. https://doi.org/10.1016/j.cemconres.2020.106211.

Chapter 2 Background

2.1 Alkali-activation process

Alkali-activated materials (AAMs) are alternative binders to traditional Portland cement (PC) and are formed through the reaction of an aluminosilicate precursor source with a highly alkaline solution. AAMs are particularly attractive substitute binders to PC due to their low carbon footprint, high durability and versatility, as well as their good mechanical properties. In AAMs, the source of alkalinity no longer lies in the presence of Portland cement, but in the activator solution that is added. This removes the need for clinker production, and therefore substantially lowers the carbon emissions associated with AAMs manufacturing [1]. Furthermore, numerous investigations on the durability of AAMs have reported largely improved resistance to many chemical degradation mechanisms such as alkali-silica reaction [2–4], as well as acid, chloride, and sulfate attacks [5–10]. The use of local raw sources is facilitated since AAMs have the potential to be manufactured with a variety of aluminosilicate precursors, including waste materials [11]. Transport costs and their associated environmental load may therefore be effectively reduced. However, the versatility of AAMs comes at a cost as high performance is not easily attained or predicted. New aluminosilicate sources must be thoroughly analyzed. Factors affecting early and long-term properties of AAMs include the precursors' amorphous Si/Al ratio and the rate of dissolution of its main oxides, as well as the molarity, anion type and soluble silica content of the activator solution [12–14]. Quality control and mix-design processes are significantly more challenging in AAMs than in PC. To understand why and how AAMs differ from PC binders, it is necessary to dive into the alkali-activation process and the main reaction products of different AAMs binders. This section will focus on these topics and provide some background on the three main categories alkali-activated binders: low calcium AAMs or geopolymers, high calcium AAMs, and hybrid AAMs. The binders studied in this thesis are hybrid AAMs, but since these materials may contain both low calcium and high calcium gels, it is important to describe them individually before studying hybrid AAMs' reaction products. Prior to these subsections, the alkali-activation process will be briefly discussed here.

The alkali-activation process is currently an active field of study. The most common model for the geopolymerization process was first proposed by Provis and van Deventer [15] and can be summarized by the steps illustrated in the figure below occurring simultaneously [15,16] (*Figure 2-1*).

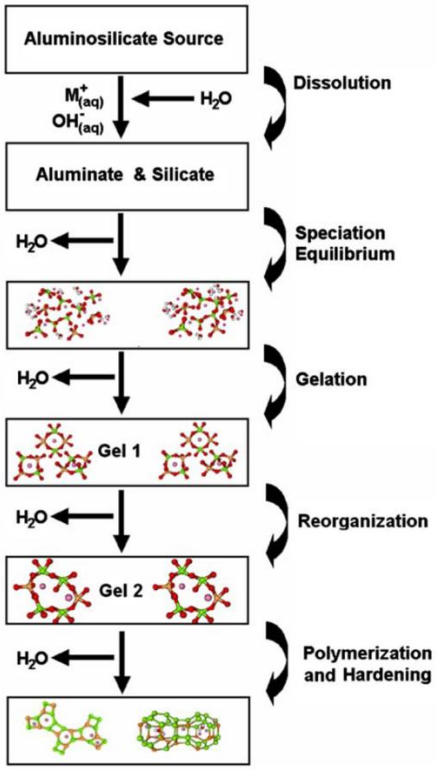

Figure 2-1 Conceptual model for geopolymerization process, adapted from [16]

In Duxson *et al.* (2007)'s conceptual model built on this theory, aluminosilicate monomers[1] are assumed to be released in solution and to form various oligomers until the formation of a first Al-rich gel ("Gel 1") [16]. The increase in silica availability over time would allow for partial substitution of Al by Si in "Gel 1", which in turn would result in the formation of a Si-rich "Gel 2". The reorganization of "Gel 1" into "Gel 2" was challenged in 2015 after a nuclear magnetic resonance (NMR) study on the interstitial phases revealed that direct polymerization of "Gel 1" might be more plausible [17]. According to Favier *et al.* (2015) [17], the evolution of "Gel 1" and oligomers in solution into "Gel 2" would be the result of a major precipitation of aluminosilicate

[1] Monomers are small molecules which consist of the basic units of polymer structures. When three to ten repeating monomer units are chemically bound, they form an oligomer. When more repeating monomer units are bound, they will form a polymer.

species, rather than the single reorganization of "Gel 1". Some degree of reorganization could however be possible in the polymerization phase. As a matter of fact, it was found that the polymerization step was associated with an exothermic peak, identified by isothermal calorimetry, which may be due to more cross-linking in the final amorphous aluminosilicate gel and thus reorganization of this final gel into a more stable structure [18]. More recent work by Li *et al.* [19] proposes a change to the original model by Provis and van Deventer [15] to include nucleation alongside gelation after the dissolution of the aluminosilicates and silicates species. According to these authors, this nucleation process would enable the formation of nano-zeolites which would act as nuclei in the polymerization process and be associated with chemical expansion.

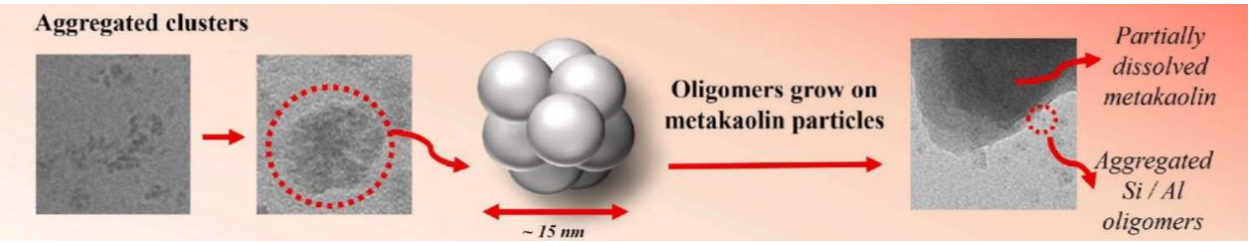

Figure 2-2 - Aggregation process during the geopolymerization, as shown in [23]

In the work of White *et al.* [21], the geopolymerization process of metakaolin activated with pure and blended hydroxide and silicate activators was investigated using Monte Carlo modeling. The simulation supported the hypothesis of Provis *et al.* (2005) [22] that the mechanism of gel growth was dependent on the silica content of the activator. In systems without soluble silica, nucleation is unlikely to occur near the surface of the metakaolin particles, which in turn enables the rapid and complete dissolution of the particle. On the other end, silicate-containing activators would allow the nucleation of aluminosilicate gel particles that attach to the surface of the metakaolin and therefore hinder its dissolution. Rather than fully dissolving, the particle starts to 'grow' as the gel forms on its surface (*Figure 2-2*). This hypothesis was introduced earlier by Wang *et al.* [24] and later further supported by the cryo-TEM imaging testing performed in the study by Tang *et al.* [23].

2.1.1 N-A-S-(H) gel formation in the low calcium AAMs (geopolymer) system

The scientific community has long been divided on the adequate terminology to be used to describe low calcium AAMs. As the issue kept dividing the community, the number of designations used continued to expand over the years. From mineral or inorganic polymers to alkali-bonded ceramics,

from soil cements to zeoceramics, the list kept on growing. In 2014, the state-of-the-art report of RILEM committee TC 224-AAM established a terminology that helped reach a consensus amongst authors [25]. The terms "low-calcium alkali-activated material" and "geopolymer" may now be used interchangeably to describe this binder system[2].

The primary reaction products in geopolymer systems are crystalline zeolitic phases (i.e., sodalite-type feldspathoids) and sodium aluminum silicate hydrates (N-A-S-(H)) [26,27]. The N-A-S-(H) gel is particularly challenging to study due to its complexity, and amorphous nature. It is best described as a three-dimensional cross-linked, highly disordered alkali aluminosilicate network [28]. While the tobermorite-like structure of calcium silicate hydrate (C-S-H), the main binding phase forming upon hydration of PC, has been studied for many decades, N-A-S-(H)'s complex polymeric structure is less well understood. It is important to keep in mind that the N-A-S-(H) gels differ largely from C-S-H and Al substituted C-S-H gels, and notably in that the water is not a major structural component [26].

In 2018, Lolli *et al.* [29] conducted computational molecular modeling to predict the structure of N-A-S-(H) gels in metakaolin geopolymers. The authors built three models with different degrees of disorder: a pure crystalline structure based on the siliceous sodalite mineral, a defective siliceous sodalite created by removing two SiO_2 molecules to the original structure, and an amorphous SiO_2 glass based on the one proposed by Sheikholeslam *et al.* [30]. To these siliceous crystal or glass structures, Na and H_2O was added, and part of the Si ions were replaced by Al to match the Si:Al ratio of the reference metakaolin. From the comparison of the XRD peaks in the simulated and experimental structures, it was found that the defective crystalline model was the most appropriate representation of N-A-S-(H) gels in metakaolin geopolymers (*Figure 2-3*).

[2] It must be observed that even though low-calcium AAMs are considered a subset of the broader AAMs family, their main reaction product differs largely from that of high AAMs. More details on the latter will be provided in section 2.1.2

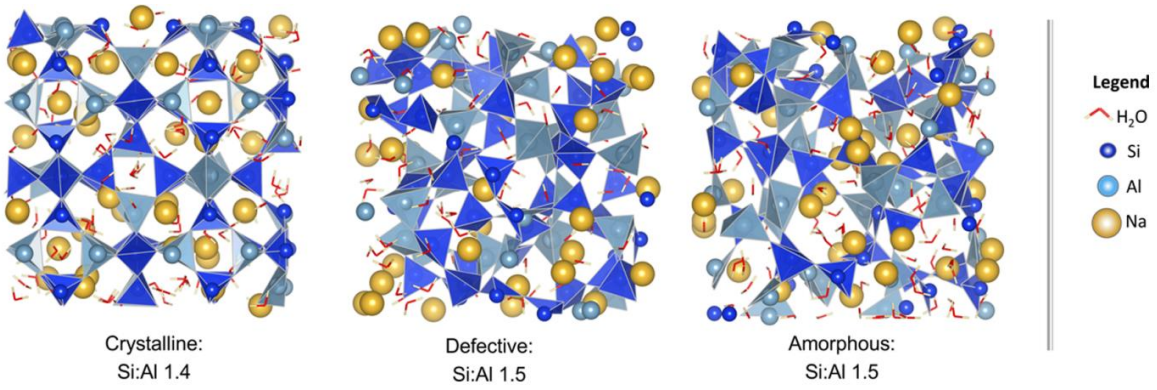

Figure 2-3 - Model of N-A-S-(H) gel with different degree of disorder, from [29]

That same year, Walkey *et al.* [28] used a different approach to shed light on the structural framework of geopolymer gels. Their team used high purity synthetic aluminosilicate powders to serve as model precursors in the geopolymer system and analyzed the molecular bonds and coordination of the aluminum, sodium and oxygen ions using ^{27}Al, ^{23}Na and ^{17}O 3QMAS NMR spectroscopy (i.e., 'Three Quantum Magic Angle Spinning Nuclear Magnetic Resonance).

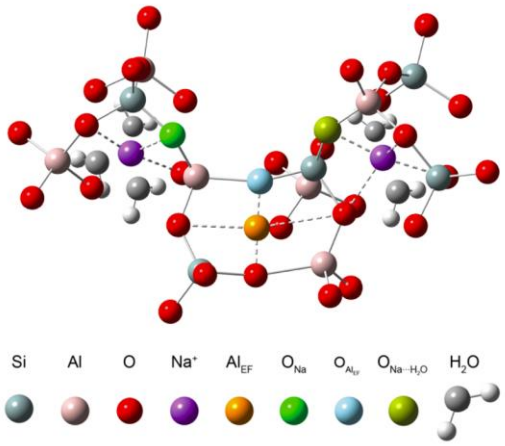

Figure 2-4 - Structural model of N-A-S-(H), proposed by [28], *where Al_{EF} is extra-framework four-fold coordinated Al (as represented by the 4 dashed lines to oxygen species O and $O_{Al,ef}$)*

In this conceptual model (*Figure 2-4*), the sodium and extra-framework aluminum ions act as negative charge balance, and the N-A-S-(H) gel mostly comprises four-fold coordinated silicon and aluminum units, which agrees with previous understanding of atoms coordination in geopolymer gels [31,32]. These authors were the first to identify that a significant portion of tetra-coordinated Al were charge-balanced by extra-framework Al species.

2.1.2 C-A-S-H gel formation in the high calcium AAM system

In high calcium systems, the main gel is a C-A-S-H gel which has presents with a similar Ca/Si ratio to C-S-H type I and a tobermorite-like structure [33] (*Figure 2-5*).

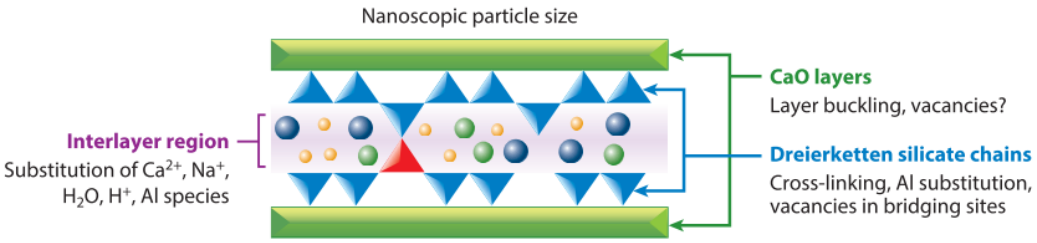

Figure 2-5 - Structure of C-A-S-H gels in high calcium AAMs, from [26]. *The blue triangles represent Si sites, and the red triangle is an example of Al substitution into a bridging site.*

Between 1993 and 1994, Richardson *et al.* [34,35] and Brydson *et al.* [36] worked on an experimental program to better understand the structure of C-S-H gels with Al inclusion. This work was fundamental in understanding the properties of C-(A)-S-H gels, typical of both high calcium AAMs and blended PC binders. In [35], Richardson *et al.* demonstrated that Al substitutes for Si only in bridging tetrahedras (*Figure 2-6*). This finding was further supported by a study by the same authors, conducted in 1994 [34]. Using Richardson's formula for the mean chain length (MCL) of C-S-H, Fernandez-Jimenez *et al.* (2003) [37] could estimate the percentages of Al and Si in bridging tetrahedras and the percentage of vacancies in bridging tetrahedras. They found that the sodium silicate and sodium carbonate activators led to increased Q_3(Si) amounts, causing a change in the morphology of C-S-H which could explain the reduced porosity and improved mechanical properties of these AAMs. On the other hand, they reported greater amounts of Al-substituted bridging sites in NaOH-activated AAMs.

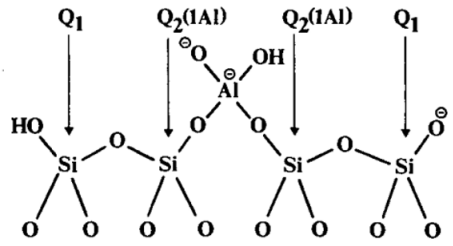

Figure 2-6 - Position of Al in C-A-S-H chain, from [35]

The early work of Faucon (1999) somehow contradicted the findings from Richardson *et al.* on the location of Al on the bridging sites only and showed that Al could also substitute Si on pairing sites at high Ca/Si ratios [38] (*Figure 2-7*). The molecular dynamics study conducted by Manzano *et al.* in 2008 [39] and NMR study of Pardal *et al.* in 2012 [40] supported this hypothesis. Nevertheless, it must be noted that the Ca/Si ratios needed for substitution on pairing sites to occur are unusual in high calcium AAMs systems.

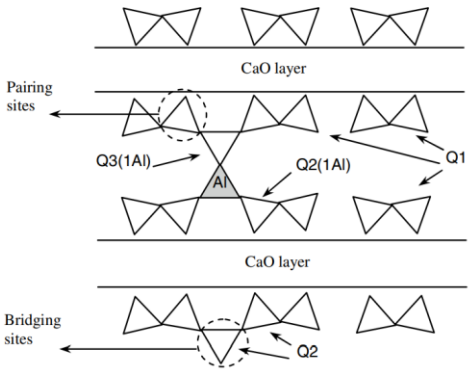

Figure 2-7 - Aluminum in C-A-S-H in pairing and bridging sites, from [39]

In Brydson *et al.* [36], it was found that the Al in C-S-H gels was predominantly in four-fold coordination. Building on this finding, the 2006's study by Sun *et al.* [41] concluded that the four-fold coordinated Al occupied tetrahedral bridging sites, while Q_5(Al) and Q_6(Al) could be found in the interlayer. Alongside some other authors [42], they found sodium cations (Na^+) to be the main charge-balancing elements for Al substituted bridging tetrahedras, but also hypothesized that Ca^{2+} and interlayer or surface Q_5(Al) and Q_6(Al) could also serve as charge-balance units.

The first study applying experimental and computational methods to understand the structure of C-A-S-H gels and correlate it to mechanical properties was conducted by Puertas *et al.* [43]. It revealed that C-A-S-H gel in NaOH-activated slags were best modelled by a combination of tobermorite 14 Å (MCL 5) and tobermorite 11 Å (MCL 14), while the C-A-S-H gels in waterglass-activated slags were found as a combination of tobermorite 14 Å (MCL 11) and tobermorite 1.1 Å (MCL 14) (*Figure 2-8*). The greater amount of tobermorite 11 Å in waterglass-activated slags was effectively correlated to the lower porosity and improved mechanical properties of this class of AAMs. Furthermore, the authors identified different C-A-S-H mechanical states based on packing. In both NaOH and waterglass activated, the lack of portlandite did not allow for the formation of

ultra-high density C-A-S-H, but most of the waterglass C-A-S-H belonged to the high density state, while the higher porosity of NaOH C-A-S-H had it belong to the low density state.

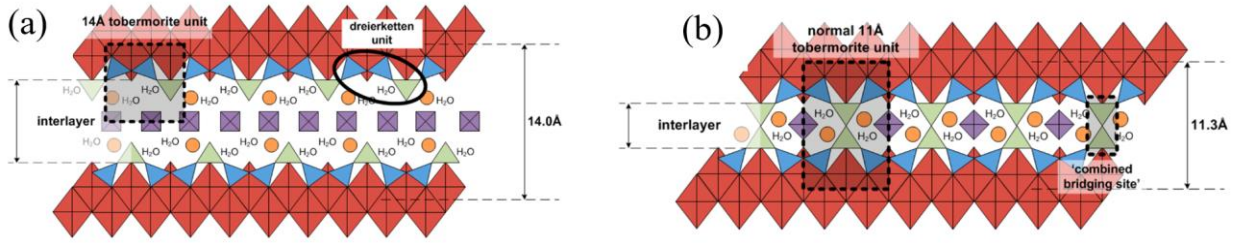

Figure 2-8 - 1.4Å and 1.1 Å tobermorite units, modified from [44]

Even though Puertas' 2011 study only identified 14 Å and 11 Å tobermorite type units, Bernal et al *et al.* [45] found XRD peaks associated with ($Ca_6Si_3O_{12}\cdot xH_2O$) which were only slightly shifted from those associated with 9 Å tobermorite ($Ca_6Si_3O_{12}\cdot xH_2O$). Therefore, in Myers et al's C-(N)-A-S-H gel model, it was hypothesized that the gel could be a combination of all tobermorite units (i.e., 9 Å, 11 Å and 14 Å) [44]. Their model was also built on the hypothesis that cross-linked and non-crosslinked tobermorite structures could represent the C-A-S-H gel more accurately than the previously discussed non-crosslinked models. The experimental results from this study correlated well with the model in terms of Ca/Si ratio, but the Al/Si ratio remained significantly underestimated. According to the authors, the most plausible explanation for the higher Al/Si ratio of the experimental AAMs is the existence of Al-containing zeolitic structure similar in composition to N-A-S-(H).

2.1.3 N-(C)-A-S-H and C-(N)-A-S-H gel formation in the hybrid AAM system

Hybrid AAMs were briefly introduced in section 1.1 of this document as an alkali-activated binder comprising approximately 70% of aluminosilicate precursors and 30% of Portland cement. The inclusion of small amounts of PC in these mixes both changes the alkali-activation process of the precursors and the hydration of PC.

While in blended Portland cement mixes, pozzolanic SCMs such as metakaolin or fly ash react directly with the portlandite resulting from PC hydration, a slightly different reaction is expected to occur in hybrid AAMs. According to Escalante-Garcia *et al.* (2023), portlandite ($Ca(OH)_2$) - reacts first with the alkaline salt [46]. The modification of the formula proposed by the authors to the particular case of sodium sulfate activators yields the following:

$$xCa(OH)_2 + Na_2SO_4 \leftrightarrow CaSO_4 + 2\,NaOH \quad (2.1)$$

Based on this reaction, it ensues that gypsum will be formed, providing the additional sulfate required to mitigate the undersulfation of a high SSA system such as those of calcined clay binders (see section 2.2.2.2 for more details). The formation of sodium hydroxide (NaOH) will also play a major role, as the presence of Portland cement alone may not be sufficient to fully dissolve the large amount of SCMs in the mixture. By helping raise the alkalinity in the fresh binder, NaOH formation leads to greater reaction from the SCMs and more reaction product formation. Knowing that portlandite will be rapidly depleted at low PC, NaOH thus substitutes for portlandite and ensures that SCMs will react.

The precise nature of the hydrates and non-hydrates forming in hybrid AAMs is a challenging matter. It may however be partially understood by correlating concepts of alkali-activation of hybrid AAMs with those of blended AAMs. The latter refers to a type of alkali-activated binder of intermediate calcium and comprising a blend of both high calcium (e.g., slag, class C fly ash, etc.) and low calcium aluminosilicate precursors (e.g., class F fly ash, metakaolin). In blended and hybrid binders, the low calcium precursors will tend to react to form N-A-S-(H) gels, but if calcium from the high calcium precursor or cement is available, C-A-S-H or C-S-H formation will be favored. Nevertheless, the formation of N-A-S-(H) and C-(A)-S-H are not mutually exclusive. Indeed, it was discovered by Yip *et al.* [47] in 2003 that C-S-H and geopolymeric gels could coexist in a binder of specific composition. In their experiment, they showed that at certain NaOH concentrations and in alkali-activated mixtures made of metakaolin and slag, a layer of NaOH ions could occur around slag particles, preventing most of the calcium to reach the geopolymeric gels forming around metakaolin particles. This resulted in the early formation of two distinct, coexisting gels.

The alkaline-activation process in hybrid binders was studied thoroughly by Garcia-Lodeiro *et al.* (2013) [48] (*Figure 2-9*). The authors developed a model to account for the differences in kinetics between these binders and traditional Portland binders. They observed notably a retardation of C-S-H formation due to alkalinity of the solution altering anhydrous silicate hydration. It also appeared that the C-S-H eventually formed had a higher degree of polymerization (i.e., more Q^2 species). This could notably be explained by the incorporation of Al from SCMs into C-(A)-S-H and the subsequent integration of $Al(OH)_4^-$ as $Q^2(Al)$ bridge unit. As for the N-A-S-(H) gel formed

from the reaction of the SCMs in the alkaline media, it stems from Garcia-Lodeiro *et al.*'s work [48] that it converted to a (N,C)-A-S-H type gel due to the incorporation of calcium ions from the pore solution into the gel. In a previous study, Garcia-Lodeiro *et al.* [49] showed that the coexistence of C-S-H, C-A-S-H and N-A-S-(H) gels was possible, but that N-A-S-(H) would tend to disintegrate in favour of C-A-S-(H) and that it ultimately could only remain stable at low pH (<12).

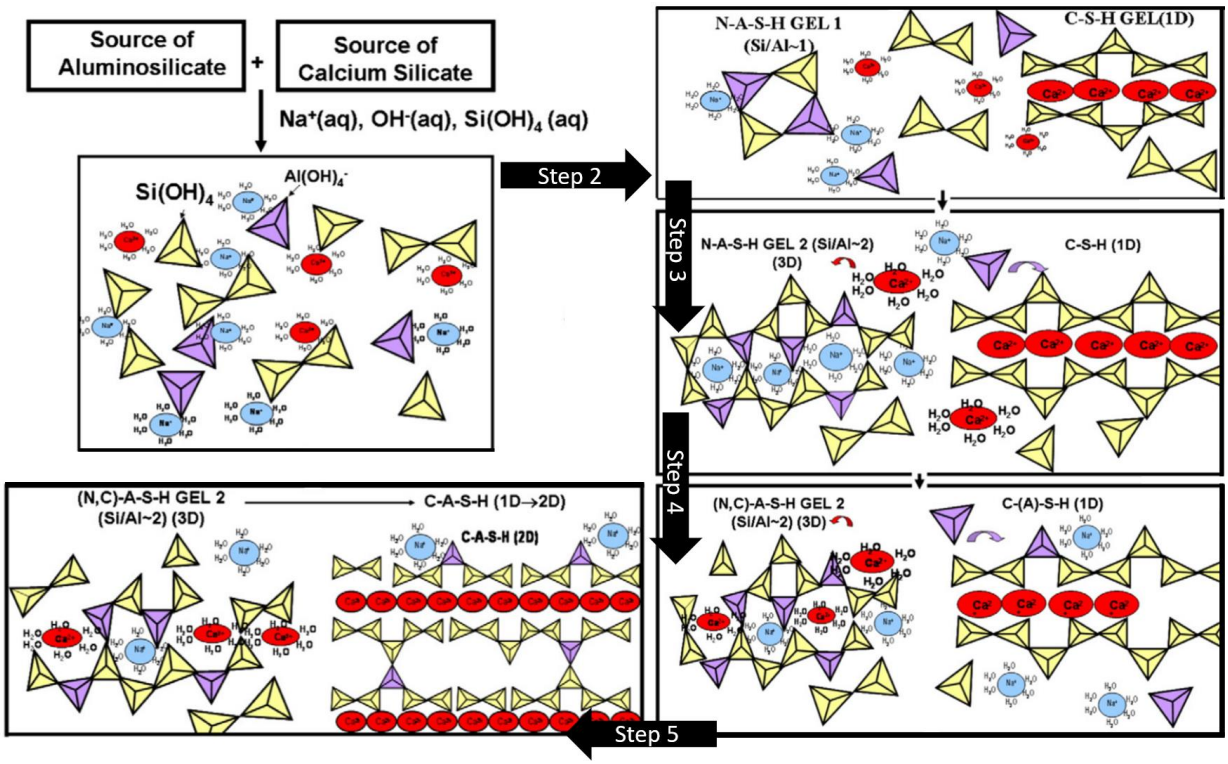

Figure 2-9 - Alkali-activation of hybrid AAMs, modified from [48]

The chemical composition of geopolymeric and hydrate gels formed in hybrid binders is depicted on the ternary diagrams developed by Garcia-Lodeiro *et al.* [49]. As shown in *Figure 2-10*, the composition of C-S-H + N-A-S-(H) and C-A-S-H + N-A-S-(H) appear in intermediate regions on the ternary diagrams, with some points also falling on the regions of the individual gels. Interestingly, and as predicted by Garcia-Lodeiro's study [49], the chemical composition of blended and hybrid gels moves towards the C-A-S-H gel region of the ternary diagram at later ages for blended low calcium (fly ash) + high calcium (slag) AAM systems [26,50].

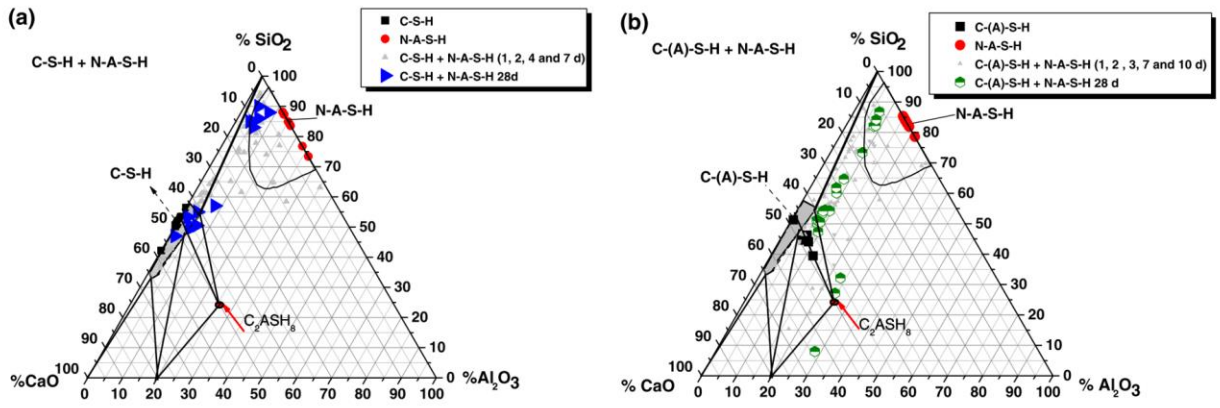

Figure 2-10 - Pseudo-ternary phase diagram proposed by [49]

2.2 Properties of binders containing metakaolin and other calcined clays

Calcined clays have been increasingly discussed in the scientific literature in the last decades. The need for widely available SCMs is a source of concern for many countries as traditional mineral additives such as fly ash and slag have started to deplete drastically [51]. The cement industry heavily relies on SCMs to reduce the carbon footprint of concrete through cement substitution, as well as to improve the durability of concrete mixtures. Calcined clays have therefore emerged as an attractive alternative to fly ash and slag. When clays rich in kaolinite are calcined at temperatures between 600 to 900 °C, they form metakaolin, a highly reactive aluminosilicate precursor. Other clays, such as illite, smectite and montmorillonite, are however more challenging to transform into suitable reactive SCMs [27].

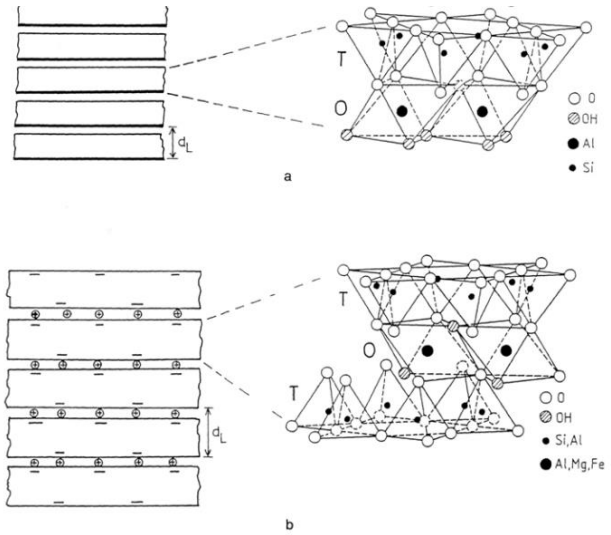

Figure 2-11 - Structure of (a) 1:1 clay and (b) 2:1 clay, adapted from [52]

2.2.1 Clay particles: morphology, surface chemistry and reactivity

2.2.1.1 Clay minerals' structure

Clay minerals are phyllosilicates, and they are formed of successive layers of silica tetrahedral and alumina octahedral sheets (*Figure 2-11*). In 1:1 clays, each layer comprises one silica sheet and one alumina sheet, while 2:1 clays have two silica sheets separated by an alumina sheet [53]. 1:1 clay minerals have electrically neutral sheets, which means that the layers can be stacked, held by van-Der-Waals forces and by the hydrogen bonds between the octahedral hydroxyl groups and tetrahedral oxygen atoms from another layer [54]. For kaolinitic clays, these O-OH bonds are sufficiently strong to prevent swelling between the successive clay units, while the 1:1 layers in halloysite clays are separated by water [55] (*Figure 2-12*).

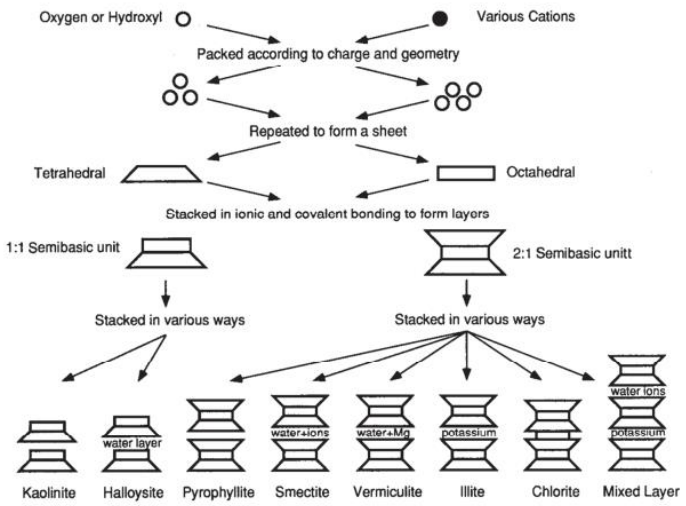

Figure 2-12 - Different clay minerals structures [56]

As for 2:1 clay minerals, the sheets may be electrically neutral (e.g., pyrophyllite and talk), or negatively charged (e.g., smectite, vermiculite and mica). In both cases, there are no available hydroxyl groups at the surface of the layers. Therefore, 2:1 clay minerals' sheets are held by either the weak van-Der-Waals forces for electrically neutral layers and coulombic bonds for negatively charged ones.

2.2.1.2 Clay calcination

Upon calcination, three processes occur: dehydration, dehydroxylation and recrystallization [57]. Dehydration is characterized by the release of water molecules adsorbed in the pores or attached to interlayer cations. The degree of humidity of the clay, as well as its mineralogy and the type of

cations in the interlayer will affect the temperature required for dehydration (80 – 300 °C). This is followed by dehydroxylation, which is critical for clay reactivity. At this point, hydroxyl ions (OH^-) are released as water, which for kaolinitic clays results in the metastable structure pictured in *Figure 2-13* [55,57].

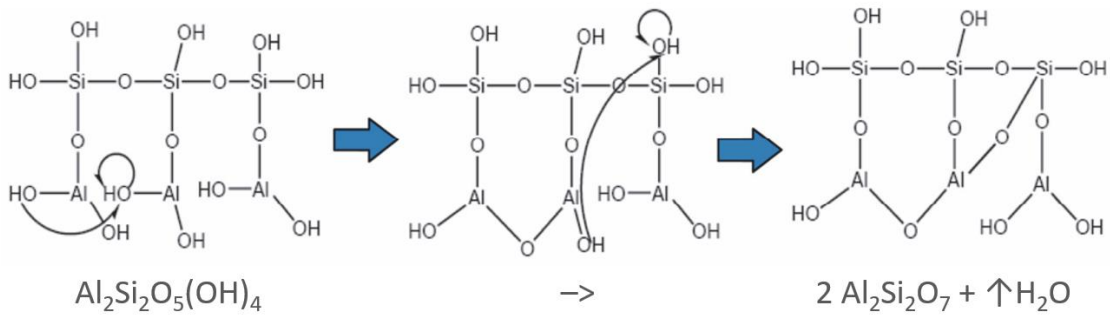

Figure 2-13 - Dehydroxylation of kaolinite, modified from [58]

The dehydroxylation process causes a loss of structural order, yet complete amorphization of the clay is not achieved even after full dehydroxylation [57]. If the clay is exposed to higher temperatures (typically, above 850 °C), recrystallization might take place. This occurs when the energy provided to the clay particles through heating is sufficient to allow the metastable structure to transform into a stable crystalline one. Since the amorphous content of calcined clays is a critical parameter for reactivity, determining the proper calcination temperature for only dehydroxylation to occur is of paramount importance.

After calcination, the hexagonal morphology of clay particles remains like that of their uncalcined counterparts. As can be seen in *Figure 2-14*, metakaolin particles consist of layered stacks of these hexagonal sheets. The plate-like shape and high specific area of clay particles have long been an issue for concrete producers as these factors negatively impact the workability of clay-containing cementitious mixtures [59]. In comparison to SCMs such as fly ash and slag, calcined clays require particular care at the mix-design stage to ensure that workability and setting time requirement will be met. If the calcined clay's shape and surface area are responsible for the decrease in workability of clay-PC blends, it is their high reactivity that is responsible for the decrease in setting time. In a study on precursors for geopolymer systems, Hajimohammadi & van Deventer (2016) [60] showed that the dissolution rate of silica and alumina species in alkaline solutions was significantly higher for metakaolin than for slag, and even more so for fly ash.

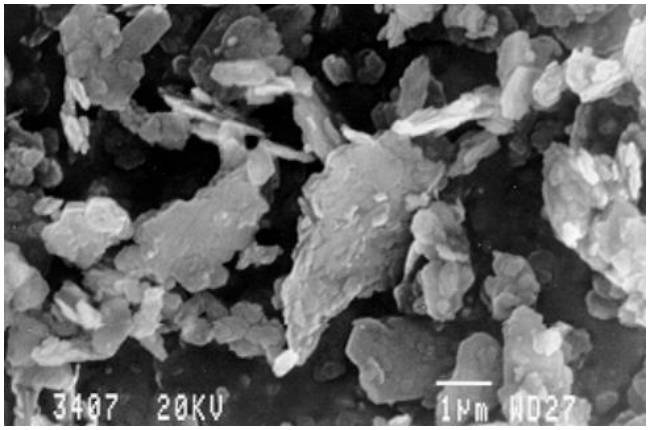

Figure 2-14 - SEM micrograph of metakaolin particle [61]

2.2.1.3 Reactivity and extent of reaction of clays and clinker

Most AAMs mix-designs rely on the knowledge of reactive silica and alumina amounts in the aluminosilicate precursors. For calcined clay and other SCMs, the development of a simple yet reliable method for quantifying the reactive oxide amounts from the raw sources is still a topic of ongoing research [27,62]. Even though no general agreement has been reached, various techniques have been proposed. One of the most efficient is the dissolution of aluminosilicate precursors in 1% hydrogen fluoride [63]. However, the health and safety issues related to the manipulation of hydrogen fluoride limit its applicability. This methodology has therefore been attempted with other acid (e.g. hydrochloric acid) and basic (e.g. NaOH) solutions and it was found reliable [64–66]. The use of X-Ray fluorescence (XRF) and X-Ray diffraction (XRD) analysis also allowed some authors to successfully quantify amorphous content from raw material [67]. Finally, reactivity techniques based on the final gel composition rather than precursors composition have been developed. In this regard, XRD with Rietveld quantification and NMR have proven to be effective but can be technical and expensive [68–70]. Furthermore, quantification of reactive content by NMR may be complexified by the overlap between resonances of some precursors and their reaction products [69].

The aforementioned techniques may be applied to most aluminosilicate precursors, but when a precursor is pozzolanic, as calcined clays are, a specific range of test is available. These tests are generally applied to predict the performance of blended cements, and therefore more work is likely needed to adapt them to AAMs systems in which the main reaction occurs without portlandite, but thanks to the presence of alkalis. According to Donatello *et al.* (2010) [71], the pozzolanic activity

of a material can be assessed both directly (through the quantification of portlandite consumption) and indirectly (through the measure of physical properties resulting from the raw material reactivity). Direct methods include the Frattini test and its simplified version, the saturated lime method, and proceed in conjunction with analytical methods such as XRD and thermogravimetric analysis (TGA) [71]. On the other hand, indirect methods are based on compressive strength, electrical conductivity and heat evolution by conduction calorimetry measurements [71]. In a study by Tironi *et al.* (2013) [72], it was found that the Frattini test and the strength activity index (i.e., representing the ratio of compressive strength of a blended cement mortar to the compressive strength of a Portland cement mortar) were the most reliable. Nevertheless, it was argued by the authors that the sole use of one method might not be enough to correlate to strength. Pozzolanic activity may be inferred more directly by the Frattini method, but prior to strength testing, it is not possible to accurately estimate the real contribution of the pozzolanic reaction to microstructure densification and strength gain. This issue motivated the search of new methods to evaluate the reactivity of clays and directly correlate them with strength in blended cements. Since strength testing takes up to 28 days, it is not always possible to apply it when searching for new raw materials. Therefore, in 2016, the R^3 method was developed by Avet *et al.* [73]. This method uses a simplified system to simulate a fresh blended paste and it comprises the investigated calcined clay, portlandite, water, alkalis and sulfates. The fresh pastes are analyzed using isothermal calorimetry for up to 7 days or may be dried in an oven to quantify bound water amounts. These two variations of the R^3 method have been found to correlate well to strength and are now standardized in ASMT C1897-2022 [74].

2.2.2 Calcined clays in binders: fresh state and early kinetics

In blended calcined clay binders, as well as in alkali-activated calcined clays (AAMKs), the role played by this binder component during early kinetics is both physical and chemical. Metakaolin and other calcined clay particles have large specific surface areas (SSA), which will enable them to contribute additional nucleation sites, a phenomenon also known as the “filler effect” [51]. Furthermore, the presence of these fine particles will tend to decrease interparticle distances, which accelerate setting significantly. On a chemical level, the addition of metakaolin provides rapidly available alumina, which affects the phase assemblage of both blended and AAMs cements [60]. In blended Portland cement, the nature of some of the C-S-H will differ as a result of the inclusion of Al and subsequent formation of C-A-S-H gel. In AAMKs, silicate and aluminate species from

the metakaolin are released in solution in similar, high amounts. This behavior has been shown in the work of Hajimohammadi *et al.* (2016). *Figure 2-15* highlights the dissolved concentrations of Si and Al in time when metakaolin is dissolved in 0.1M NaOH. In such cases, the high early availability of alumina leads to faster reaction kinetics and more homogeneous gel formation [75]. Early age strength is benefited by this process, but it may come with impediments in strength development due to the lack of silicon ions available [75]. Indeed, the presence of high levels of alumina in solution is known to hinder silica dissolution, a phenomenon of interest in the study of alkali-silica reaction in blended and AAMs binders.

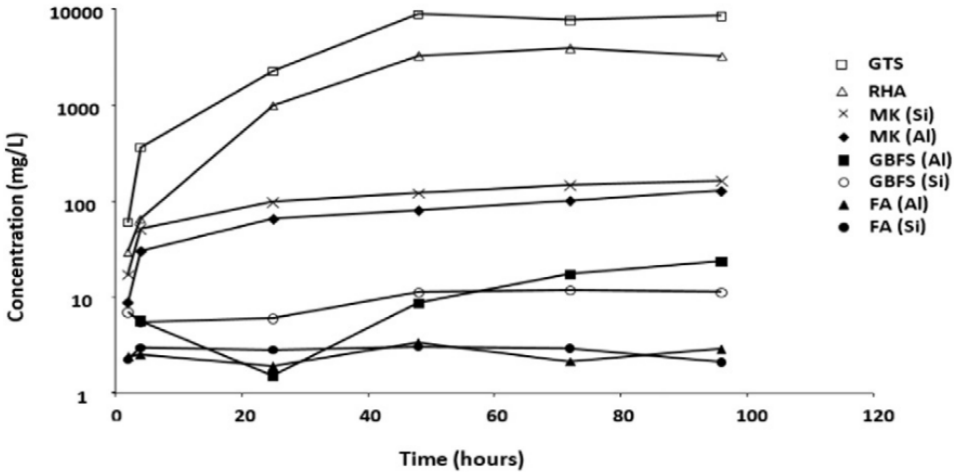

Figure 2-15 Concentrations of dissolved silica and alumina in 0.1M NaOH of geothermal sludge (GTS), rice husk ash (RHA), MK, ground-blast furnace slag (GBFS), and fly ash (FA), from [60]

2.2.2.1 Admixture interaction

The large surface area of calcined clay, and their typically high amorphous content renders them particularly reactive, which will directly impact the reaction kinetics and therefore the setting time. To address the workability and setting time challenges, superplasticizers and retarders are sometimes combined. It has been shown that standard PCEs (polycarboxylate ether) admixtures remain effective in clay-containing mixtures through the same electrostatic repulsion mechanisms as in PC mixtures [59]. In some cases, intercalation of the PCEs macromolecules in the interlayer space of the clays can lead to the deformation of some clay particles and to the 'loss' of part of the PCE added [76]. However, this phenomenon only occurs in some clays and has not been reported in kaolinite and illite clays. A more common issue is that the greater surface area of calcined clay particles compared to PC particles leads to greater adsorption of PCEs on their surface, hereby leading to greater PCE demand to achieve the same level of fluidity in the mix [59].

2.2.2.2 Mix-design adjustments

Addressing the workability issue caused by calcined clay in cementitious mixtures can also be done through changes to the mix-design. Higher water-to-cement ratios, lower fine aggregate content and an optimized paste volume can all contribute to a more fluid mix without admixtures [59]. The incorporation of calcined clays in concrete mixes also requires sulfate adjustments to be made. Indeed, the presence of clay particles will promote C-A-S-H gel formation, and therefore more sulfate ions will be adsorbed onto the surface of the C-A-S-H gels [53]. This will lead to an undersulfated system if no additional source of sulfate alkali or gypsum is provided.

2.2.3 Calcined clay in binders: porosity evolution and strength development

The pore structure of cementitious materials plays an important role in their mechanical properties and transport behavior. Understanding the size repartition of pores, their interconnectivity and tortuosity, and how these parameters may affect the durability and mechanical performance of the binder is thus crucial. In the case of cementitious binders containing calcined clays, the porosity and strength development will vary significantly between AAMs and PC systems. Therefore, this section will focus individually on the case of metakaolin AAMs (AAMKs) and MK-PC or MK-PC-LS (LC3) blends without activators.

2.2.3.1 Metakaolin alkali-activated materials (AAMKs)

AAMKs are a class of low calcium AAMs. This class of binders, regardless of the precursor (usually fly ash or metakaolin), share the following three factors which will influence porosity features, i.e., the Si/Al ratio, the molarity of the activating solution and the curing temperature [77]. Since AAMKs form N-A-S-(H) type gels, with small amounts of water bound, water-to-cement ratio does not play a role as significant as in traditional PC mixes.

In terms of Si/Al ratio, ratios of 1 to 5 are generally suitable in terms of strength and thermal stability [78], but a Si/Al ratio of 2 is generally found ideal as it promotes metakaolin dissolution [79,80]. The silica to aluminum ratio does not only matters in terms of precursors' composition, but also in terms of silica availability. Yang *et al.* (2020) found that for systems without soluble silicates (e.g., activated by pure NaOH), the pore structure contains a high number of nanopores, which is believed to be related to the presence of zeolites [81]. Pores in the mesoscale are scarcer for this type of binder, and instead "macro" pores in the 40 to 120 nm range are responsible for bridging the gel pores within the larger pore system. In the case of systems activated by alkali

silicates, pure or combined with sodium hydroxide, few nanopores are found and large amounts of mesopores in the 3-13 nm range are present.

Regarding the molarity of the activator, higher molarities will usually benefit greater dissolution of the metakaolin and thus larger amounts of reaction products formation, and consequently strength by decreasing porosity. This behavior diverges from that of high calcium systems, in which high amounts of alkalis can be detrimental to strength. Studies have indeed found that high molarities could negatively impact the later age strength and durability of activated slag binders. This would be caused by the excess hydroxide and sodium ions, the poor dispersion of silicon and sodium oxide in solution, and the rapid formation of a high-density inner product ring, which inhibits later-age product formation [82,83]. In Portland systems, alkalis can also negatively impact strength by increasing the capillary porosity of the system. From this, it can be expected that metakaolin AAMs blended with calcium rich precursors may be sensitive to high molarities in the activating solution.

Regarding curing temperature, contradicting results have emerged in the literature. Rovnanik *et al.* (2010) found that AAMKs experience lower strength at 28 days when heat curing is used, although it also increases early age strengths. The authors attributed the phenomenon to the formation of larger pores when heat was applied during alkali-activation [84]. This effect could also be related to the nanocrystalline nature of N-A-S-(H) gels, which means that their amorphous state is only metastable. When geopolymers are heated at high temperatures, their amorphous phases may convert to crystalline ones, leading to increased amounts of zeolites at a microscale level [85]. These zeolites are associated with greater amounts of gel porosity and their rapid formation may be linked with the conversion of small pores into large ones. Nevertheless, Aredes *et al.* (2015) [86,87] and Mo *et al.* (2014) [87] both found an optimum curing temperature of about 60°C and a reduced porosity at this optimum. More studies are therefore needed to understand how curing should be performed to enhance strength of AAMKs binders.

It is finally important to highlight that despite the similarities in the reaction products of geopolymers independently of their precursors, metakaolin AAMs differ from their fly ash counterparts [77]. These two precursors differ mostly in terms of their reactivity, and particle shape and surface area. The high reactivity of metakaolin is typically beneficial to the refinement of porosity since it enables the rapid formation of reaction products. On the other hand, fly ash has a

significant glassy content, and its reactivity is low unless subjected to high temperatures [77]. This may cause the presence of large amounts of unreacted particles, which will lead to higher porosity. Conversely, the high surface area and platy shape of metakaolin particles cause them to increase the water demand of the system [59] and this typically increases the average size of the pores since, as mentioned previously, the added water to ensure sufficient workability will generally not end up chemically bound in hydrates. This "excess" water will thus eventually evaporate, leaving pores in the cementitious structure.

2.2.3.2 Metakaolin-Portland cement blends (MK-PC) and metakaolin-limestone-Portland cement blends (LC3)

For decades, metakaolin was not a commonly used SCMs in the cement industry, and therefore, MK-PC blends were not very extensively studied [59]. This came down to the workability issue associated with the use of calcined clays, as well as their higher cost and environmental impact compared to fly ash and slags, both of which were first considered as waste (null environmental impact), and later as by- or co-products of the coal and steel industries respectively (assigned portion of the environmental impact of coal and steel production). About 15 years ago, limestone-calcined clay cements started being developed and it was found that similar or higher mechanical properties could be reached at high degrees of PC substitution by adding a combination of metakaolin and limestone to traditional PC binders [51]. These materials are now widely known as limestone calcined clay cements or LC_3. Much of the research on the impact of metakaolin in MK-PC blends now emanates from LC3 studies, which is why both binders will be discussed simultaneously in this section.

When adding metakaolin to a PC system, the first parameter which will influence porosity of the end product is the pozzolanic reaction between the metakaolin and portlandite ($Ca(OH)_2$) [88]. Due to the high availability of aluminum from metakaolin, this reaction will cause the formation of Al-containing C-S-H gels, or C-A-S-H, which have a similar composition to the C-A-S-H forming in high calcium AAMs. If limestone is added alongside the metakaolin, its calcium carbonate will react with the C_3A from cement and the alumina from metakaolin to form monocarboaluminate and hemicarboaluminate phases [53]. The formulas governing these chemical reactions are as follows in cement chemist notation [88]:

$$AS_2 + 3CH + 6H \rightarrow C - A - S - H + C_2ASH_8 \quad (2.2)$$

$$C_3A + 0.5Cc + \ 0.5CH + 11.5H \rightarrow C_4Ac_{0.5}H_{12} \quad (2.3)$$

$$AS_2 + 0.5Cc + 3.5CH + 8.5\,H \rightarrow C_4Ac_{0.5}H_{12} \quad (2.4)$$

The formation of these products has significant implications for porosity by contributing to the quantity of hydrates. Furthermore, the preferential formation of hemi and monocarboaluminate phases over monosulfoaluminate phases will allow for more sulfate remaining in solution, and thus greater ettringite precipitation [88]. Since ettringite is a high-volume hydrate, it will also contribute greatly to space filling within the binder. In the study conducted by Zunino and Scrivener (2021) [88], it was found that the additional formation of hemi and monocarboaluminate through reaction (2.4) was strongly related to the early refinement of porosity. This finding supports the evidence of [89] who showed that the porosity of LC_3 was significantly finer at early age compared to that of traditional PC and even fly ash-PC blends. Moreover, it was shown by [90] that the total porosity of LC_3 binders was lower than that of Portland cement pastes at 3 days, but that the opposite was observed after 28 days. This behavior could be linked to the refinement of porosity reported by multiple authors, and which is due to the high reactivity of metakaolin and synergetic reaction with limestone to form AFm phases [88,91,92]. In such conditions, the fine porosity might be responsible for a premature plateau in reaction product growth and stunt further terms of porosity reduction. It is important to note that this plateau is also associated with an important slowing down of metakaolin reaction in LC_3, typically occurring around 7 days.

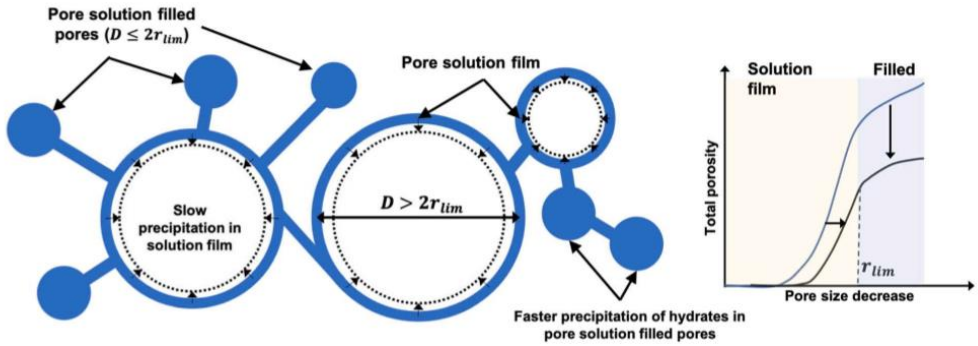

Figure 2-16 Schematic of potential mechanism of reaction at later ages, adapted from [93]

Briki *et al.* (2021) [91] further investigated this mechanism, for which they had found three potential causes: (1) the lack of portlandite, (2) the presence of Al in pore solution, and (3) the lack of water-filled pores. To test the first hypothesis, the authors added extra portlandite to one of the

cementitious systems but it was later found that it remained in excess. Aluminum was also a suspected cause for the slow down mechanisms due to its known role in inhibiting C_3S dissolution and pozzolanic glasses [94,95]. However, even when silica fume was used to replace metakaolin, a similar slowing down was observed. It was found by the authors that when the LC_3 paste samples were fully hydrated during curing (i.e., thin slices were kept immersed in water to ensure that the pores remained saturated), the extent of reaction from metakaolin kept increasing after 7 days, thereby achieving a higher extent of reaction, and preventing the kinetic slow down typically observed. Later ages studies conducted by Zunino *et al.* [93] corroborated the findings of Briki *et al.* [91] and additionally showed that in later ages (3-year samples), the lack of sufficiently large, saturated pores limited further hydrate growth in the pore system (*Figure 2-16*).

2.3 Research gaps

Despite significant advances over the last decades on hybrid AAMs, much remains to be further investigated. In particular, the addition of alkali sources in PC-MK and PC-MK-limestone (LS) mixes has scarcely been studied in the literature. The present work strives to contribute to the understanding of these promising sustainable binders.

The addition of alkalis and high SSA particles to cementitious systems containing PC are known to accelerate the kinetics, but ultimately tend to result in a loss of longer-term compressive strength. Future-proofing hybrid AAMs will require the knowledge of how mix-design must be conducted to reach moderate to high early strengths, while preserving 28-days strength. To address this issue, it is important to better understand how alkalis, metakaolin, limestone, and Portland cement content impact the alkali-activation process of AAMs and the hydration of PC. The impact of binder composition on compressive strength requires further investigation and must be correlated to microscale properties to shed light on the underlying mechanisms.

In this thesis, statistical design of experiment (DOE) will be used to assess the individual and combined effects of binder components and activator composition on macroscale properties such as strength, setting time and bulk resistivity. Multiscale testing related to the fresh state, hardened state, and chemical amorphous and crystalline phases will be performed to relate the macroscale performance to microscale features.

2.4 References

[1] Y.H.M. Amran, R. Alyousef, H. Alabduljabbar, M. El-Zeadani, Clean production and properties of geopolymer concrete; A review, J Clean Prod 251 (2020). https://doi.org/10.1016/j.jclepro.2019.119679.

[2] Z. Shi, C. Shi, R. Zhao, S. Wan, Comparison of alkali–silica reactions in alkali-activated slag and Portland cement mortars, Materials and Structures/Materiaux et Constructions 48 (2015) 743–751. https://doi.org/10.1617/s11527-015-0535-4.

[3] A. Fernández-Jiménez, F. Puertas, The alkali-silica reaction in alkali-activated granulated slag mortars with reactive aggregate, Cem Concr Res 32 (2002) 1019–1024. https://doi.org/10.1016/S0008-8846(01)00745-1.

[4] J. Lei, W.W. Law, E.H. Yang, Effect of calcium hydroxide on the alkali-silica reaction of alkali-activated slag mortars activated by sodium hydroxide, Constr Build Mater 272 (2021). https://doi.org/10.1016/j.conbuildmat.2020.121868.

[5] T.A. Aiken, J. Kwasny, W. Sha, M.N. Soutsos, Effect of slag content and activator dosage on the resistance of fly ash geopolymer binders to sulfuric acid attack, Cem Concr Res 111 (2018) 23–40. https://doi.org/10.1016/j.cemconres.2018.06.011.

[6] H.J. Zhuang, H.Y. Zhang, H. Xu, Resistance of geopolymer mortar to acid and chloride attacks, Procedia Eng 210 (2017) 126–131. https://doi.org/10.1016/j.proeng.2017.11.057.

[7] A. Koenig, A. Herrmann, S. Overmann, F. Dehn, Resistance of alkali-activated binders to organic acid attack: Assessment of evaluation criteria and damage mechanisms, Constr Build Mater 151 (2017) 405–413. https://doi.org/10.1016/j.conbuildmat.2017.06.117.

[8] J. Osio-Norgaard, J.P. Gevaudan, W. V. Srubar, A review of chloride transport in alkali-activated cement paste, mortar, and concrete, Constr Build Mater 186 (2018) 191–206. https://doi.org/10.1016/j.conbuildmat.2018.07.119.

[9] N. Džunuzović, M. Komljenović, V. Nikolić, T. Ivanović, External sulfate attack on alkali-activated fly ash-blast furnace slag composite, Constr Build Mater 157 (2017) 737–747. https://doi.org/10.1016/j.conbuildmat.2017.09.159.

[10] M. Komljenović, Z. Baščarević, N. Marjanović, V. Nikolić, External sulfate attack on alkali-activated slag, Constr Build Mater 49 (2013) 31–39. https://doi.org/10.1016/j.conbuildmat.2013.08.013.

[11] J.L. Provis, Alkali-activated materials, Cem Concr Res 114 (2018) 40–48. http://dx.doi.org/10.1016/j.cemconres.2017.02.009.

[12] Y.K. Cho, S.W. Yoo, S.H. Jung, K.M. Lee, S.J. Kwon, Effect of Na2O content, SiO2/Na2O molar ratio, and curing conditions on the compressive strength of FA-based geopolymer, Constr Build Mater 145 (2017) 253–260. https://doi.org/10.1016/j.conbuildmat.2017.04.004.

[13] C. Ruiz-Santaquiteria, J. Skibsted, A. Fernández-Jiménez, A. Palomo, Alkaline solution/binder ratio as a determining factor in the alkaline activation of aluminosilicates, Cem Concr Res 42 (2012) 1242–1251. https://doi.org/10.1016/j.cemconres.2012.05.019.

[14] S. Yaseri, G. Hajiaghaei, F. Mohammadi, M. Mahdikhani, R. Farokhzad, The role of synthesis parameters on the workability, setting and strength properties of binary binder based geopolymer paste, Constr Build Mater 157 (2017) 534–545. https://doi.org/10.1016/j.conbuildmat.2017.09.102.

[15] J.L. Provis, J.S.J. van Deventer, Geopolymerisation kinetics. 2. Reaction kinetic modelling, Chem Eng Sci 62 (2007) 2318–2329. https://doi.org/10.1016/j.ces.2007.01.028.

[16] P. Duxson, A. Fernández-Jiménez, J.L. Provis, G.C. Lukey, A. Palomo, J.S.J. Van Deventer, Geopolymer technology: The current state of the art, J Mater Sci 42 (2007) 2917–2933. https://doi.org/10.1007/s10853-006-0637-z.

[17] A. Favier, G. Habert, N. Roussel, J.B. D'Espinosede Lacaillerie, A multinuclear static NMR study of geopolymerisation, Cem Concr Res 75 (2015) 104–109. https://doi.org/10.1016/j.cemconres.2015.03.003.

[18] Z. Zhang, J.L. Provis, H. Wang, F. Bullen, A. Reid, Quantitative kinetic and structural analysis of geopolymers. Part 2. Thermodynamics of sodium silicate activation of metakaolin, Thermochim Acta 565 (2013) 163–171. https://doi.org/10.1016/j.tca.2013.01.040.

[19] Z. Li, S. Zhang, Y. Zuo, W. Chen, G. Ye, Chemical deformation of metakaolin based geopolymer, Cem Concr Res 120 (2019) 108–118. https://doi.org/10.1016/j.cemconres.2019.03.017.

[20] W. Wang, T. Noguchi, Alkali-silica reaction (ASR) in the alkali-activated cement (AAC) system : A state-of-the-art review, Constr Build Mater 252 (2020).

[21] C.E. White, J.L. Provis, T. Proffen, J.S.J. van Deventer, Molecular mechanisms responsible for the structural changes occurring during geopolymerization: Multiscale simulation, AIChE Journal 58 (2012) 2241–2253. https://doi.org/10.1002/aic.12743.

[22] J.L. Provis, G.C. Lukey, J.S.J. van Deventer, Do Geopolymers Actually Contain Nanocrystalline Zeolites? A Reexamination of Existing Results, Chemistry of Materials 17 (2005) 3075–3085. https://doi.org/10.1021/cm050230i.

[23] Z.Q. Tang, F.B. de Souza, R.J. Mulder, KwesiSagoe-Crentsil, W. Duan, Multistep nucleation and growth mechanism of aluminosilicate gel observed by cryo-electron microscopy, Cem Concr Res 159 (2022) 106873. https://doi.org/10.1016/j.cemconres.2022.106873.

[24] H. Wang, H. Li, F. Yan, Synthesis and mechanical properties of metakaolinite-based geopolymer, Colloids Surf A Physicochem Eng Asp 268 (2005) 1–6. https://doi.org/10.1016/J.COLSURFA.2005.01.016.

[25] J.L. Provis, Introduction and scope, in: J.L. Provis, J.S.J. van Deventer (Eds.), RILEM State-of-the-Art Reports, Springer Netherlands, Dordrecht, 2014: pp. 1–8. https://doi.org/10.4324/9780203223512_chapter_7.

[26] J.L. Provis, S.A. Bernal, Geopolymers and related alkali-activated materials, Annu Rev Mater Res 44 (2014) 299–327. https://doi.org/10.1146/annurev-matsci-070813-113515.

[27] A.Z. Khalifa, Ö. Cizer, Y. Pontikes, A. Heath, P. Patureau, S.A. Bernal, A.T.M. Marsh, Advances in alkali-activation of clay minerals, Cem Concr Res 132 (2020) 106050. https://doi.org/10.1016/j.cemconres.2020.106050.

[28] B. Walkley, G.J. Rees, R. San Nicolas, J.S.J. van Deventer, J. V Hanna, J.L. Provis, New Structural Model of Hydrous Sodium Aluminosilicate Gels and the Role of Charge-Balancing

Extra-Framework Al, Journal of Physical Chemistry. C 122 (2018) 5673–5685. https://doi.org/10.1021/acs.jpcc.8b00259.

[29] F. Lolli, H. Manzano, J.L. Provis, M.C. Bignozzi, E. Masoero, Atomistic Simulations of Geopolymer Models: The Impact of Disorder on Structure and Mechanics, ACS Appl Mater Interfaces 10 (2018) 22809–22820. https://doi.org/10.1021/acsami.8b03873.

[30] Sa. Sheikholeslam, H. Manzano, C. Grecu, A. Ivanov, Reduced hydrogen diffusion in strained amorphous SiO2: understanding ageing in MOSFET devices, Journal of Materials Chemistry. C, Materials for Optical and Electronic Devices 4 (2016) 8104–8110. https://doi.org/10.1039/c6tc02647h.

[31] J. Davidovits, Geopolymer chemistry and applications, 4th ed., Institut Géopolymère, Saint-Quentin, 2015.

[32] J.L. Provis, J.S.J. Van Deventer, Introduction to geopolymers, Woodhead Publishing Limited, 2009. https://doi.org/10.1533/9781845696382.1.

[33] E. L'Hôpital, B. Lothenbach, D.A. Kulik, K. Scrivener, Influence of calcium to silica ratio on aluminium uptake in calcium silicate hydrate, Cem Concr Res 85 (2016) 111–121. https://doi.org/10.1016/j.cemconres.2016.01.014.

[34] I.G. Richardson, A.R. Brough, G.W. Groves, C.M. Dobson, The characterization of hardened alkali-activated blast-furnace slag pastes and the nature of the calcium silicate hydrate (C-S-H) phase, Cem Concr Res 24 (1994) 813–829. https://doi.org/10.1016/0008-8846(94)90002-7.

[35] I.G. Richardson, A.R. Brough, R. Brydson, G.W. Groves, C.M. Dobson, Location of Aluminum in Substituted Calcium Silicate Hydrate (C-S-H) Gels as Determined by 29Si and 27Al NMR and EELS, Journal of the American Ceramic Society 76 (1993) 2285–2288. https://doi.org/10.1111/j.1151-2916.1993.tb07765.x.

[36] R. Brydson, I.G. Richardson, D.W. McComb, G.W. Groves, Parallel electron energy loss spectroscopy study of al-substituted calcium silicate hydrate (C□S□H) phases present in hardened cement pastes, Solid State Commun 88 (1993) 183–187. https://doi.org/10.1016/0038-1098(93)90404-B.

[37] A. Fernández-Jiménez, F. Puertas, I. Sobrados, J. Sanz, Structure of Calcium Silicate Hydrates Formed in Alkaline-Activated Slag: Influence of the Type of Alkaline Activator, Journal of the American Ceramic Society 86 (2003) 1389–1394. https://doi.org/10.1111/j.1151-2916.2003.tb03481.x.

[38] P. Faucon, A. Delagrave, C. Richet, J.M. Marchand, H. Zanni, Aluminum Incorporation in Calcium Silicate Hydrates (C−S−H) Depending on Their Ca/Si Ratio, J Phys Chem B 103 (1999) 7796–7802. https://doi.org/10.1021/jp990609q.

[39] H. Manzano, J.S. Dolado, M. Griebel, J. Hamaekers, A molecular dynamics study of the aluminosilicate chains structure in Al-rich calcium silicate hydrated (C-S-H) gels, Physica Status Solidi A Appl Res 205 (2008) 1324–1329. https://doi.org/10.1002/pssa.200778175.

[40] X. Pardal, F. Brunet, T. Charpentier, I. Pochard, A. Nonat, 27Al and 29Si Solid-State NMR Characterization of Calcium-Aluminosilicate-Hydrate, Inorg Chem 51 (2012) 1827–1836. https://doi.org/10.1021/ic202124x.

[41] G.K. Sun, J.F. Young, R.J. Kirkpatrick, The role of Al in C–S–H: NMR, XRD, and compositional results for precipitated samples, Cem Concr Res 36 (2006) 18–29. https://doi.org/10.1016/J.CEMCONRES.2005.03.002.

[42] F. Puertas, S. Martínez-Ramírez, S. Alonso, T. Vázquez, Alkali-activated fly ash/slag cements. Strength behaviour and hydration products, Cem Concr Res 30 (2000) 1625–1632. https://doi.org/10.1016/S0008-8846(00)00298-2.

[43] F. Puertas, M. Palacios, H. Manzano, J.S. Dolado, A. Rico, J. Rodríguez, A model for the C-A-S-H gel formed in alkali-activated slag cements, J Eur Ceram Soc 31 (2011) 2043–2056. https://doi.org/10.1016/j.jeurceramsoc.2011.04.036.

[44] R.J. Myers, S.A. Bernal, R. San Nicolas, J.L. Provis, Generalized structural description of calcium-sodium aluminosilicate hydrate gels: The cross-linked substituted tobermorite model, Langmuir 29 (2013) 5294–5306. https://doi.org/10.1021/la4000473.

[45] S.A. Bernal, J.L. Provis, V. Rose, R.M. de Gutiérrez, High-Resolution X-ray Diffraction and Fluorescence Microscopy Characterization of Alkali-Activated Slag-Metakaolin Binders,

Journal of the American Ceramic Society 96 (2013) 1951–1957. https://doi.org/10.1111/jace.12247.

[46] J.I. Escalante-Garcia, P. Castro Borges, A. Duran-Herrera, Sustainable Cements: Hybrid Alkaline Cements Overview, in: Proceedings of the 75th RILEM Annual Week 2021, Springer International Publishing AG, Switzerland, 2023: pp. 626–639. https://doi.org/10.1007/978-3-031-21735-7_68.

[47] C.K. Yip, J.S.J. Van Deventer, Microanalysis of calcium silicate hydrate gel formed within a geopolymeric binder, J Mater Sci 38 (2003) 3851–3860. https://doi.org/10.1023/A:1025904905176.

[48] I. García-Lodeiro, A. Fernández-Jiménez, A. Palomo, Variation in hybrid cements over time. Alkaline activation of fly ash-portland cement blends, Cem Concr Res 52 (2013) 112–122. https://doi.org/10.1016/j.cemconres.2013.03.022.

[49] I. Garcia-Lodeiro, A. Palomo, A. Fernández-Jiménez, D.E. MacPhee, Compatibility studies between N-A-S-H and C-A-S-H gels. Study in the ternary diagram Na2O-CaO-Al2O3-SiO 2-H2O, Cem Concr Res 41 (2011) 923–931. https://doi.org/10.1016/j.cemconres.2011.05.006.

[50] I. Ismail, S.A. Bernal, J.L. Provis, R. San Nicolas, S. Hamdan, J.S.J. Van Deventer, Modification of phase evolution in alkali-activated blast furnace slag by the incorporation of fly ash, Cem Concr Compos 45 (2014) 125–135. https://doi.org/10.1016/j.cemconcomp.2013.09.006.

[51] M. Antoni, J. Rossen, F. Martirena, K. Scrivener, Cement substitution by a combination of metakaolin and limestone, Cem Concr Res 42 (2012) 1579–1589. https://doi.org/10.1016/J.CEMCONRES.2012.09.006.

[52] R.A. Kühnel, Tonminerale und tone. Struktur, eigenschaften, anwendung and einsatz in industrie und umwelt: K. Jasmund and G. Lagaly (Editors). Steinkopf Verlag, Darmstadt, 1993. xiv+490 pp. ISBN 3-7985-0923-9, Appl Clay Sci 10 (1996) 411–412. https://doi.org/10.1016/0169-1317(96)90003-4.

[53] F. Zunino, Y. Dhandapani, M. Ben Haha, J. Skibsted, S. Joseph, S. Krishnan, A. Parashar, M.C.G. Juenger, T. Hanein, S.A. Bernal, K.L. Scrivener, F. Avet, Hydration and mixture design

of calcined clay blended cements: review by the RILEM TC 282-CCL, Mater Struct 55 (2022). https://doi.org/10.1617/s11527-022-02060-1.

[54] J. Gardolinski, Interlayer grafting and delamination of Kaolinite, 2005. https://www.researchgate.net/publication/321907277.

[55] M. Antoni, Investigation of cement substitution by blends of calcined clays and limestone, EPFL, 2013.

[56] I. Jefferson, I. Smalley, Fundamentals of Soil Behaviour, Geoderma 63 (1994) 310–312. https://doi.org/10.1016/0016-7061(94)90074-4.

[57] T. Hanein, K.-C. Thienel, F. Zunino, A.T.M. Marsh, M. Maier, B. Wang, M. Canut, M.C.G. Juenger, M. Ben Haha, F. Avet, A. Parashar, L.A. Al-Jaberi, R.S. Almenares-Reyes, A. Alujas-Diaz, K.L. Scrivener, S.A. Bernal, J.L. Provis, T. Sui, S. Bishnoi, F. Martirena-Hernández, Clay calcination technology: state-of-the-art review by the RILEM TC 282-CCL, Mater Struct 55 (2022). https://doi.org/10.1617/s11527-021-01807-6.

[58] R.C. Mielenz, Thermogravimetric Analysis of Clay and Clay-Like Minerals, Clays Clay Miner 2 (1953) 285–314. https://doi.org/10.1346/CCMN.1953.0020124.

[59] Y. Dhandapani, S. Joseph, D.A. Geddes, Z. Zhao, P. Boustingorry, S. Bishnoi, M. Vieira, F. Martirena, A. Castel, F. Kanavaris, K.A. Riding, Fresh properties of concrete containing calcined clays: a review by RILEM TC-282 CCL, Mater Struct 55 (2022). https://doi.org/10.1617/s11527-022-01971-3.

[60] A. Hajimohammadi, J.S.J. van Deventer, Dissolution behaviour of source materials for synthesis of geopolymer binders: A kinetic approach, Int J Miner Process 153 (2016) 80–86. https://doi.org/10.1016/j.minpro.2016.05.014.

[61] M. Cyr, Contribution à la characterisation des fines minérales et à compréhension de leur rôle joué dans le comportement rhéologique des matrices cimentaires, Institut national des sciences appliquées de Toulouse, 1999.

[62] X. Li, R. Snellings, M. Antoni, N.M. Alderete, M. Ben Haha, S. Bishnoi, Ö. Cizer, M. Cyr, K. De Weerdt, Y. Dhandapani, J. Duchesne, J. Haufe, D. Hooton, M. Juenger, S. Kamali-Bernard, S. Kramar, M. Marroccoli, A.M. Joseph, A. Parashar, C. Patapy, J.L. Provis, S. Sabio, M.

Santhanam, L. Steger, T. Sui, A. Telesca, A. Vollpracht, F. Vargas, B. Walkley, F. Winnefeld, G. Ye, M. Zajac, S. Zhang, K.L. Scrivener, Reactivity tests for supplementary cementitious materials: RILEM TC 267-TRM phase 1, Mater Struct 51 (2018) 1–14. https://doi.org/10.1617/s11527-018-1269-x.

[63] C. Ruiz-Santaquiteria, A. Fernández-Jiménez, A. Palomo, Quantitative Determination of Reactive SiO2 and Al2O3 in Aluminosilicate Materials, in: ICCC, Madrid, 2011.

[64] A. Sanalkumar, U. Krishnan, M. Lahoti, E.-H. Yang, Investigating the potential reactivity of fly ash for geopolymerization, Constr Build Mater 225 (2019) 283–291. https://doi.org/10.1016/j.conbuildmat.2019.07.140.

[65] A. Buchwald, M. Hohmann, K. Posern, E. Brendler, The suitability of thermally activated illite/smectite clay as raw material for geopolymer binders, Appl Clay Sci 46 (2009) 300–304. https://doi.org/10.1016/j.clay.2009.08.026.

[66] H. Xu, J.S.J. Van Deventer, The geopolymerisation of alumino-silicate minerals, Int J Miner Process 59 (2000) 247–266. https://doi.org/10.1016/S0301-7516(99)00074-5.

[67] L.H. Buruberri, D.M. Tobaldi, A. Caetano, M.P. Seabra, J.A. Labrincha, Evaluation of reactive Si and Al amounts in various geopolymer precursors by a simple method, Journal of Building Engineering 22 (2019) 48–55. https://doi.org/10.1016/j.jobe.2018.11.017.

[68] A. Fernández-Jimenez, A.G. De La Torre, A. Palomo, G. López-Olmo, M.M. Alonso, M.A.G. Aranda, Quantitative determination of phases in the alkali activation of fly ash. Part I. Potential ash reactivity, Fuel 85 (2006) 625–634. https://doi.org/10.1016/j.fuel.2005.08.014.

[69] X. Gao, Q.L. Yu, H.J.H. Brouwers, Apply 29Si, 27Al MAS NMR and selective dissolution in identifying the reaction degree of alkali activated slag-fly ash composites, Ceram Int 43 (2017) 12408–12419. https://doi.org/10.1016/j.ceramint.2017.06.108.

[70] O. Vogt, N. Ukrainczyk, C. Ballschmiede, E. Koenders, Reactivity and microstructure of metakaolin based geopolymers: Effect of fly Ash and liquid/solid contents, Materials 12 (2019) 1–21. https://doi.org/10.3390/ma12213485.

[71] S. Donatello, M. Tyrer, C.R. Cheeseman, Comparison of test methods to assess pozzolanic activity, Cem Concr Compos 32 (2010) 121–127. https://doi.org/10.1016/J.CEMCONCOMP.2009.10.008.

[72] A. Tironi, M.A. Trezza, A.N. Scian, E.F. Irassar, Assessment of pozzolanic activity of different calcined clays, Cem Concr Compos 37 (2013) 319–327. https://doi.org/10.1016/j.cemconcomp.2013.01.002.

[73] F. Avet, R. Snellings, A. Alujas Diaz, M. Ben Haha, K. Scrivener, Development of a new rapid, relevant and reliable (R3) test method to evaluate the pozzolanic reactivity of calcined kaolinitic clays, Cem Concr Res 85 (2016) 1–11. https://doi.org/10.1016/J.CEMCONRES.2016.02.015.

[74] ASTM C1897, Standard Test Methods for Measuring the Reactivity of Supplementary Cementitious Materials by Isothermal Calorimetry and Bound Water Measurements, ASTM International, West Conshohocken, PA 04 (2020) 7–11. https://doi.org/10.1520/C1897-20.2.

[75] A. Hajimohammadi, J.L. Provis, J.S.J. Van Deventer, Effect of alumina release rate on the mechanism of geopolymer gel formation, Chemistry of Materials 22 (2010) 5199–5208. https://doi.org/10.1021/cm101151n.

[76] Y. Ma, C. Shi, L. Lei, S. Sha, B. Zhou, Y. Liu, Y. Xiao, Research progress on polycarboxylate based superplasticizers with tolerance to clays - A review, Constr Build Mater 255 (2020) 119386. https://doi.org/10.1016/J.CONBUILDMAT.2020.119386.

[77] S. Chen, S. Ruan, Q. Zeng, Y. Liu, M. Zhang, Y. Tian, D. Yan, Pore structure of geopolymer materials and its correlations to engineering properties: A review, Constr Build Mater 328 (2022) 127064. https://doi.org/10.1016/J.CONBUILDMAT.2022.127064.

[78] J.L. Provis, A. Fernández-Jiménez, E. Kamseu, C. Leonelli, A. Palomo, Binder chemistry – Low-calcium alkali-activated materials, in: RILEM State-of-the-Art Reports, 2014: pp. 93–123. https://doi.org/10.1007/978-94-007-7672-2_4.

[79] P. Duxson, S.W. Mallicoat, G.C. Lukey, W.M. Kriven, J.S.J. van Deventer, The effect of alkali and Si/Al ratio on the development of mechanical properties of metakaolin-based

geopolymers, Colloids Surf A Physicochem Eng Asp 292 (2007) 8–20. https://doi.org/10.1016/j.colsurfa.2006.05.044.

[80] Q. Wan, F. Rao, S. Song, R.E. García, R.M. Estrella, C.L. Patiño, Y. Zhang, Geopolymerization reaction, microstructure and simulation of metakaolin-based geopolymers at extended Si/Al ratios, Cem Concr Compos 79 (2017) 45–52. https://doi.org/10.1016/j.cemconcomp.2017.01.014.

[81] K. Yang, C.E. White, Multiscale pore structure determination of cement paste via simulation and experiment: The case of alkali-activated metakaolin, Cem Concr Res 137 (2020). https://doi.org/10.1016/j.cemconres.2020.106212.

[82] M. Shariati, A. Shariati, N.T. Trung, P. Shoaei, F. Ameri, N. Bahrami, S.N. Zamanabadi, Alkali-activated slag (AAS) paste: Correlation between durability and microstructural characteristics, Constr Build Mater 267 (2021) 120886. https://doi.org/10.1016/j.conbuildmat.2020.120886.

[83] B.S. Gebregziabiher, R.J. Thomas, S. Peethamparan, Temperature and activator effect on early-age reaction kinetics of alkali-activated slag binders, Constr Build Mater 113 (2016) 783–793. https://doi.org/10.1016/j.conbuildmat.2016.03.098.

[84] P. Rovnaník, Effect of curing temperature on the development of hard structure of metakaolin-based geopolymer, Constr Build Mater 24 (2010) 1176–1183. https://doi.org/10.1016/j.conbuildmat.2009.12.023.

[85] J.L. Provis, Geopolymers and other alkali activated materials: Why, how, and what?, Materials and Structures/Materiaux et Constructions 47 (2014) 11–25. https://doi.org/10.1617/s11527-013-0211-5.

[86] F.G.M. Aredes, T.M.B. Campos, J.P.B. Machado, K.K. Sakane, G.P. Thim, D.D. Brunelli, Effect of cure temperature on the formation of metakaolinite-based geopolymer, Ceram Int 41 (2015) 7302–7311. https://doi.org/10.1016/j.ceramint.2015.02.022.

[87] B. Mo, H. Zhu, X. Cui, Y. He, S. Gong, Effect of curing temperature on geopolymerization of metakaolin-based geopolymers, Appl Clay Sci 99 (2014) 144–148. https://doi.org/10.1016/j.clay.2014.06.024.

[88] F. Zunino, K. Scrivener, The reaction between metakaolin and limestone and its effect in porosity refinement and mechanical properties, Cem Concr Res 140 (2021) 106307. https://doi.org/10.1016/j.cemconres.2020.106307.

[89] Y. Dhandapani, M. Santhanam, Assessment of pore structure evolution in the limestone calcined clay cementitious system and its implications for performance, Cem Concr Compos 84 (2017) 36–47. https://doi.org/10.1016/J.CEMCONCOMP.2017.08.012.

[90] F. Avet, E. Boehm-Courjault, K. Scrivener, Investigation of C-A-S-H composition, morphology and density in Limestone Calcined Clay Cement (LC3), Cem Concr Res 115 (2019) 70–79. https://doi.org/10.1016/j.cemconres.2018.10.011.

[91] Y. Briki, F. Avet, M. Zajac, P. Bowen, M. Ben Haha, K. Scrivener, Understanding of the factors slowing down metakaolin reaction in limestone calcined clay cement (LC3) at late ages, Cem Concr Res 146 (2021) 106477. https://doi.org/10.1016/J.CEMCONRES.2021.106477.

[92] F. Avet, K. Scrivener, Investigation of the calcined kaolinite content on the hydration of Limestone Calcined Clay Cement (LC3), Cem Concr Res 107 (2018) 124–135. https://doi.org/10.1016/j.cemconres.2018.02.016.

[93] F. Zunino, K. Scrivener, Microstructural developments of limestone calcined clay cement (LC3) pastes after long-term (3 years) hydration, Cem Concr Res 153 (2022) 106693. https://doi.org/10.1016/J.CEMCONRES.2021.106693.

[94] R. Snellings, Solution-Controlled Dissolution of Supplementary Cementitious Material Glasses at pH 13: The Effect of Solution Composition on Glass Dissolution Rates, Journal of the American Ceramic Society 96 (2013) 2467–2475. https://doi.org/10.1111/jace.12480.

[95] L. Nicoleau, E. Schreiner, A. Nonat, Ion-specific effects influencing the dissolution of tricalcium silicate, Cem Concr Res 59 (2014) 118–138. https://doi.org/10.1016/j.cemconres.2014.02.006.

Chapter 3 Preliminary investigation

This chapter is based on the published conference paper *Optimization of Hybrid Portland Cement – Metakaolin Binders*[3], presented in the 16th International Congress on the Chemistry of Cement (ICCC) 2023 and published here with the written permission of the ICCC Permanent Secretariat. I would like to acknowledge the contribution of co-authors Professor Leandro Sanchez and Professor Susan Bernal in the data analysis and revision process of this paper. Further discussion and data treatment on some of the results presented here can be found in Chapter 6.

3.1 Abstract

The urgent need to develop sustainable and durable alternatives to Portland cement (PC) concrete has been a major drive for research on alkali-activated materials (AAMs). Amongst AAMs, hybrid alkaline binders appear to be the most industry-ready option, as their manufacturing process is similar to that of PC binders, they use milder doses of alkali-activators compared with other AAMs, and materials produced with those binders can develop excellent mechanical properties and high chemical resistance. However, the added complexity of these binders raises the need for further research to better understand and optimize them on a micro- to macroscale level. This study focuses on the optimization of hybrid alkali-activated metakaolin (MK) paste with varying PC content. The effect of the activator dose, in this case a sodium sulfate (NS) solution, was also evaluated. On a meso-to macroscale, the setting time and compressive strength of the samples were appraised, while conducting XRD and TGA on the hydrated cement pastes allowed for a microscale assessment of the chemical features. This study has shown that setting time may be decreased with NS addition. Improvements in early mechanical performance are also found at higher levels of PC substitution and with moderate amounts of activator, as shown by the strength of the 30%PC-5NS and 50%PC-10NS mixes surpassing that of the 50PC-0NS mix. These findings correlated well with microscale results which indicated greater extent of reaction from the raw precursors in the NS-activated mixes.

KEYWORDS: *Hybrid alkali-activated binders, calcined clay, multi-scale testing*

[3] C. Monin, L.F.M. Sanchez, S.A. Bernal, Optimization of Hybrid Portland Cement – Metakaolin Binders, in: 16th International Congress on the Chemistry of Cement 2023 (ICCC2023), Thailand Concrete Association, Bangkok, 2023: pp. 286–289.

3.2 Introduction

The growing cement consumption worldwide is causing the construction industry to face crucial sustainability challenges. Finding sustainable and economical alternatives to traditional PC-based concrete has thus been a major focus of the scientific community in recent years and has driven the research in alkali-activated materials (AAMs) [1,2]. AAMs are a class of binders comprising amorphous aluminosilicate precursors activated with an alkaline activator solution such as sodium silicate, sodium hydroxide, or sodium sulfate (NS). These materials are promising and more sustainable alternatives to traditional concrete materials. However, their most common activator, sodium silicate, is unsustainable with respect to many non-carbon environmental categories [3]. Furthermore, both sodium silicate and sodium hydroxide are expensive and highly corrosive, which are major roadblocks on the path to large-scale industrialization of AAMs. Near-neutral salts, such as NS, have emerged as sustainable, user-friendly, and cost-effective alternatives to traditional activators [4]. Research on NS-activated binders remain scarce due to the delayed setting and strength gain that were observed for these materials [5]. The addition of PC clinker has however been found to improve the performance of NS-activated AAMs [6,7]. To better understand the behaviour of this class of binders, this study will discuss the setting time, mechanical performance, and microscopic chemical features (i.e., XRD and TGA) of NS-activated MK-PC paste blends.

3.3 Experimental methodology

3.3.1 Materials and sample preparation

In this study, different blends of hybrid NS activated MK–PC paste samples were manufactured. The chemical composition of the raw MK and PC precursors was evaluated by X-ray fluorescence (XRF) and can be found in Table 3-1. The mix-design follows a 2-level factorial design. The water/binder ratio and binder (MK+PC) content are kept constant for all mixes and their value are fixed at 0.55 and 480 kg/m^3 respectively, while PC content is varied between 10 and 50 wt.% and NS content between 0 to 5 wt.% of total binder weight. NS solutions were made by magnetic stirring of the dry anhydrous NS powder in water at elevated temperature (40° – 80°C) until complete dissolution. The solutions were then left at room temperature to cool down. Prior to batching, the dry precursors were weighted and blended to ensure proper distribution of the MK

and PC particles in the cast samples. The solutions were then incorporated gradually to the dry ingredients. After 5 minutes of mixing, the paste samples were cast in 50 mm x 100 mm molds for 24 hours, until demolding. They were then sealed to prevent carbonation and kept at room temperature (21 °C) until testing.

Table 3-1 Chemical composition of raw materials, determined by X-ray fluorescence (XRF)

Material	**CaO**	**SiO_2**	**Al_2O_3**	**Fe_2O_3**	**MgO**	**SO_3**	**K_2O**	**Na_2O**	**Others**
Metakaolin	0.385	62.5	29.8	1.23	0.42	-	1.75	0.18	0.77
Portland cement	61.5	19.4	4.9	3.7	2.4	3.9	0.95	-	3.25

3.3.2 Tests conducted

The setting time of the samples was determined following ASTM C191 [8] using a manual Vicat needle apparatus. In between measurements, samples were kept under a wet cloth to simulate high relative humidity conditions. Samples at 1 and 6 days of curing were tested in compression after being ground at both ends. 3 samples of each mix were tested each time and the test followed the procedure of ASTM C39 with 50 x 100 mm cylinders and an applied load of 0.25 MPa/s [9]. At 6 days of curing, a sample from each mix design was crushed in large chunks and their hydration process was arrested with isopropanol. Two filtrations with ethanol were then conducted, 10 minutes apart. The pieces were then dried at 60 °C for 20 minutes and ground in an agate crucible. Before testing, the dried powders were kept in a desiccator to prevent carbonation. Powder X-ray diffraction (XRD) was performed on powdered samples using the Rigaku Ultima IV diffractometer equipped with a copper source and a diffracted beam monochromator. The samples were scanned over a 2θ range between 5º and 50ºC. Thermogravimetric analysis (TGA) was conducted on powdered samples using the Q5000 TGA instrument at an ending temperature of 1000°C and ramping rate of 20°C/min.

3.4 Results and discussion

3.4.1 Meso to macroscale analysis

The results of Vicat needle testing illustrated in *Figure 3-1* show that for mixtures with low PC content (10PC-0NS and 10PC-5NS), the final setting time was slower for the mix with 5NS. This result is surprising, as the incorporation of NS would typically raise the alkalinity of the fresh paste, which in turn would accelerate the reaction kinetics of cement [10]. On the other hand, for mixtures with high PC content (50PC-0NS and 50PC-5NS), the effect of NS was as anticipated, with the high NS content mix setting faster than its low NS counterpart. Regarding the impact of PC content, the 50PC mixes took the longest to set, but it is unlikely to be the direct consequence of their higher PC content. Higher calcium AAMs tend to have a shorter setting time, which would explain the faster setting of mix 30PC-5NS in comparison with mixes 10PC-5NS and 10PC-0NS. The longer setting of 50PC-0NS and 50-5NS might be more correlated with the w/b of these mixes. Because the high surface area and plate-like shape of MK significantly reduces the workability of high MK content mixes, the w/b ratio for all mixtures was based on minimal workability of the 10PC mixes (i.e., 10PC-5NS and 10PC-0NS). For the two 50PC mixes, the high w/b chosen led to a very flowable mix which may have artificially prolonged the setting of these mixes.

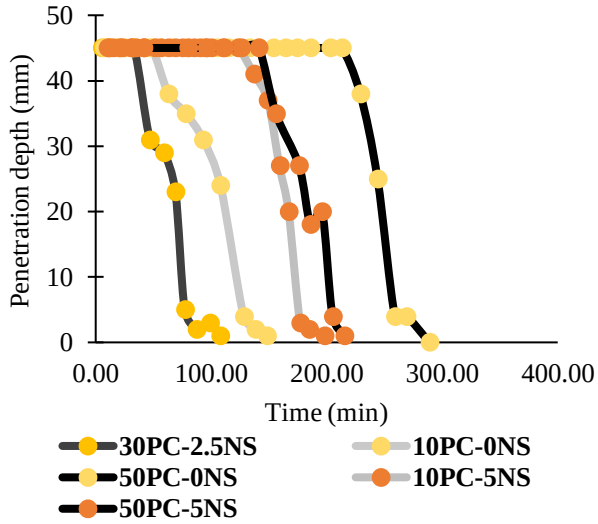

Figure 3-1. Vicat needle testing measurements

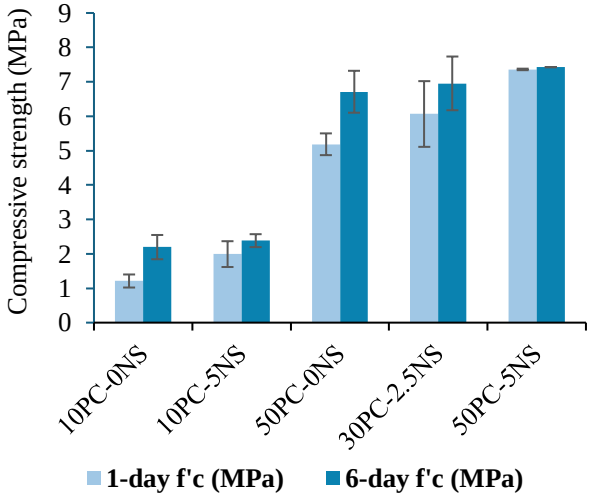

Figure 3-2. Compressive strength at 1 and 6 days

The compressive strength of the mixes at 1 and 6 days is shown in *Figure 3-2*. From this figure, it is possible to see that higher PC and higher NS contents generally provided higher strength to the samples. At low PC, the increase of strength due to NS was more significant after 1 day than at 6

days. Similar results are found for mixes 50PC-5NS and 50PC-0NS: strength is 42% higher for the 5NS mix after 1-day curing, and only 11% higher after 6 days. Those results may indicate that the presence of NS accelerates the early reaction kinetics but may not have a significant impact on strength at later ages. It is also interesting to observe that the 30PC-2.5NS mix performed similarly to the 50PC-0NS mixture, especially after 1 day of curing. This might indicate that the addition of NS could prevent the loss in mechanical properties typically associated with higher levels of PC replacement. Nonetheless, these preliminary findings are drawn based on early age results, with cement paste samples of less than a week's age. Longer testing duration are therefore needed to confirm this conclusion. Finally, it is important to note that the strength of all cement pastes remained quite low. This could be related to the natural tendency of metakaolin particles to agglomerate, thus hindering the dispersion of the raw material particles during mixing. It is also possible that the Portland cement clinker phases content could be optimized for use of this cement in hybrid AAMs. Therefore, the use of superplasticizers suited to calcined clays and the conduction of additional testing with various Portland cements may be useful in investigating further the low strength of the mixes and how to address it.

3.4.2 Microscale analysis

The diffraction patterns of all mixtures illustrated in *Figure 3-3* reveals that both PC and NS content had a strong impact on the types of crystalline phases found in the binders.

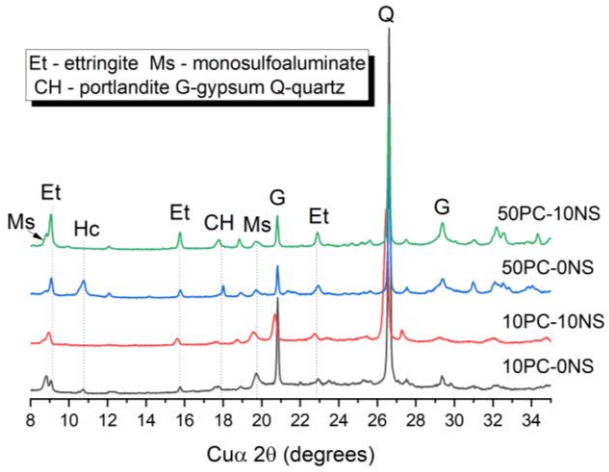

Figure 3-3 XRD patterns of 6-days samples

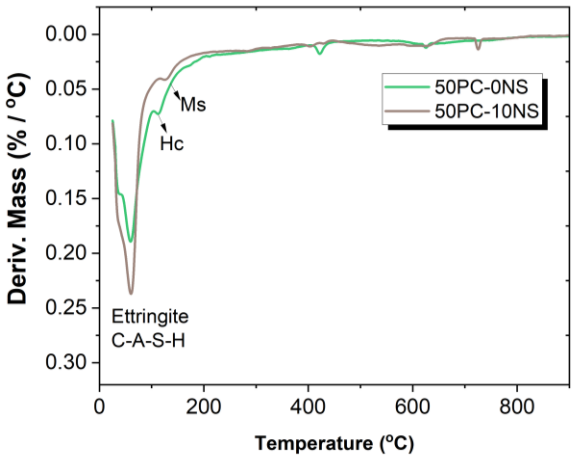

Figure 3-4 TGA of the 6-days 50PC samples

Hemicarboaluminate (HC) appears to be only forming in samples with no NS and is barely distinguishable at low PC (10PC-0NS). Low PC and low NS conditions seemed to favour the

formation of monosulfoaluminate (Mc), while ettringite (E) seemed to be preferably formed at high PC and high NS conditions. A small peak due to portlandite (CH) appears in mixes with high PC content only. The presence of a strong quartz peak in all mixes is found to be due to the raw precursors. Finally, all mixes showed traces of gypsum, except for the one with low PC and high NS (10PC-5NS).

Figure 3-4 illustrates TGA results on the two mixes with the highest PC content (i.e., 50PC-5NS and 50PC-0NS). It is possible to observe that the thermal decomposition peaks vary in location and intensity. The first peak is observed in both samples from 55°C to 200°C. This peak is likely associated with the decomposition of evaporable water and C-S-H, as well as the dehydration of ettringite [11,12]. The difference in intensity of this peak between the samples could be explained by a higher degree of dissolution of the precursors in the 5NS mix, and because of the greater degree of ettringite formation in sulfate-activated binders. The former hypothesis would correlate with the compressive strength and setting time results reported for the two mixes. Indeed, faster reaction kinetics and improved dissolution of the PC and MK may have occurred due to the addition of NS. The presence of a peak around 450°C for the 50PC-0NS paste only is further supporting this hypothesis. This peak indicates the decomposition of portlandite, but it is not observed in 50PC-5NS due to the consumption of the mineral by MK [13]. This suggests that more MK reacted in the sulfate-activated mix.

3.5 Conclusions

In this work, the properties of hybrid NS-activated MK-PC have been investigated on a micro to macroscale. The fresh state testing revealed that NS could accelerate the setting of cement paste with at least 30% of PC but may slow setting at low PC contents (i.e., 10%PC). Furthermore, at the same level of PC content, the addition of NS benefited the strength of the samples. For the intermediate mix 30PC-2.5NS, the strength at 1 and 6 days was similar to that of the 50PC-0NS mix, thereby suggesting that higher levels of cement replacement could potentially be achieved with NS alkali-activation. This finding was correlated by the conduction of chemical analyses which revealed greater amounts of reaction products in NS-activated mixes.

Finally, based on the overall low strength results obtained for all hybrid AAMs, it is suggested that further testing is conducted with a wide range of Portland cements and using superplasticizer to

ensure proper dispersion. The addition of sample replicates for Vicat needle testing and the use of a central composite design (i.e., a factorial DOE with axial points) are also suggested for future work. Replicate measurements of the setting time test would help confirm the trends shown in this research. Furthermore, a central composite design would provide additional data points that may be used to plot the response surface of strength as a function of PC and NS contents.

3.6 References

[1] P. Duxson, A. Fernández-Jiménez, J.L. Provis, G.C. Lukey, A. Palomo, J.S.J. Van Deventer, Geopolymer technology: The current state of the art, J Mater Sci 42 (2007) 2917–2933. https://doi.org/10.1007/s10853-006-0637-z.

[2] Y. Wu, B. Lu, T. Bai, H. Wang, F. Du, Y. Zhang, L. Cai, C. Jiang, W. Wang, Geopolymer, green alkali activated cementitious material: Synthesis, applications and challenges, Constr Build Mater 224 (2019) 930–949. https://doi.org/10.1016/j.conbuildmat.2019.07.112.

[3] G. Habert, Environmental impact of Portland cement production, Eco-Efficient Concrete (2013) 3–25. https://doi.org/10.1533/9780857098993.1.3.

[4] S.A. Bernal, Advances in near-neutral salts activation of blast furnace slags, RILEM Technical Letters 1 (2016) 39. https://doi.org/10.21809/rilemtechlett.v1.8.

[5] S.A. Bernal, J.L. Provis, A. Fernández-Jiménez, P. V. Krivenko, E. Kavalerova, M. Palacios, C. Shi, Binder chemistry - High-calcium alkali-activated materials, in: RILEM State-of-the-Art Reports, 2014: pp. 59–91. https://doi.org/10.1007/978-94-007-7672-2_3.

[6] M.A. Nawaz, B. Ali, L.A. Qureshi, H.M. Usman Aslam, I. Hussain, B. Masood, S.S. Raza, Effect of sulfate activator on mechanical and durability properties of concrete incorporating low calcium fly ash, Case Studies in Construction Materials 13 (2020). https://doi.org/10.1016/j.cscm.2020.e00407.

[7] A. Dakhane, S. Tweedley, S. Kailas, R. Marzke, N. Neithalath, Mechanical and microstructural characterization of alkali sulfate activated high volume fly ash binders, Mater Des 122 (2017) 236–246. https://doi.org/10.1016/j.matdes.2017.03.021.

[8] ASTM, ASTM C191 − 21 Standard Test Methods for Time of Setting of Hydraulic Cement by Vicat Needle, ASTM International (2021). https://doi.org/10.1520/C0191-21.

[9] ASTM, ASTM C39/C39M - 21 Standard Test Method for Compressive Strength of Cylindrical Concrete Specimens, ASTM International (2021). https://doi.org/10.1520/C0039_C0039M-21.

[10] B. Mota, T. Matschei, K. Scrivener, Impact of NaOH and Na2SO4 on the kinetics and microstructural development of white cement hydration, Cem Concr Res 108 (2018) 172–185. https://doi.org/10.1016/j.cemconres.2018.03.017.

[11] R.J. Myers, E. L'hôpital, J.L. Provis, B. Lothenbach, Effect of temperature and aluminium on calcium (alumino)silicate hydrate chemistry under equilibrium conditions, (2014). https://doi.org/10.1016/j.cemconres.2014.10.015.

[12] Christopher Hall, Paul Barnes, Andrew D. Billimore, Andrew C. Jupeb, Xavier Turrillasb, Thermal decomposition of ettringite Ca, [Al(OH)6]2(S04)3 26H2, Journal of Chemistry Society 92 (1996). https://pubs.rsc.org/en/content/articlepdf/1996/ft/ft9969202125 (accessed February 26, 2023).

[13] M. Antoni, J. Rossen, F. Martirena, K. Scrivener, Cement substitution by a combination of metakaolin and limestone, (2012). https://doi.org/10.1016/j.cemconres.2012.09.006.

Chapter 4 Multiscale statistical investigation of hybrid metakaolin alkali-activated pastes

4.1 Introduction

Sustainability concerns over traditional Portland cement (PC) production are at the center of a number of modern initiatives in the world of cement and concrete. Clinker manufacturing for PC production is the leading cause for the release of large amounts of CO_2. This is due to the high temperature required for calcination (i.e., over 1300°C) and the decomposition of calcium carbonate ($CaCO_3$). PC is therefore the most pollutant component in concrete, and one of the most direct approaches to address this problem is therefore to replace it in concrete production by alternative binders or partial replacements referred to as supplementary cementitious materials (SCMs). The amount of PC that can be replaced by a SCMs is dependent on the type of SCM used, and it is often limited by the reduction in the compressive strength development that can be achieved at high replacement levels. To increase early strength development, the addition of an alkaline activator has been explored. The principle is the central idea behind alkali-activated materials (AAMs), which are a class of alternative binders formed through the reaction of aluminosilicate precursors[4] with alkaline solutions such as sodium silicate, sodium hydroxide, or sodium sulfate (NS). Decades of work have focused on mostly low calcium and high calcium AAMs, while blended alkali-activated binders (i.e., blend of low + high calcium aluminosilicate precursors) and hybrid alkali-activated binders (i.e., 20-30% PC + reactive aluminosilicate) remain less understood. These binders have been regarded by many authors as the most industry-ready and promising alkali-activated binder type [1–4].

Hybrid AAMs are of particular interest, since they may be produced at milder alkalinity conditions to those required without PC. This is because PC acts as another source of alkalinity, and therefore, lower the need for highly alkaline activators. The main benefit of this technology is the extremely high PC replacement levels that can be achieved, as well as the potential to use near-neutral salts as activators in place of sodium silicate and sodium hydroxide. Indeed, contrary to these activators which are largely unsustainable [5], costly, and highly corrosive, NS is an eco-friendly, user-

[4] SCMs are part of the group of aluminosilicate precursors, but AAMs may also be formed with aluminosilicate waste materials that would not meet the criteria for SCMs in terms of reactivity or impurities content.

friendly, and cost-effective alternative [6]. These advantages of NS have raised interest in the scientific community, and specifically for accelerating Portland cement hydration in traditional cements [7,8], or for reacting with various SCMs in AAMs [6,9,10]. In non-hybrid AAMs however, research on NS-activated binders remained scarce due to the delayed setting and strength gain that were observed for these materials compared to other activators [11]. Nevertheless, since the addition of PC clinker has been found to significantly improve the performance of NS-activated AAMs [12–14], the fresh and hardened state performance of NS-activated hybrids requires further investigation to help understand whether these behaviors would still occur.

The impact of NS on alkali-activated and Portland cement binders has been studied by a few authors in recent years [6,8,10,11,15–20]. Bernal *et al.* found that hybrid AAMs made with metakaolin and PC could be successfully activated with NS, and reach high levels of PC replacement without losses in performance [11]. Based on their NMR testing, these authors observed that the formation of ettringite was enhanced at high levels of NS addition, which inhibited the formation of AFm phases. Millán-Corrales *et al.* [15] investigated the behavior of NS-activated fly ash hybrid AAMs that incorporated 10% of limestone filler and found that regardless of limestone addition, the presence of 5% of sodium sulfate reduced setting time and improved compressive strength at early and later ages. They also observed that the incorporation of limestone did not lead to changes in the chemical composition of the reaction products. However, they found that the inclusion of limestone filler indeed led to an acceleration of the kinetics and a densification of the pore structure. These findings were supported by the work of Marsh *et al.* on NS-activated limestone-containing slag AAMs [20].

Interestingly, the work of Fu *et al.* on NS addition to slag AAMs showed that while NS did improve early age strength, comparable strength was achieved at 7 days across mixes with varying NS content, and 28-days strength was highest for the mix without added NS [10]. In a subsequent microstructural study [16], these authors correlated these findings to the lower capillary pore volume and pore size prior to 3 days for samples with added NS compared to those without, and the higher capillary pore volume and pore size from 3 days onwards. Their analysis also showed that this behavior was due to the early refinement of porosity induced by NS addition, which consequently caused the reduction in later age strengths. This finding aligns with what was found through the work of Mota *et al.* on the impact of sodium hydroxide and sodium sulfate on white

cement [8]. In their study, Mota *et al.* showed that the degree of hydration of a pure Portland cement paste was affected by the addition of alkalis, and that a higher degree of hydration was reached at early age for alkali-boosted cements compared to cements without added alkalis. Nonetheless, they found that a lower degree of hydration was reached at later ages for the same alkali-boosted cements. Sodium sulfate appeared less detrimental to later age strength than sodium hydroxide due to its promotion of ettringite formation, a high-volume hydrate which decreased capillary porosity. Recently, the study published by Zhou *et al.* on the impact of inorganic salts (including NS) on limestone calcined clay cements (LC_3) showed that the behavior observed in slag AAMs by Fu *et al*. [10,16] and the one observed in pure Portland cement by Mota *et al*. [8] may also occur in these cements. Indeed, Zhou *et al.* also observed an acceleration of kinetics and improvement of early strength induced by NS addition and a detrimental impact on strength at later ages. These authors linked this behavior to the excessive formation of AFm phases, which temporarily enhanced compressive strength, but ultimately led to early porosity refinement, causing the lack of pozzolanic reaction at later ages.

On the other hand, it was discussed previously that Millán-Corrales *et al*. [15] had found improved mechanical performance at both early and later ages due to the addition of NS. Moreover, other authors found that the performance of hybrid AAMs could be improved at later ages by alkali addition [7,8,10,16,21]. The effect of NS addition to hybrid binders thus remains highly debated amongst authors and few studies have yet been performed on NS-activated metakaolin hybrid AAMs. In this context, this study strives to shed light on the fresh and hardened state properties of NS-activated hybrid binders by use of multi-scale techniques and statistical design of experiment (DOE) methods. It is necessary to investigate whether NS addition will impair the long-term strength of hybrid binders, and if so, to which extent. The factors which may be impacting the synergetic or antagonistic behavior of NS at different ages will be studied in this work by evaluating the fresh and hardened state performance of different binder compositions. Statistical analysis of the macroscale results will be conducted using ANOVA analysis, as well as main effect, interaction, contour, and response surface methodology (RSM) plots. Microscale testing will also be conducted to provide additional insight on the macroscale properties measured.

4.2 Scope of the work

The binders studied in this study are hybrid sodium sulfate-activated metakaolin (MK)-limestone (LS)-PC AAMs. The binder compositions were optimised based on the statistical analysis of the results of the preliminary investigation (see Appendix A – Factorial design rationale). The complexity of the ternary cementitious binders studied, and the novelty of the work raised the need to approach the goals of this research sequentially. Therefore, this study was divided into two sets of experiments, illustrated in the visual below. Throughout this work, the term "early age properties" is used to refer to the cement pastes' properties measured at 7 days and earlier, while the term "later age properties" refers to those measured after 7 days.

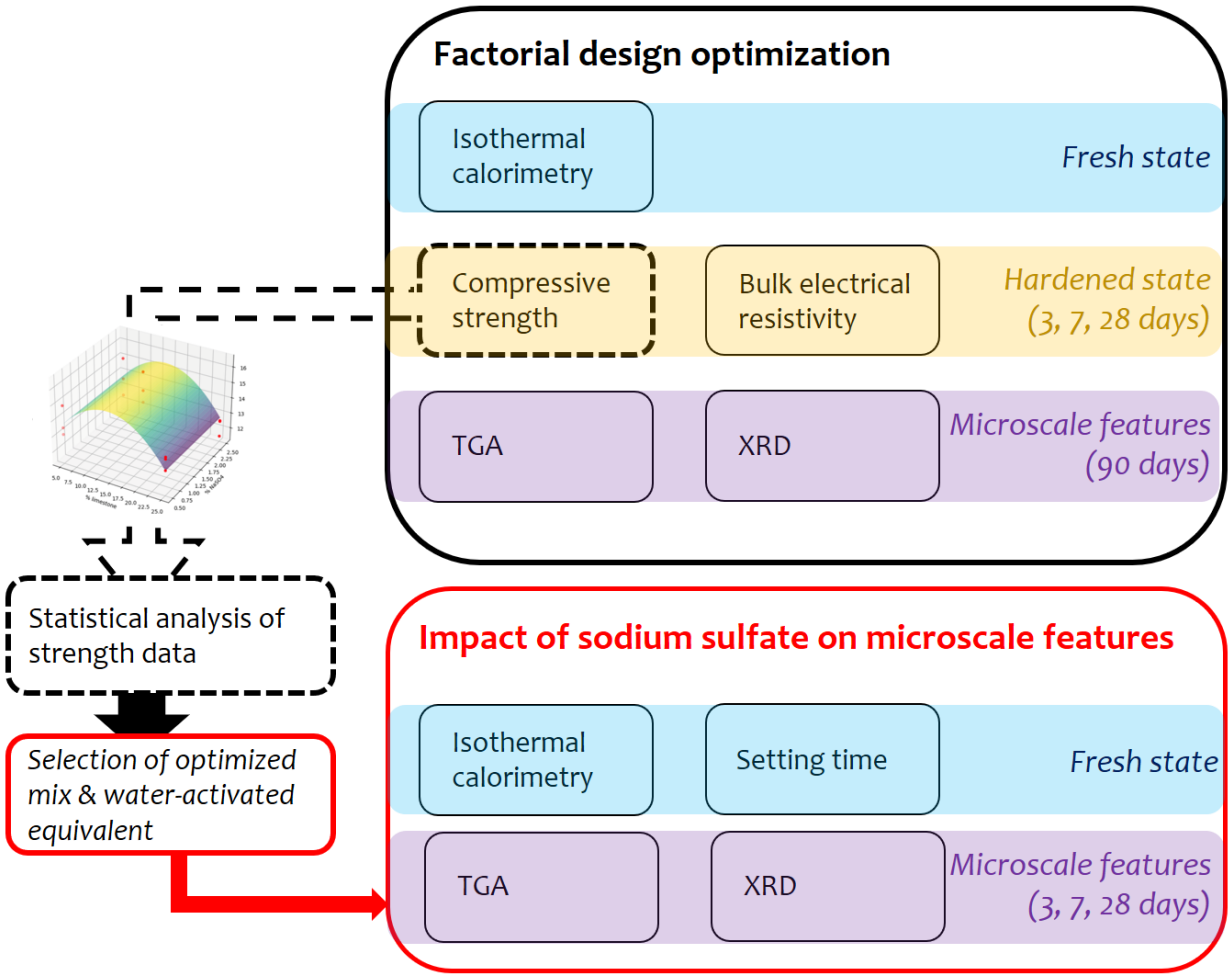

Figure 4-1 Flowchart summarizing the scope of the study

The factorial optimization experiment is presented in section 4.4, while the impact of sodium sulfate experiment is presented in section 4.5. In these sections, the results and discussion are

presented together for clarity purposes. Finally, section 4.6 contains a framework for the mix-design of hybrid AAMs.

4.2.1 Factorial optimization of ternary hybrid binders

First, this research explores the impact of binder composition at the macroscale and microscale levels applying a factorial design of experiment (DOE) optimization. The proportion of limestone and the amount of added sodium sulfate were determined based on the factorial design shown in *Figure 4-2*. Isothermal calorimetry is performed on the hybrid binders to evaluate the early reaction kinetics of all binders, while compressive strength and bulk resistivity testing are conducted at 3, 7 and 28 days to assess the evolution of mechanical properties and infer the microstructure (porosity and pore connectivity). A statistical analysis of the strength results is performed and used as a basis for the choice of optimal binders for the second set of experiment. Fresh and hardened state performance are also correlated to microscale properties by testing thermogravimetric analysis (TGA) and X-Ray diffraction (XRD) after 90 days for the factorial points of the mix-design. The testing matrix of this first part can be found in Table 4-1.

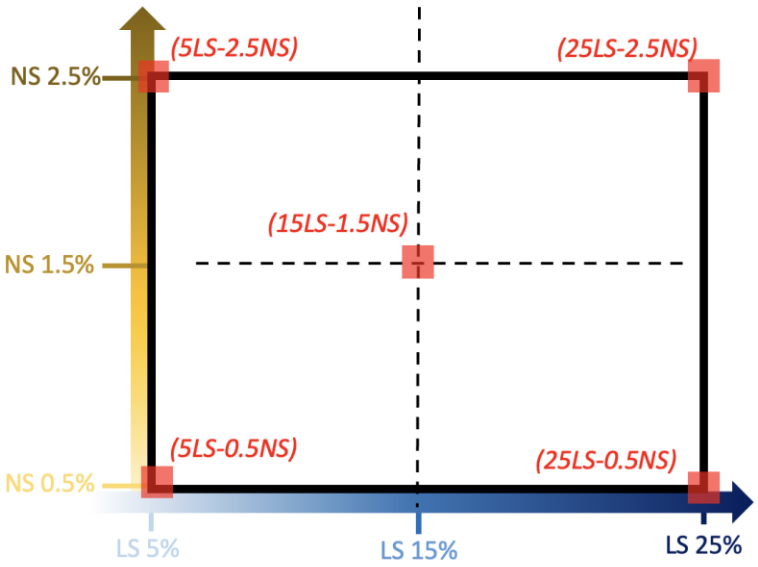

Figure 4-2 Illustration of the factorial design

Table 4-1 – Summary of mixes and testing matrix for ternary optimization

Binder families	PC (%)	MK (%)	LS (%)	NS[1] (%)	w/b	Isothermal calorimetry	Compressive strength	Bulk ER	XRD	TGA
5LS-0.5NS	30	65	5	0.5	0.5	X	X	X	X	X

25LS-0.5NS	30	45	25	0.5	0.5	X	X	X	X	X
5LS-2.5NS	30	65	5	2.5	0.5	X	X	X	X	X
25LS-2.5NS	30	45	25	2.5	0.5	X	X	X	X	X
15LS-1.5NS	30	55	15	1.5	0.5	X	X	X		

[1]Sodium sulfate is proportioned as w/w of total binder.

4.2.2 Impact of Na_2SO_4 on microscale features

Upon completion of the first set of experiments, the impact of sodium sulfate on the early kinetics and evolution of microscale features is explored. The hybrid AAM selected for this experiment is the binder with highest early strength (i.e., 3 and 7 days) in the first set investigated. This binder is compared with a binder made of the same metakaolin, Portland cement and limestone proportions, but without added NS. For these two binders, isothermal calorimetry is performed over 3 days and XRD and TGA are performed at 3, 7 and 28 days. Since a slowing down of strength gain at 7 days and onwards is usually observed for high early strength binders containing both alkalis and PC, this experiment is anticipated to shed light on the underlying microscale mechanisms behind such a decrease of strength evolution.

4.3 Materials and methods

The amount of PC and the range of added NS in the hybrid binders were determined based on the statistical analysis of the results of the preliminary investigation (see Appendix A – Factorial design rationale). For all mixtures, Portland cement content was fixed at 30 wt.% and water-to-binder ratio was set at 0.5. This w/b ratio is the minimal one to achieve suitable workability of the stiffest mix (i.e., mix with highest MK content). The limestone fraction of the total binder content was varied between 5 and 25 wt.%, while sodium sulfate content was added as 0.5 to 2.5 wt.% of total binder (see factorial DOE in *Figure 4-2*). The oxide composition of Portland cement and metakaolin can be found in Table 4-2.

For the two experimental parts of this work, the preparation of the samples started with 5 minutes of dry mixing of the powder ingredients. This included sodium sulfate powder, which was blended in a solid form, as per [22]. Afterwards, water was gradually incorporated, and the paste mixtures were mixed for an additional 5 minutes. The samples were cast in 50 by 100 mm cylinder molds

and sealed until demolding, 24 hours after casting. Following that, the samples were cured at 100% relative humidity (RH) until they reached the testing ages.

Since the limestone and sodium sulfate amounts varied between mixes, the sample mixes were identified as follows: xx%LS – xx%NS, where the xx represented the percentage fraction of LS and the percentage of NS per total binder weight. MK was used as replacement of PC + LS.

Table 4-2 – Oxide composition (wt.%) of Portland cement and metakaolin determined by XRF

	CaO	SiO_2	Al_2O_3	Fe_2O_3	MgO	K_2O	Na_2O	P_2O_5	TiO_2	MnO	S	Zn	Sr	LOI* & others
PC	66.4	18.6	4.1	4.0	1.3	0.7	0.2	0.1	0.3	0.1	1.2	0.0	0.2	2.9
MK	0.4	62.5	29.8	1.2	0.4	1.8	0.2	0.0	0.7	0.0	0.0	0.0	0.0	2.9

**LOI stands for loss on ignition*

4.3.1 Fresh state testing

Isothermal calorimetry to determine the hydration kinetics of the tested binders was performed on all mixes, based on the ASTM C1702 [23] method B. All cementitious powders were equilibrated to the temperature of the isothermal calorimeter room (23°C) for 24 hours and then mixed outside the vial with water to attain a w/c of 0.5. The test was conducted over three days.

Setting time was determined by the Vicat needle testing on the two mixtures, following the ASTM C191 [24]. In between measurements, the samples were kept under a wet cloth to prevent drying. As per ASTM C191, initial setting was calculated as the time difference between initial contact of water with the cementitious blend, and the time to reach 25 mm of needle penetration in the paste. Final setting was considered as the time interval between initial contact of water and the time for the needle to no longer leave a circular trace on the paste.

4.3.2 Mechanical testing

Mechanical testing was performed on all samples of the factorial optimization. After 3, 7 and 28 days, three samples per mixture were taken from the 100% relative humidity container and the cylinder's ends were ground for compressive strength testing. Compressive strength was conducted on 50 x 100 mm cylindrical samples at a load rate of 490 N/s, following the guidelines of ASTM C39 [25]. Prior to testing for compressive strength, uniaxial electrical resistivity, also known as bulk electrical resistivity, was performed using Giatec's instrument, RCON. The

conduction of this test was done on paste cylinders in accordance with ASTM C1876-24 [26]. Three cement paste cylinders of each mix were placed between two electrodes positioned at the ends of the sample. A wet sponge covered each electrode to ensure electrical connection between the specimen and the electrode. From the resistance in ohms obtained by the instrument, electrical resistivity (ρ) was calculated according to the equation below:

$$\rho = \frac{A * R}{L} \tag{4.1}$$

where A is the cross-sectional area of the specimen, L is the specimen's length, and R is the specimen's electrical resistance.

4.3.3 Microscale testing

In the first set of experiments, during the factorial optimization of the samples, one sample of each factorial point (i.e., 5LS-0.5NS, 5LS-2.5NS, 25LS-0.5NS and 25LS-2.5NS) was removed from the humidity chamber after 90 days, while in the second set of experiments, one sample per mix was removed at 3, 7 and 28 days. The goal of microscale testing was to determine the type of reaction products forming in the binders, with the aim to understand in more detail how the reaction of these novel cements is occurring. To achieve this, two techniques were applied: XRD and TGA. XRD provided information about the crystalline reaction products forming, as well as information about how the PC clinker phases might be reacting as hydration progresses, while TGA provided indirect information about the potential degree of reaction of the binders and was useful in verifying the interpretation of the XRD results.

The powders for TGA and XRD were prepared by grinding cement paste chunks in an agate mortar. The cement pastes' hydration process was arrested with isopropanol. Two consequent filtrations with ethanol were then conducted, 10 minutes apart. The pieces were dried at 40 °C for 30 minutes and ground in an agate crucible. Before testing, the dried powders were kept in a desiccator to prevent carbonation. XRD was performed on powdered samples using the Rigaku Ultima IV diffractometer equipped with a copper source and a diffracted beam monochromator. The samples were scanned over a 2θ range between 5º and 60ºC. TGA was conducted on powdered samples using the Q5000 TGA instrument at an ending temperature of 800 °C and ramping rate of 20 °C /min.

Several phases were quantified from the TGA results, based on the procedure in [27]. It is commonly agreed upon that the weight loss occurring below 105 °C is mostly due to evaporable water loss [27]. As presented in [28], hydrate water (H) can be quantified as follows:

$$H = \frac{w_{40} - w_{550}}{w_{550}} \tag{4.2}$$

where w_{40} is the weight loss at 40 °C and w_{550} is the weight loss at 550 °C.

Portlandite ($Ca(OH)_2$) generally decomposes to calcium oxide (CaO) and water between 400 and 500 °C. To recalculate portlandite content from the weight loss between 400 and 500 °C, the following formula is suggested by [27,28]:

$$Ca(OH)_2 = \frac{w_{400} - w_{500}}{w_{500}} * \frac{74}{18} \tag{4.3}$$

where 74/18 corresponds to the molar mass ratio of $Ca(OH)_2$ (74 g/mol) and H_2O (18 g/mol). Finally, calcium carbonate ($CaCO_3$) decomposes to CaO and water above 600 °C. Taking again in consideration the molar mass of $CaCO_3$ of 100 g/mol and the molar mass of CO_2 of 44 g/mol, the following formula may be used:

$$CaCO_3 = \frac{w_{600} - w_{800}}{w_{800}} * \frac{100}{44} \tag{4.4}$$

4.4 Factorial optimization of ternary hybrid binders

4.4.1 Isothermal calorimetry

In traditional cements, three kinetic periods can be identified from the calorimetry curve. The first is the induction period, which lasts approximately 3 hours and ends with the precipitation of calcium hydroxide and start of the acceleration period. This induction period can be easily identified as it corresponds to a period of very low heat flow prior to the beginning of the curve. The left side of this curve corresponds to the acceleration period, and in Portland cements, it is characterized by the growth of calcium silicate hydrate (C-S-H) needles. The right side of the curve corresponds to the deceleration period, during which reaction product formation still occurs, but at an increasingly slower rate.

4.4.1.1 Early age reaction

In *Figure 4-3*a, it is possible to observe that limestone contents of 25% decreased the height of the first peak (commonly known as C_3A peak). However, it is interesting to note that the central mix (15LS-1.5NS) did not display the same decrease and had a similar height to that of the 5LS-0.5NS mix. Mix 5LS-2.5NS had the highest peak out of all mixes. Since this mix had the highest MK and NS content, it appears that these factors might have enhanced the aluminate reaction and thus increased the first peak. Limestone is known to have the potential to enhance the early age reactivity by providing additional nucleation sites [6,9,10], but since metakaolin is rich in alumina and has a higher specific surface area, and thus the capacity to increase the surface available for nucleation as well, a larger amount of metakaolin is more beneficial to the increase in aluminate peak than a higher limestone content. Across mixes, another interesting phenomenon is the broadening of the aluminate peaks for sodium sulfate contents of 2.5%. At 0.5NS, peaks are steeper, and they reach a lower optimum, while for mixes with 2.5NS, the peaks are broader and higher. This shows that the additional sodium sulfate provided benefited the reaction in the first hours of hydration. The fact that 15LS-1.5NS performed similarly to 5LS-0.5NS also illustrates that the slightly detrimental impact of lower amounts of metakaolin may be balanced by an increase in NS content. To further analyze the impact of sodium sulfate on the calorimetry curves, mixes 5LS-0.5NS and 5LS-2.5NS, as well as mixes 25LS-0.5NS and 25LS-2.5NS were plotted separately in *Figure 4-4*.

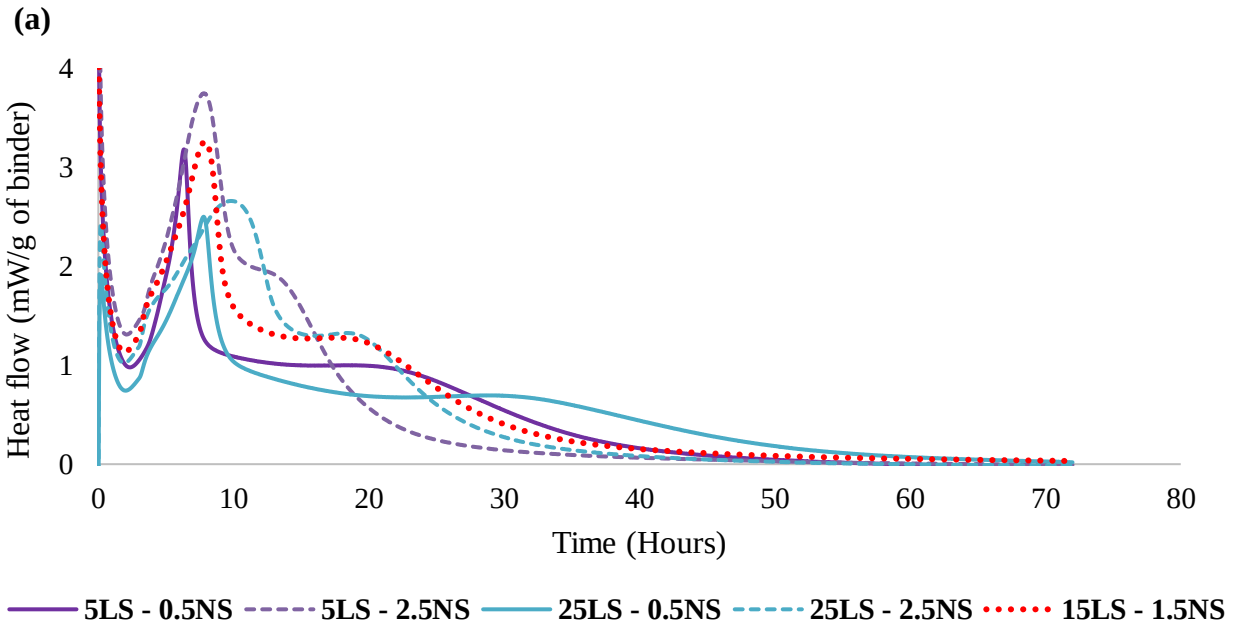

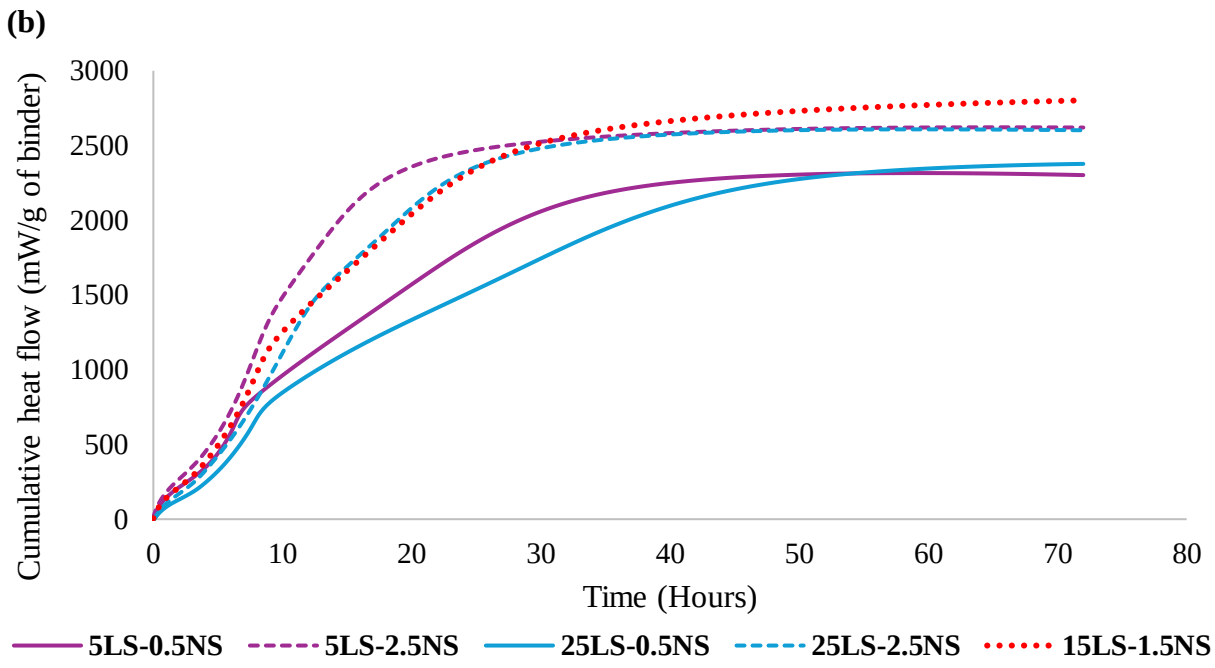

Figure 4-3 (a) Isothermal calorimetry and (b) cumulative calorimetry curves of hybrid alkali-sulfate activated metakaolin/limestone pastes

The cumulative heat flow of the different mixes reveals that the 5LS-2.5NS mix has higher values for the first day of testing, but from 30 hours onwards, both 5LS-2.5NS and 25LS-2.5NS appear to attain the same plateau. The behavior of mixes 5LS-0.5NS and 25LS-0.5NS is similar, however, their plateau occurs after more than 2 days, or 50 hours. The mix 15LS-1.5NS has the highest cumulative heat flow, slightly above both 2.5NS mixes. From this discussion, it appears that the kinetics are heavily influenced by the proportion of sodium sulfate, with limestone content only impacting the cumulative heat flow for the first one or two days of alkali-activation.

4.4.1.2 Understanding the impact of sulfates

Zunino (2020) [29] identified that Portland cement binders with limestone and metakaolin may be affected by undersulfation. This phenomenon arises from the high specific surface area of limestone and metakaolin, which drives calcium silicate hydrates (C-S-H) formation, which is the main strength giving phase and raises the need for more sulfate to cover all available surface areas and temporarily inhibit the aluminate reaction. In *Figure 4-4*a and b, for each curve, it is possible to observe two peaks, the first one being much higher and narrower. In properly sulfated systems, the second peak is expected to be higher than the first. It is the sign that the silicate peak (i.e., the smaller peak) occurred first, and then the aluminate peak occurred after the depletion of gypsum.

However, when the highest peak comes first, it shows that there was not enough sulfate to temporarily arrest C_3A reaction. The aluminate reaction thus occurs first, consuming all the sulfate ions available. The silicate peak that follows is much lower and broader than it would have been in a system with sufficient sulfate content. Based on the geometry of the curves, it is possible that even with the addition of 2.5% of sodium sulfate, sulfate balance was not achieved in any of the hybrid binders. However, it is important to observe that the hydration mechanisms in alkali-containing systems may differ largely from that of water-activated systems. Increasing sulfate content might therefore not resolve this behavior in the kinetics and a deeper look into them is necessary to further understand the present results.

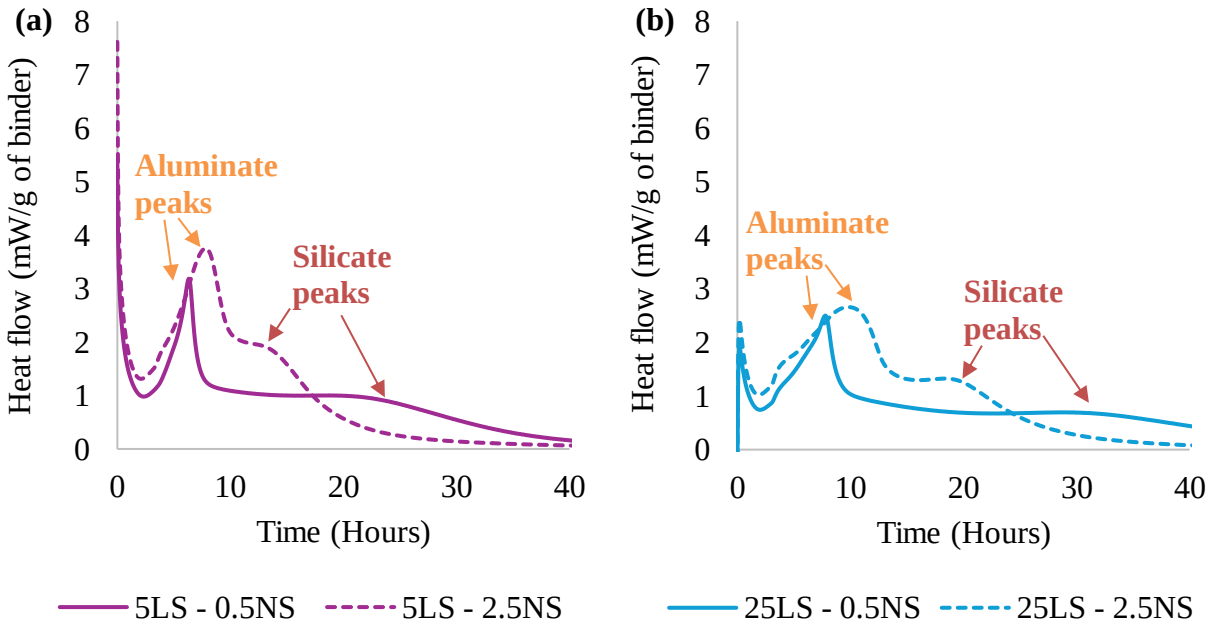

Figure 4-4 Isothermal calorimetry curves of (a) 5LS binders and (b) 25LS binders

4.4.2 Macroscale testing

4.4.2.1 Compressive strength

The evolution of compressive strength for the mixes of the factorial design is reported in *Figure 4-5*. At day 3, the best performing mixes were 15LS-1.5NS (13 MPa) and 5LS-0.5NS (13.6 MPa). Both mixes incorporating 25% of limestone displayed lower strengths, independently of their sodium sulfate content. For the mix with 5LS-2.5NS, there was a reduction in strength of 10% associated with the increase of sodium sulfate content but no such reduction was observed between 25LS-2.5NS and 25LS-0.5NS. It is interesting to observe that the opposite phenomenon occurs at

day 7: mixes with 25% of limestone experience almost 10% of strength reduction when $NaSO_4$ content is raised from 0.5 to 2.5%, while mixes with 5% of limestone have comparable strength (13.9 and 13.7 MPa) independently of sodium sulfate content. Compared to the other mixes, the central point of the factorial design (15LS-1.5NS) performed better at day 7, with an average strength of 15.4 MPa. At day 28 however, all mixtures presented very similar strength (19-21 MPa), apart from the 5LS-0.5NS mix which reached a strength of almost 26 MPa at day 28.

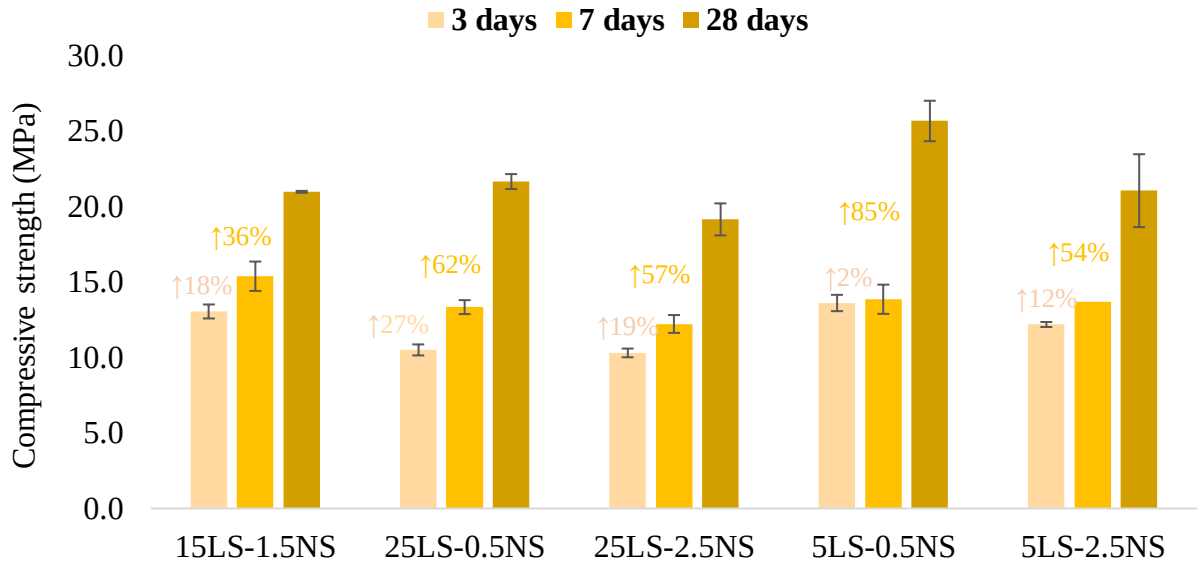

Figure 4-5 - Compressive strength of hybrid alkali-sulfate activated metakaolin/limestone pastes as a function of Na_2SO_4 content, and curing duration

From these results, it appears that the impact of limestone and sodium sulfate, as well as their interaction, are complex. Depending on the time of testing and the levels of limestone/sodium sulfate, their respective and combined impact on strength appears to change. It is however possible to draw some general observations. Firstly, limestone contents of 25% are detrimental to early strength, particularly at 3 days, but it appears to be less significant for 28 days' strength. Secondly, the sodium sulfate content does not seem to have the same effect at 3 and 7 days depending on the limestone content. At lower metakaolin and higher limestone contents, a detrimental impact of Na_2SO_4 is observable at 7 days and onwards, while it occurs as early as 3 days for low limestone/higher metakaolin contents. From past studies [30–32], it is already known that stronger concentrations of alkalis or higher content of high SSA materials such as both metakaolin and limestone will negatively impact strength once the refinement of porosity starts to limit hydrate growth. This behavior can be expected to occur earlier for 5LS samples than 25LS ones since

limestone was used to replace metakaolin and the latter will react to a much greater extent. The slower strength gain of 25LS mixes could therefore be related to slower hydrates formation compared to that of 5LS mixes. After 7 days, it is possible that the limits on hydration growth in smaller pores may have impacted the strength gain of 25LS-2.5NS mixes. The same behavior likely occurred earlier for low limestone mixes, as their strength increased more quickly, and hydrates formation occurred more rapidly.

The increase in strength between two testing ages is also reported in *Figure 4-5*. From the values shown, it appears that between day 3 and day 7, the smallest increments in strengths are associated with mixes 5LS-0.5NS (2% increase) and 5LS-2.5NS (12% increase), respectively. This behavior may hint that metakaolin content will govern the very early age strength gain (i.e., between 1 and 3 days). Indeed, the strength that is achieved by 25LS mixes at day 7 are achieved at day 3 by 5LS mixes. On the other hand, between 7 and 28 days, the highest strength increments are for mixes 25LS-0.5NS (62% increase) and 5LS-0.5NS (85% increase). Mixes with 2.5NS also experienced strength gain between 7 and 28 days, but they were lower, with 54% and 57% of increase. Moreover, the 15LS-2.5NS mix, which had the highest strength at 3 and 7 days, only saw a 36% increase in strength between the ages of 7 and 28 days. From this discussion, it appears that the strength increases between 3 and 7 days were more governed by binder composition (limestone and metakaolin content), while strength gains between 7 and 28 days were more influenced by sodium sulfate content. The impact of the limestone and sodium sulfate factors will be further discussed in the statistical analysis of this work (section 4.4.3).

4.4.2.2 Bulk electrical resistivity

The bulk resistivity of all families at different testing ages is shown in *Figure 4-6*a. It shows that while an increasing trend of the values may be observed over time, the variability between the different mixes also significantly increases with time. This finding may be explained by the behavior of individual families displayed in *Figure 4-6*b. This graph shows that half of the families follow a similar pattern (i.e., 15LS-1.5NS, 25LS-0.5NS and 5LS-0.5NS), while the other half (i.e., 25LS-2.5NS and 5LS-2.5NS) display a different behavior. The first group, containing 1.5% of sodium sulfate or less, displays resistivity values ranging from 40 to 60 Ω-mm at 3 days, 130 to 170 Ω-mm at 7 days, and 260 to 390 Ω-mm at 28 days. On the other hand, the mixes with 2.5% Na_2SO_4 reached 140 Ω-mm at most at 28 days. The 5LS-2.5NS mix was performing the worst,

with resistivity values ranging from 22 Ω-mm at 3 days, to 40 Ω-mm at 28 days. From these results, it appears that high sodium sulfate concentrations significantly affect resistivity past a certain threshold, found to be around 1.5% for limestone contents of 5 to 25%. This appears particularly critical for low limestone contents (i.e., 5LS-2.5NS mix), which may again be related to porosity changes in the system in the early days. Indeed, bulk resistivity measurements are often found to correlate to the porosity of cementitious systems. It must however be noted that other factors than porosity may affect these results, such as the moisture in the cement pastes and the chemistry of their pore solution. Therefore, direct porosity measurements are needed to confirm these findings.

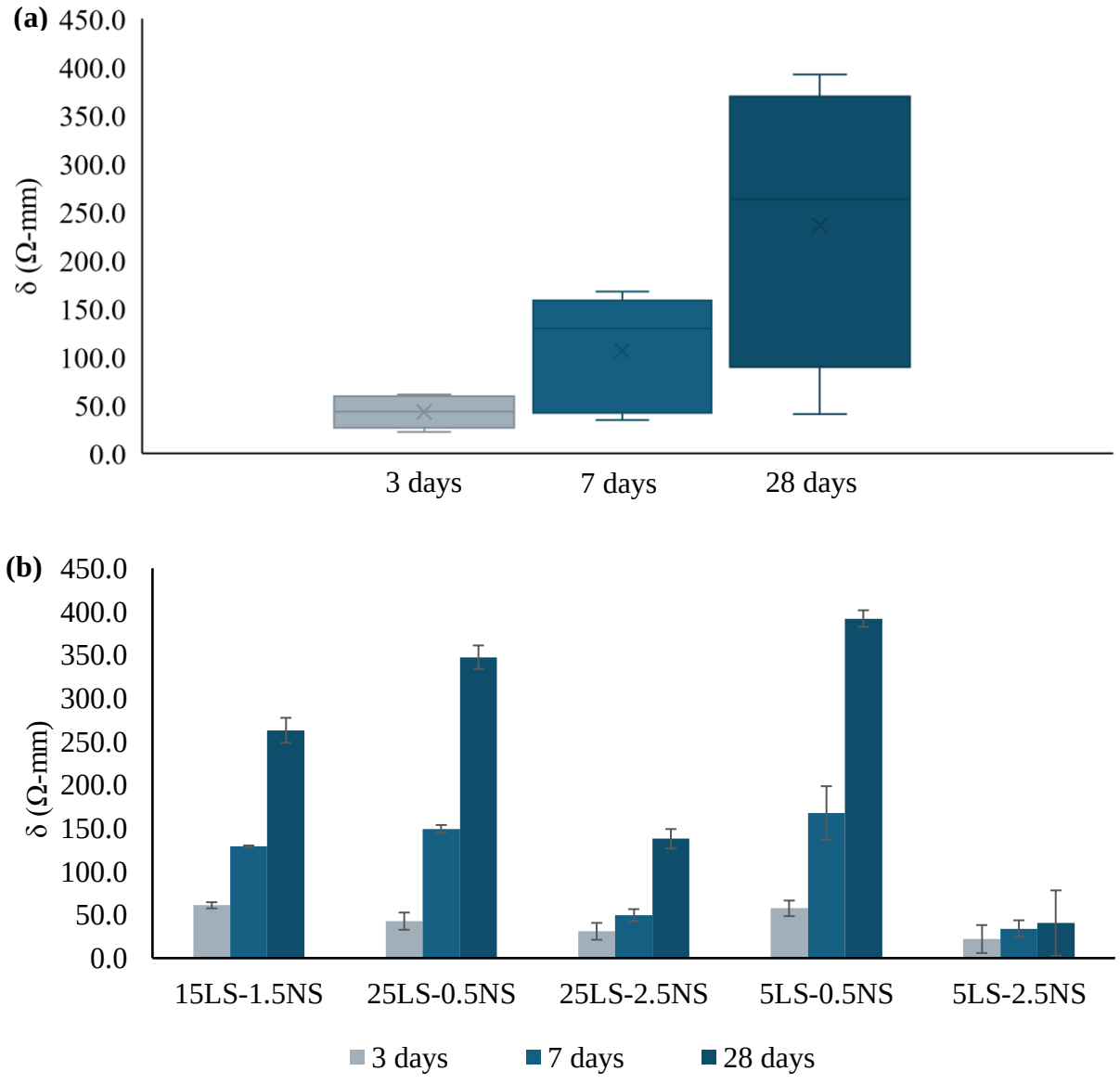

Figure 4-6 –(a) Box plot and (b) individual families plot for bulk resistivity measurements.

Mota *et al.* (2018) [8], showed that the presence of alkalis can lead to greater capillary porosity in Portland cement-containing systems due to the interaction between alkalis and Portland cement. A greater NS content would lead to more alkalis, and therefore, might affect the capillary porosity. However, the difference in bulk resistivity between 25LS-2.5NS and 5LS-2.5NS cannot be explained by this interaction as both alkalis and Portland cement content are constant for both mixes. At all testing ages, the 5LS-0.5NS mixes had higher resistivity values than their 25LS-0.5NS counterparts, while the opposite behavior is displayed for -2.5NS mixes. The reason for this behavior could be related to the reaction kinetics of the binder systems. At high levels of metakaolin and sodium sulfate, the reaction might take place even faster than at lower levels of metakaolin. This is corroborated by the high heat flow shown in the isothermal calorimetry testing. Therefore, the extent of reaction might plateau early on, leading to the slowing down of the increase in resistivity values. On the other hand, the slight increase in resistivity at 28 days for 25LS-2.5NS might hint that this mixture did not experience to the same extent an acceleration of the kinetics, thus allowing for a small improvement of resistivity at later ages.

4.4.3 Macroscale statistical analysis

4.4.3.1 Factorial design analysis

In *Figure 4-7*, the main effects of LS and NS on strength at 3, 7 and 28 days are shown for the factorial points of the design (i.e., excluding the central point 15LS-1.5NS).

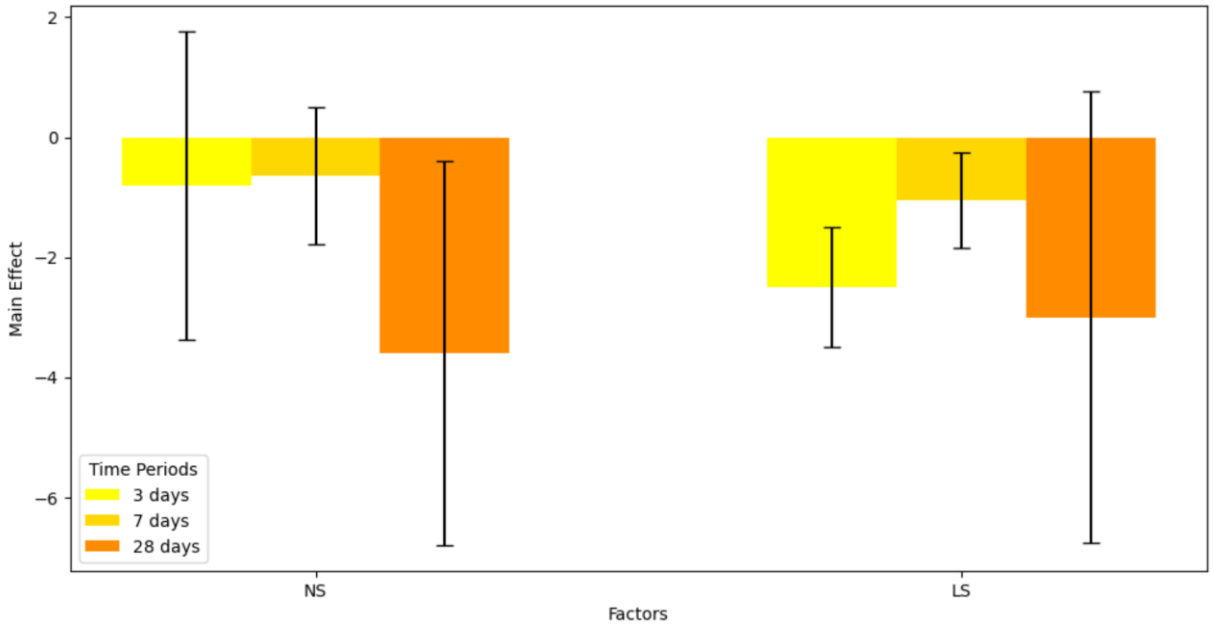

Figure 4-7 Main effects plot of limestone (LS) and sodium sulfate (NS) for compressive strength

It is first interesting to notice that the initial average impact (3 - 7 days) of NS going from 0.5 to 2.5% is small, but that this impact rapidly increases at 28 days, even exceeding the impact of the limestone concentration. The error bars on the average impact of NS reveal that, depending on its concentration, NS may benefit or hinder the early strength from 3 to 7 days, but that even at low concentrations, its impact on 28-days strength will be negative. This behavior is understandable from a kinetics point of view, as a proper dosage of sodium sulfate is generally expected to enhance early age strength but may also lead to an early plateau in strength. On the other hand, for both NS and LS, the factors have a smaller influence at 7 days. This behavior is linked to the similar strengths that all mixtures displayed at 7 days. As discussed in section 4.4.2, strength gain between 3 and 7 days was governed by the limestone content used to replace metakaolin. Higher amounts of metakaolin accelerated the kinetics and improved 3 days' strength, but did not substantially affect 7 days strength, while the opposite occurred for mixes with higher amounts of limestone. This may partially explain why most mixes had similar 7-day strength, independently of their limestone and sodium sulfate content. Lastly, the impact of adding 5 to 25% of limestone to the mixes was generally negative at 3 and 7 days, but the error bars on the 28-days strength illustrate that at certain ratios of replacement, the limestone reaction slightly benefits later age strength.

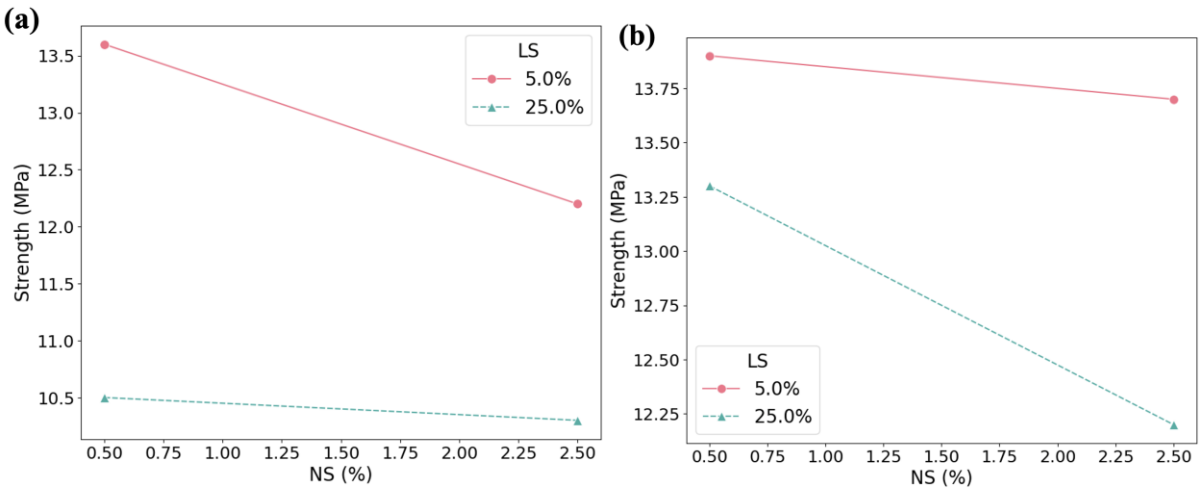

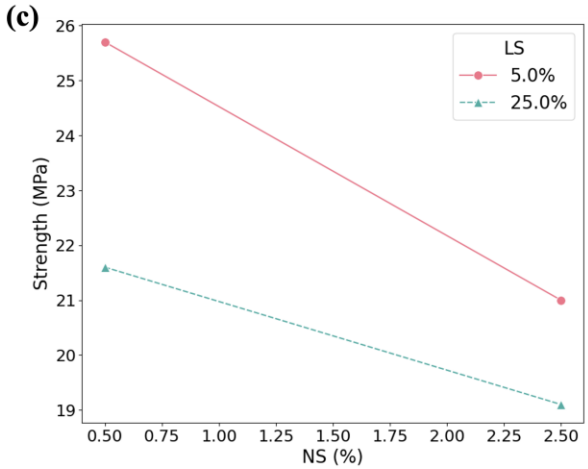

Figure 4-8 Interaction plots of strength (a) 3 days, (b) 7 days and (c) 28 days

In the interaction plots, only the factorial points were considered again. For these plots, it is important to look at the difference in the slope of the two lines corresponding to the different concentrations of LS (5 and 25%). When two factors are independent from one another, their lines are parallel, meaning that the difference in concentration of one factor does not affect the behavior of the second. However, as shown in *Figure 4-8* and in Table 4-3, the slope of the two lines varies significantly, showing that there is indeed an interaction of NS and LS, and that the effect of NS on strength is affected by the level of LS. Moreover, except at 7 days, the slope associated with the decrease in strength as a function of NS content is larger for the 5% LS line than for the 25% LS line. This behavior highlights that NS content tends to have a greater impact on samples with larger amounts of metakaolin/lower amounts of limestone.

Table 4-3 Slopes of interaction lines

Time	% LS	Slope
3 days	5%	0.35MPa/% of NS
	25%	0.05MPa/% of NS
7 days	5%	0.05MPa/% of NS
	25%	0.275MPa/% of NS
28 days	5%	1.175MPa/% of NS
	25%	0.625MPa/% of NS

4.4.3.2 Two-way ANOVA

To further understand the impact that the individual factors and their interactions had on the strength of the mixes, a two-way analysis of variance (ANOVA) was performed for each testing age results. Table 4-4 shows that the most significant impact of limestone and sodium sulfate occurred at day 3. At this testing age, the *p*-values for LS, NS, and their interaction (LS:NS) are all well below 0.05, meaning a confidence level above 95% that these factors are significantly affecting strength. The high sum of squares (SS) of LS also shows that this factor plays the largest role in explaining strength variation between mixes at day 3.

Table 4-4 Two-way ANOVA - compressive strength results

3-days f'c

	df	Sum of squares	F	PR(>F)
LS	1	18.51	123.233	0.0000006
NS	1	2.02	13.4377	0.0043
LS:NS	1	1.09	7.241	0.023
I(LS²)	1	4.65	30.9475	0.00024
I(NS²)	1	0.06	0.3818	0.55
Residual	10	1.50	NaN	NaN

7-days f'c

	df	Sum of squares	F	PR(>F)
LS	1	2.90	3.627	0.086
NS	1	1.28	1.59774	0.23
LS:NS	1	0.64	0.80281	0.39
I(LS²)	1	10.68	13.3565	0.004
I(NS²)	1	0.78	0.97894	0.35
Residual	10	7.99	NaN	NaN

28-days f'c

	df	Sum of squares	F	PR(>F)
LS	1	17.49	9.72961	0.026
NS	1	25.34	14.1023	0.013
LS:NS	1	2.23	1.2392	0.32
I(LS²)	1	1.31	0.72969	0.43
I(NS²)	1	1.98	1.09945	0.34
Residual	5	8.99	NaN	NaN

The behavior at day 7 is less straightforward to explain. Indeed, it is possible to observe that most factors do not bear statistical significance at this age, which may be explained by the similar strength that all mixes displayed. On the other hand, at day 28, the individual factors (LS and NS) are statistically significant, but their interaction is not. Furthermore, the NS content has a much larger SS at day 28 than at day 3 or 7, and it even surpasses the SS of LS. This result shows that high NS mixes did not have much lower strength than their low NS counterparts in early days, but that this difference increased significantly with time. On the other hand, LS impact slightly reduced between 3 and 28 days, indicating that LS addition may have contributed to a slight increase in strength in later ages, thus slightly reducing the gap in strength between high and low LS content mixes. The results of the ANOVA confirm what was discussed in section 4.4.2 and show that strength is first governed by limestone/metakaolin content (from 3 to 7 days), and then by sodium sulfate content (from 7 to 28 days).

4.4.3.3 Response surface methodology optimization

The response surface of all mixes at 3, 7 and 28 days are plotted in *Figure 4-9*. RSM plots were designed based on strength (f'c) modelling with the formula below:

$$f'c = aNS + bLS + c(NS * LS) + dNS^2 + eLS^2$$

Where a, b, c, d and e are constants, and NS and LS are the individual factors. Residual plots based on the fitting of the data to this model can be found in Chapter 7 Appendix B – Residual plots.

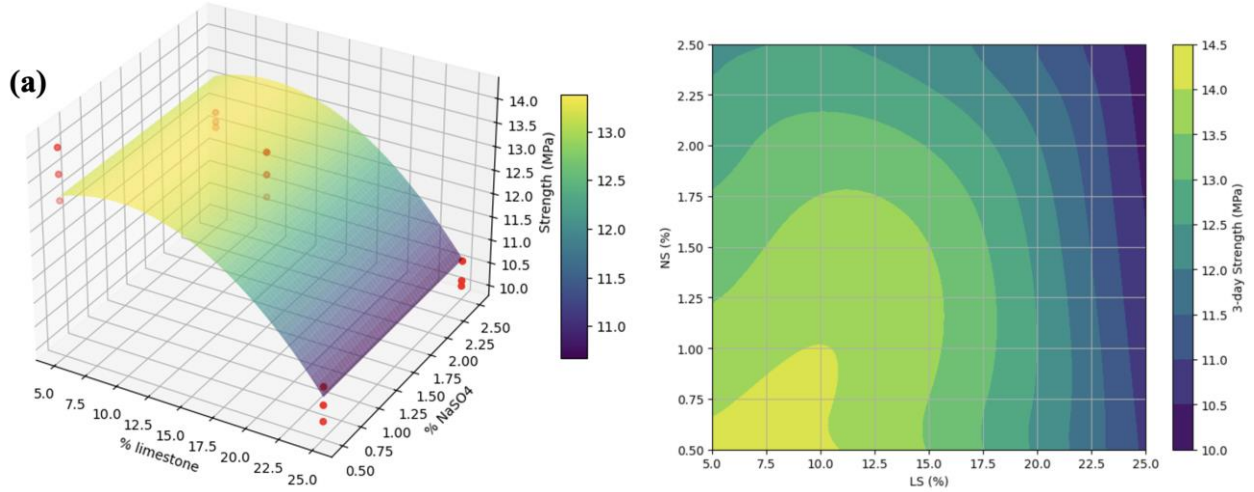

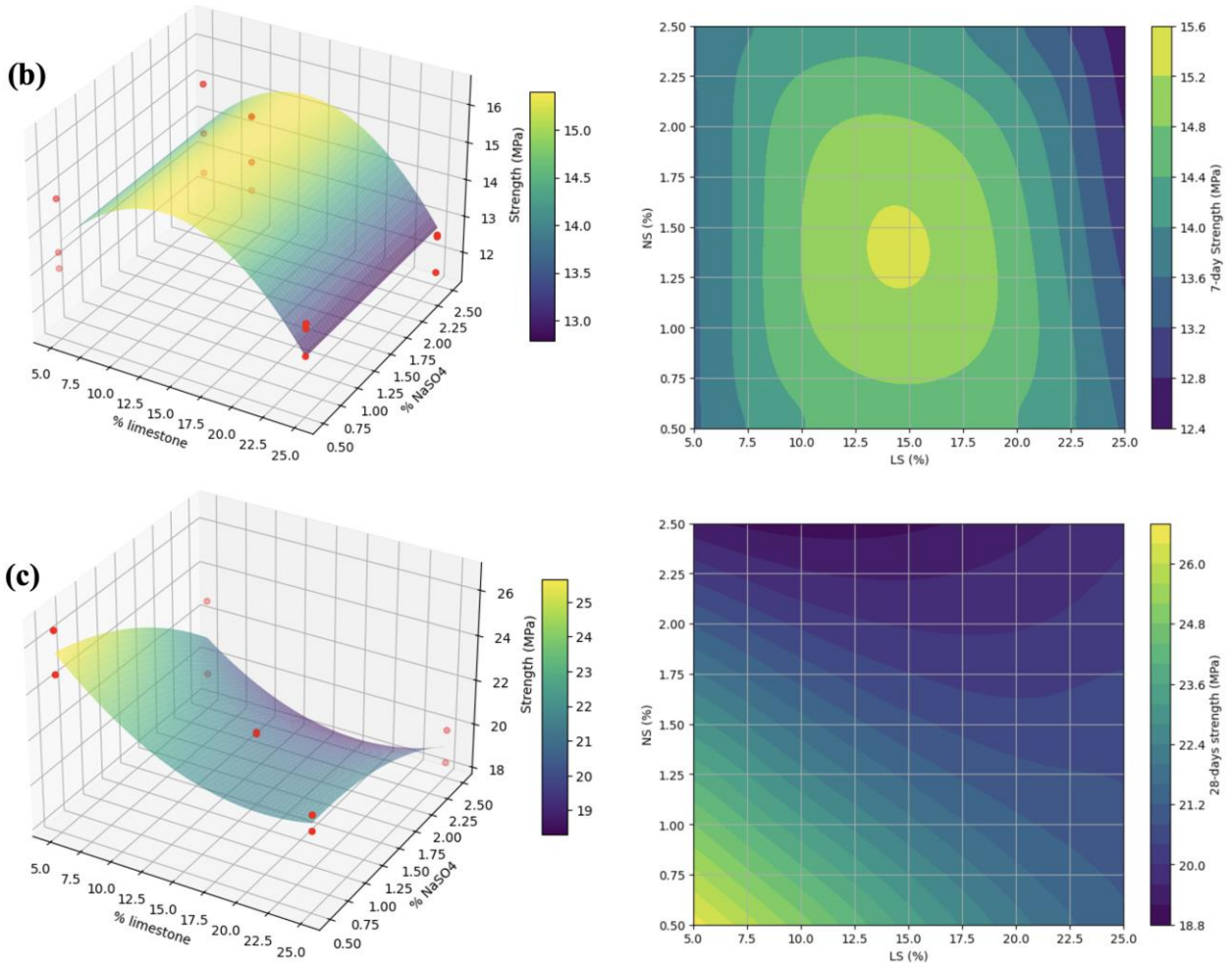

Figure 4-9 RSM of strengths at (a) 3 days, (b) 7 days and (c) 28 days

These plots highlight how the composition of the binders with respect to limestone and sodium sulfate content influences the strength differently in time. For early age strength, a sodium sulfate content of 1.5% is optimal. At 3 days, the 15LS-1.5NS mix has similar strength to the 5LS-0.5NS one, despite having 3 times more limestone. At 7 days, this mix is also the best performing, as the curvature of the RSM plot shows (*Figure 4-9*b). Metakaolin being the most reactive component apart from the fixed Portland cement, it could have been expected that 5LS-0.5NS or 5LS-2.5NS would have better early age properties than 15LS-1.5NS. The results obtained therefore show that the level of NS matters more than the amount of metakaolin to determine the early strength of ternary hybrid cement pastes. However, at 28 days, the impact of sodium sulfate bears more consequences and mixes with 0.5% of NS perform better. This can be easily observed in *Figure 4-9*c, as strength values first start to go down along the y(NS)-axis. From *Figure 4-10*, it can be

further confirmed that NS plays a determining role in how much strength will increase between 3 and 28 days.

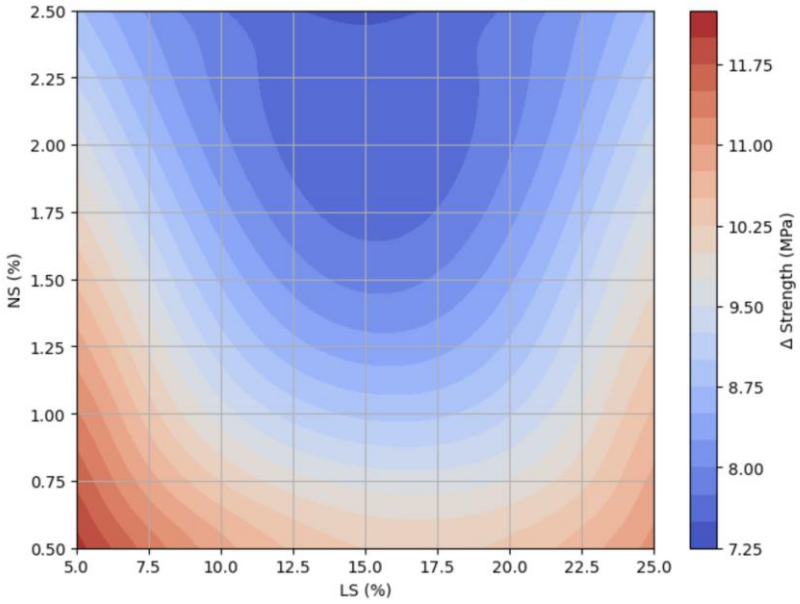

Figure 4-10 Contour plot of the difference in strength between 3 and 28 days

4.4.4 Microscale testing

To understand how the phase assemblage (type and amount of reaction products forming) of hybrid ternary AAMs were affected by their binder composition, this section will focus on the characterization and analysis of crystalline and amorphous phases in the binders.

4.4.4.1 TGA

Thermogravimetric analysis (TGA) was conducted after 90 days of curing for all factorial points (i.e., mixes 5LS-0.5NS, 5LS-2.5NS, 25LS-0.5NS and 25LS-2.5NS). The peak around 120 °C associated with hydrate products and the amount of hydrate water calculated from equation (4.2) (see section 4.3.3) are shown in *Figure 4-11* and *Figure 4-12*, respectively. Both the peak and calculated amount of hydrate water show little variation across different mixes. This means that the variation in LS from 5 to 25% and NS from 0.5 to 2.5% did not significantly alter the final extent of hydrate formation. The variations in LS and NS contents played a role at earlier ages, but after 90 days of curing, all mixes appear to have reached a similar extent of product formation.

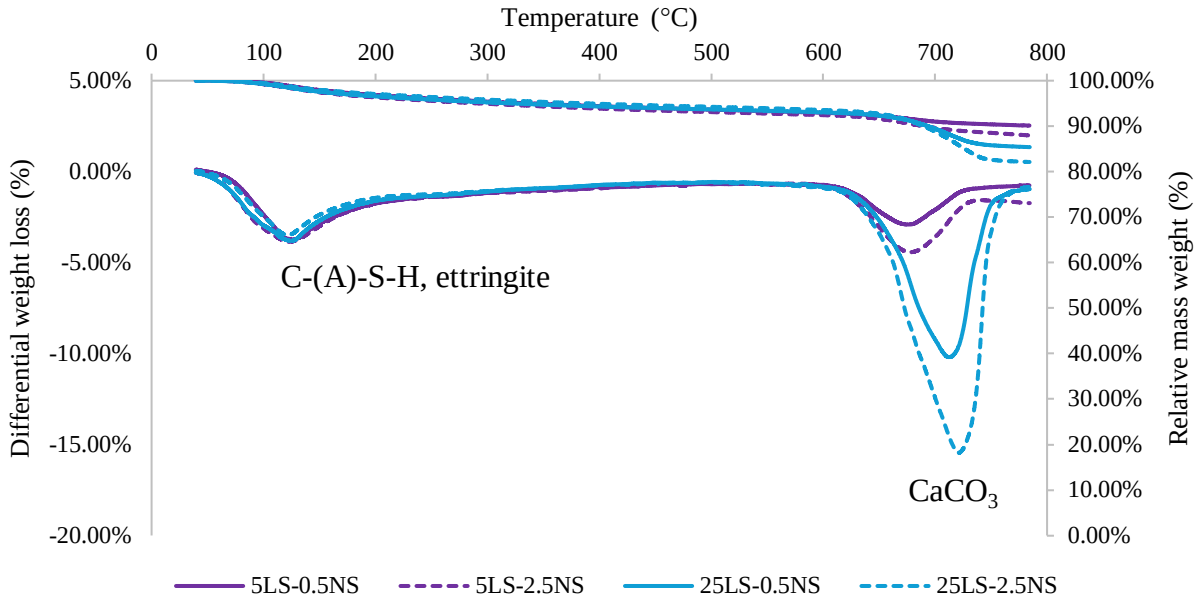

Figure 4-11 TGA and DTG of hybrid binders at 90 days

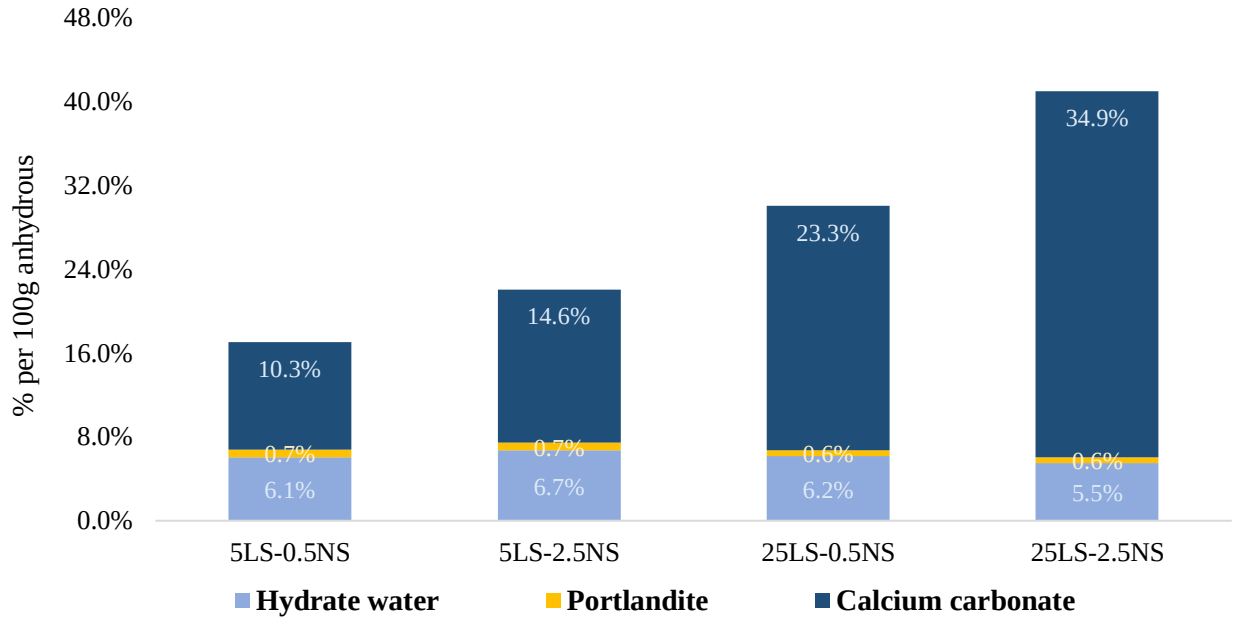

Figure 4-12 Calculated percentage of hydrate water, portlandite and calcium carbonate

In *Figure 4-11*, it is also possible to observe a peak around 700 °C. This peak is associated with the decomposition of calcium carbonate or calcite from limestone and may also be attributed to carbonation in the samples. The difference in peak depth between 5LS and 25LS mixes is attributable to the difference in LS content. However, the calculated amounts of calcite from *Figure 4-12* show that there is a small increase in calcite content for mixes with 2.5 NS% compared

with mixes with 0.5 NS%. Moreover, since the only difference between these two mixes was their NS content, the difference in calculated calcite content may only be explained by one of these two following hypotheses: either a product in a similar range of thermal decomposition as calcite was formed, because of the added Na_2SO_4, or more calcite participated in the formation of other products for mixes with lower amounts of Na_2SO_4. This could occur if the excess of NS would have hindered the reaction of limestone to form AFm phases. This is the most probable hypothesis, since even if a new product was forming with a similar thermal decomposition range as calcite, it is unlikely that it would decompose at the exact same temperature. However, a shift in the peak would have probably been observed, which was not the case here. The issue with the second hypothesis (i.e., more calcite reacted in mixes with lower amounts of NS) is that it would be expected for limestone to participate in the formation of additional AFm phases such as hemicarboaluminate and monosulfoaluminate. However, as summarized in Lothenbach *et al.* [27], AFm phases will mostly decompose between 60 °C and 350 °C, with minor CO_2 losses occurring around 650 °C. Since the thermal changes in the hydrate water range (40 °C to 550 °C) were not significant between 0.5NS samples and 2.5NS samples, it is not possible to verify whether the reduced amount of calcite in 0.5NS mixes would be associated by greater AFm product formation from the reaction of limestone with metakaolin and portlandite. Since no other notable peak appears in the TGA, further testing would be required to identify the products formed from $CaCO_3$. Finally, since the calculated calcite amounts are superior to the amount of limestone added in all samples, it may be suggested that carbonation must have taken place prior to TGA testing.

4.4.4.2 XRD

XRD was conducted after 90 days for all of the factorial binders and the results are shown in *Figure 4-13*. Most crystalline phases appear in all mixes, with the main peaks attributed to ettringite, monosulfoaluminate, gypsum, hemicarboaluminate, quartz and calcite. Mixes 25LS-0.5NS and 25LS-2.5NS displayed very similar heights for their diffraction peaks, with only the calcite peak of 25LS-2.5NS appearing to be higher than that of its 0.5NS counterpart. From this observation, it appears that the increase in Na_2SO_4 dosage did not play a significant influence in the crystalline phases profile of the 25LS mixes.

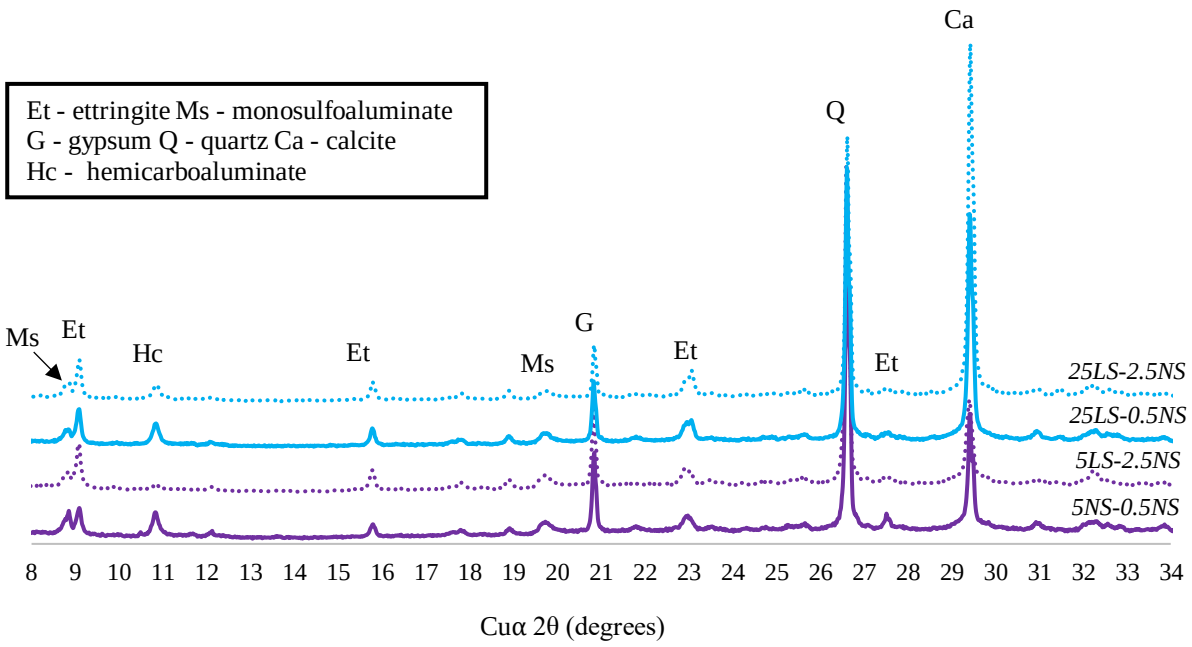

Figure 4-13 XRD of hybrid binders at 90 days

Regarding 5LS mixes, it is possible to observe a few notable differences between samples with 0.5NS and samples with 2.5NS. Mix 5NS-0.5NS had a larger monosulfoaluminate peak slightly before 9° and a reduced ettringite peak at 9°. It also displayed a hemicarboaluminate peak around 11° that did not appear in mix 5NS-2.5NS. Calcite peaks were very similar for the two mixes, independently of NS content. These findings show that the addition of sodium sulfate may be influencing more significantly the crystalline phases forming in mixes with higher amounts of metakaolin and lower amounts of limestone. The absence of the hemicarboaluminate peak in 5LS-2.5NS may hint that the presence of NS in excess hindered the formation of AFm phases, as was hypothesized based on the TGA data. Since AFm phases formation is stimulated by the addition of limestone, this could be a potential explanation for the reduced calcite peak in 0.5NS mixes compared to 2.5NS mixes. It is important to note that 25LS-0.5NS and 25LS-2.5NS both displayed a diffraction peak around 11° which was attributed to hemicarboaluminate. However, due to the much higher limestone percentage of these mixes, it is possible that more AFm phases will form, regardless of NS content. It is also possible that 25LS-0.5NS had a higher hemicarboaluminate content, but the sole observation of the diffraction peaks and their respective height are not sufficient to conclude that this was the case.

4.5 Impact of Na_2SO_4 on microscale features

The previous section of this chapter highlighted the macroscale and microscale properties of binders of different LS and NS composition. The results of these investigations, in addition to the statistical analysis performed on strength values, showed the interaction of limestone and sodium sulfate. It also showed that the most successful mix with respect to early strength, mix 15LS-1.5NS, had lower strength values than both 5LS- and 25LS-0.5NS mixes. Based on the microscale analysis of the factorial mixes at 90 days (see section 4.4.4), the hydrate water at 90 days is constant independently of the binder composition of the mixes. It is therefore possible that the variation in NS content led to an acceleration of the kinetics between 1 and 7 days and slowing down of the strength development from 7 days and onwards. However, from the microscale analysis in the previous section, it does not appear that the amount of hydrate products formed after 90 days was affected by NS, and only that retardation and acceleration effects occurred.

The goal of this section will therefore be to shed light on the behavior of hybrid binders at early ages on a microscale level and on what may explain the effects of NS on kinetics and strength development. The mix 15LS-1.5NS is compared to a "15LS-0NS" mix of similar binder composition (constant MK-LS-PC content) but made without sodium sulfate. Isothermal calorimetry, XRD and TGA will be the tools used in this section to compare the kinetics and microscale properties of the two binders.

4.5.1 Early kinetics

4.5.1.1 Isothermal calorimetry

The first observation that can be made about the isothermal curves of 1.5NS and 0NS in *Figure 4-14*a are that they both have an initially high peak, followed by a lower and broader peak. As discussed in section 4.4.1, this geometry of the curves is indicative of an undersulfated system. The C_3S or "silicate" peak seems particularly affected in the case of 0NS, as it is possible to notice that it is reduced to a very low and broad peak. Nevertheless, even with the addition of 1.5% of Na_2SO_4, the amount of sulfate ions added did not manage to inhibit the aluminate reaction in the 15LS-1.5NS mix sufficiently, and the silicate peak was low and occurred after the aluminate one. From this finding, it appears that in addition to the sodium sulfate amounts incorporated to the mixes, gypsum should be added until sulfate balance is reached.

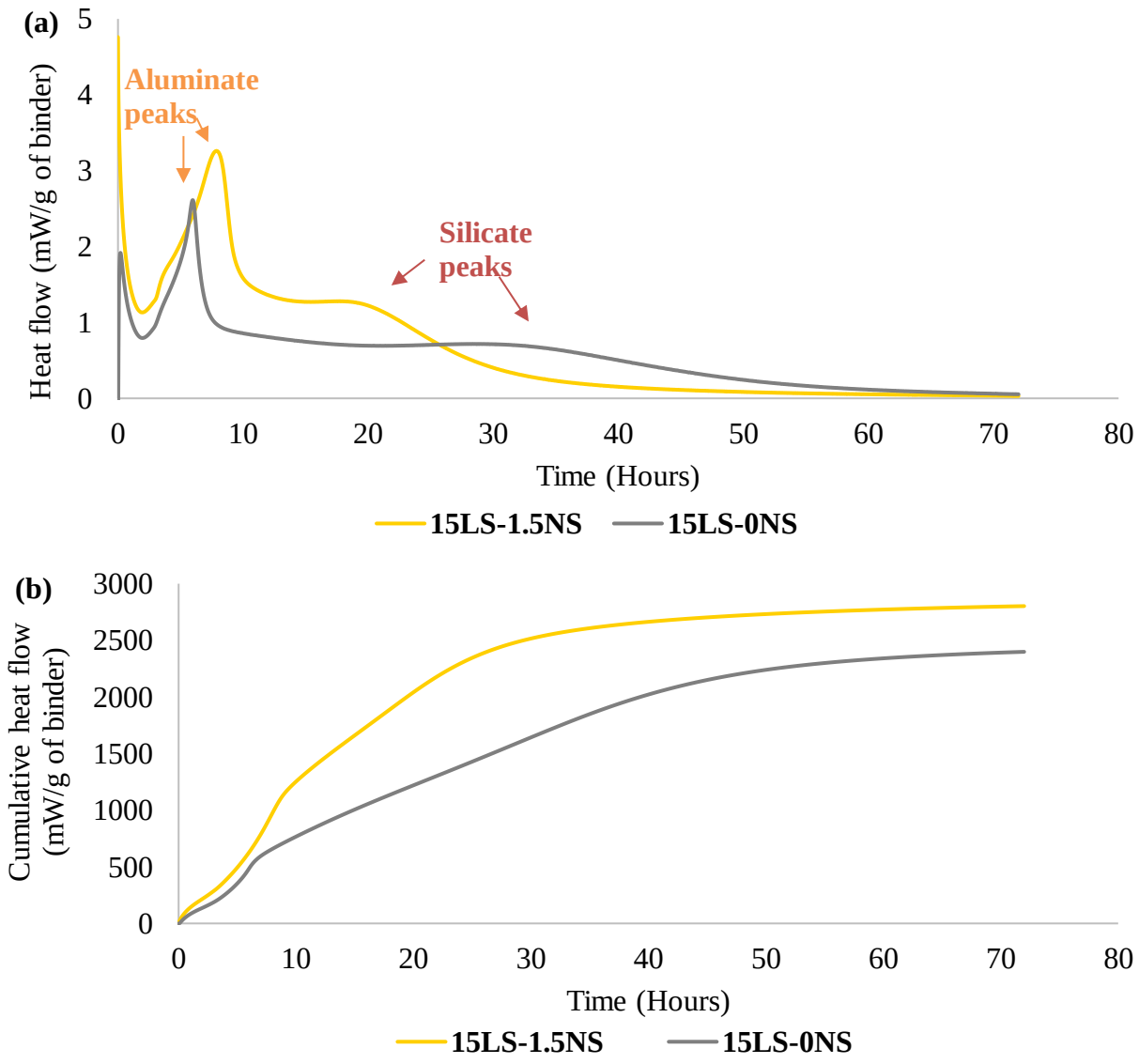

Figure 4-14 (a) Isothermal calorimetry curves and (b) cumulative heat release of NaSO4-activated pastes vs non-activated pastes

Another finding which emerged from the isothermal calorimetry testing is that the NS content did enhance the aluminate reaction, but that it appears to have retarded its peak slightly. While the 0NS aluminate peak occurred after 6 hours, the 1.5NS aluminate peak occurred after more than 7.5 hours. Comparing the two peaks reveals that the 0NS aluminate peak is less high, but steeper, showing a shorter aluminate reaction than the 1.5NS, and therefore an earlier peak. This may be explained by the fact that NS content would promote the dissolution of metakaolin which is expected to participate significantly in the aluminate reaction. This is also highlighted in *Figure 4-14*b, which shows the final heat release in both 1.5 and 0NS binders. Indeed, the higher heat

release by 1.5NS can be attributed to greater reaction from the raw materials in the first three days of hydration. This supports the strength findings of section 4.4.2 which had shown that higher NS amounts were beneficial to the initial strength (3-days strength).

4.5.1.2 Setting time

To assess the influence of sodium sulfate on the setting time of hybrid AAMs, the Vicat needle penetration test was performed on binders 1.5NS and 0NS. In *Figure 4-15*, it is possible to observe that the $NaSO_4$-activated mix reached setting quickly, with 25 mm penetration depth reached at 75 min. On the other hand, Vicat Needle testing had to be stopped after 4 hours for the 15LS-0NS mixture and the sample still had not reached complete setting. A penetration depth of 25 mm was achieved after 155 mins for this mixture, which is more than twice the time it took for the sodium sulfate activated mix.

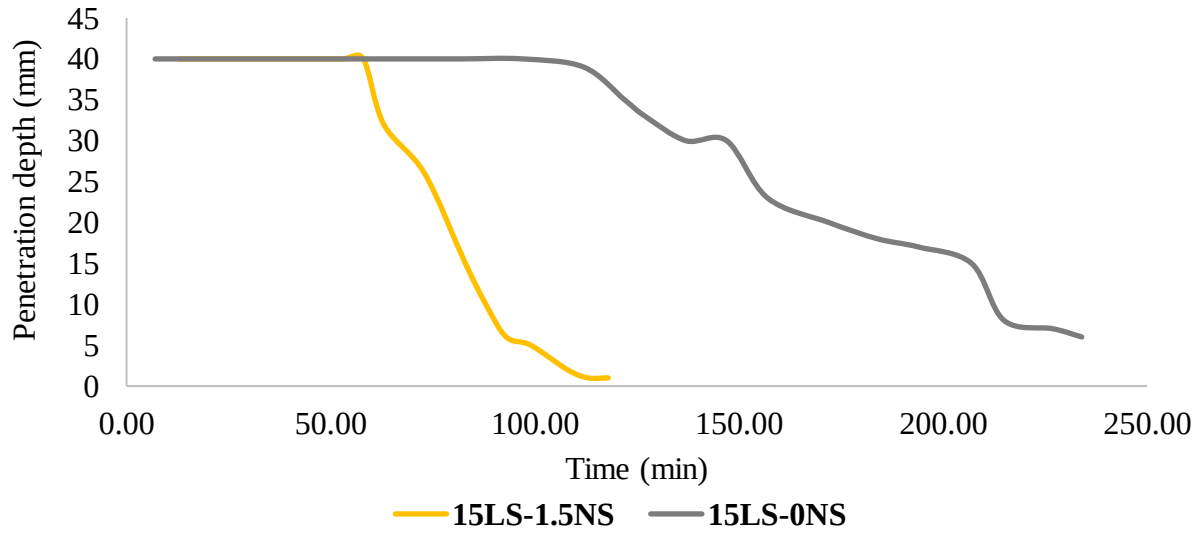

Figure 4-15 Setting time of NaSO4-activated pastes vs non-activated pastes

From these results, the role of $NaSO_4$ in accelerating the kinetics is obvious. It also correlates with the isothermal calorimetry results discussed in the previous section. This is an important consideration for potential industry applications, as most projects require hardening to occur within one to two hours of placement.

4.5.2 Microscale testing

4.5.2.1 TGA

Thermogravimetric analysis (TGA) was run on the water and sodium sulfate activated samples at 3, 7 and 28 days (*Figure 4-16*). In *Figure 4-16*a and b, four peaks may be identified: a peak around 70 °C, one around 120 °C, another around 300 °C and finally one around 700 °C. Typically, C-S-H type phases and ettringite are found around 100-120°C [27], so the peak at 120 °C may be attributed to these phases.

However, the presence of the peak at 70 °C is not easy to explain. First, this peak appears to be larger in the 1.5NS sample than in the 0NS sample (i.e., -7% derivative weight loss versus -5% for 0NS) and it is drastically reducing at day 28 in both samples. This may indicate that a metastable phase is forming in early ages, and that it later converts to another product. In the 0NS sample, it appears that the 120°C peak increases as the 70 °C peak is getting smaller, which may be a sign that the metastable phase converts into C-S-H or ettringite. However, in the 1.5NS mix, the 120 °C peak remains constant. Other phases in 1.5NS such as portlandite and calcium carbonate both remain constant or diminish. It is possible that this mix experienced carbonation, but it would have normally been associated with an increase in calcite. Additionally, the 65-75 °C peak is not present in the factorial samples' TGA run after 90 days (see *Figure 4-11*). This reinforces the hypothesis that the product forming between 3 and 7 days, and which appears to be stimulated by the presence of NS, does not correspond a stable hydrate phase. In a study by Chaipanich *et al.* (2019), the authors attributed a peak around 85 °C to N-A-S-(H) gel. N-A-S-(H) gel may convert to C-A-S-H gel, which would explain the reduction in the peak over time. However, with 30% of Portland cement and little alkalis provided, it is unlikely that N-A-S-(H) would form in either of the binders. Instead, C-S-H and C-A-S-H formation are likely to be favored. Moreover, many studies conducted on AAMs did not report the observation of any peak at a temperature lower than 100 °C., even with pure low calcium binders [33–35].

A more plausible explanation for this peak is that it corresponds to the first water loss from monosulfate, which occurs between 50 and 100 °C [27,36]. This hypothesis would explain why the peak is larger for 1.5NS samples than for 0NS ones. Monosulfate formation normally occurs because of the reaction of C_3A with gypsum to form ettringite (equation 4.4) which then reacts with the remaining C_3A to convert to monosulfate (equation 4.5) [37].

$$C_3A + 3CaSO_4 \cdot 2H_2O + 27H_2O \rightarrow C_3A \cdot 3CaSO_4 \cdot 33H_2O \quad (4.4)$$

$$2C_3A + C_3A \cdot 3CaSO_4 \cdot 33H_2O + 9H_2O \rightarrow 3C_3A \cdot CaSO_4 \cdot 14H_2O \quad (4.5)$$

Monosulfate is usually not as common in limestone and metakaolin containing binders. This is because the carbonate ions will usually consume the excess of calcium sulfate ($CaSO_4$) that would have reacted with C_3A to form monosulfate and instead react with portlandite and the alumina and silica from metakaolin to form monocarbonate phases [38]. Therefore, there remains two issues with the hypothesis that the 65 to 75 °C peak is associated with monosulfate. The first is that ettringite should be spared from converting to monosulfate due to the addition of 15% of limestone to the mixes. The second is that it remains unclear why monosulfate would form between 3 and 7 days and disappear at day 28. If it was forming a new product, other peaks should be increasing, which is not the case for sample 1.5NS. As for the sample without added sodium sulfate (0NS), the 120 °C peak does increase, which could show a conversion to another hydrate phase. Based on this data, the 70 °C peak may not be attributed to a particular phase with full confidence.

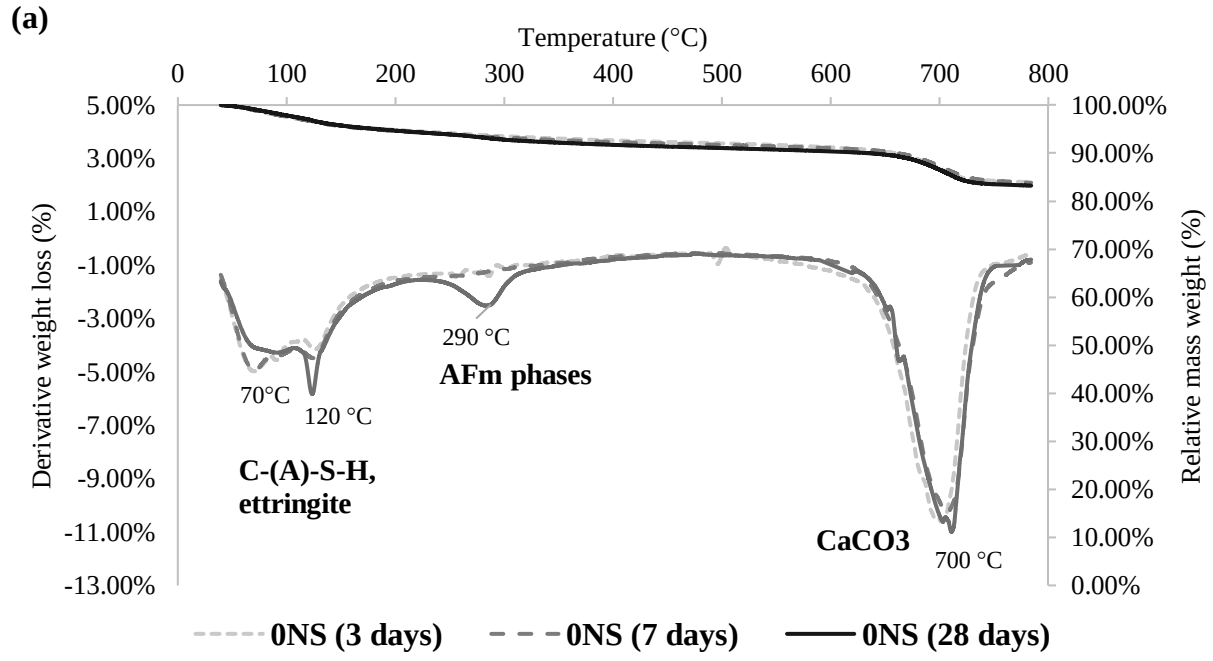

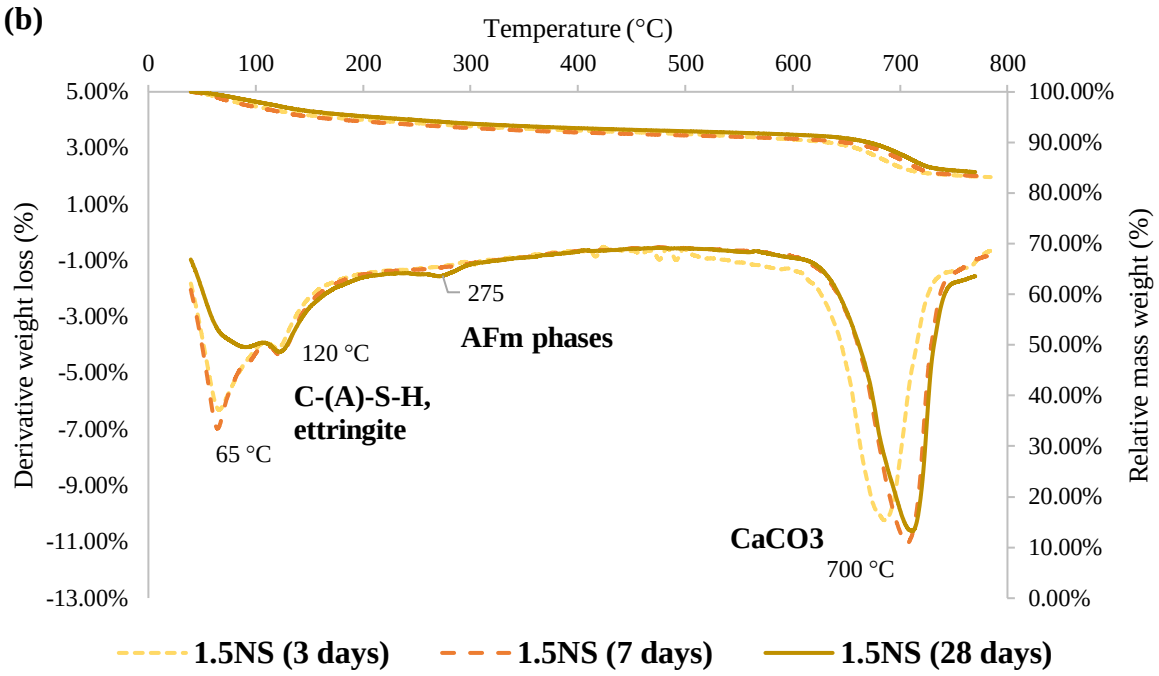

Figure 4-16 TGA and DTG of (a) 0% NaSO4 and (b) 1.5% NaSO4 at 3, 7 and 28 days

The third peak of interest is the one slightly below 300 °C for both 0NS and 1.5NS samples. As reported by Lothenbach [27], a peak of 260 °C can be associated with the loss of water from the aluminum hydroxide of ettringite (AFt). It could also be associated with monosulfate or monocarbonate (AFm) decomposition as they both have a peak near 300 °C. In the case of monocarbonate, the first and main thermal loss occurs around 150 °C. This is interesting, since the peak at 290 °C for 0NS sample appears at day 28 and is associated with a notable increase in the 120 °C peak, located in the range of the first main peak of monocarbonate. Monocarbonate's thermal decomposition occurs in three steps: (1) thermal loss at 150 °C associated with interlayer dehydration, (2) thermal loss at 300 °C associated with depletion of octahedral water, and finally (3) thermal loss at 650 °C associated with the loss of CO_2 [27]. It is thus very likely that monocarbonate could be the main product responsible for the third peak. It could have also contributed to the 120 °C peak attributed to C-(A)-S-H and ettringite, as well as the 700 °C peak attributed to calcite. The 1.5NS sample had a smaller peak at 275 °C and did not display the increase of the 120 °C peak that was observed for the water-activated sample. The lower extent of formation of AFm phases in 1.5NS could potentially indicate that the addition of sodium sulfate promotes the formation of non-hydrate products, such as zeolites. A deeper look into the crystalline phases with XRD might help shed light on this behavior.

Finally, the fourth peak of interest can be attributed mainly to calcite. Since this peak is mostly determined by limestone content, it is expected that both 0NS and 1.5NS have similar peaks at this temperature. Moreover, the depth of the peaks does not seem to change over time, showing that limestone remained largely unreacted. This finding is confirmed in *Figure 4-17* which shows a constant calcite content from 3 to 28 days.

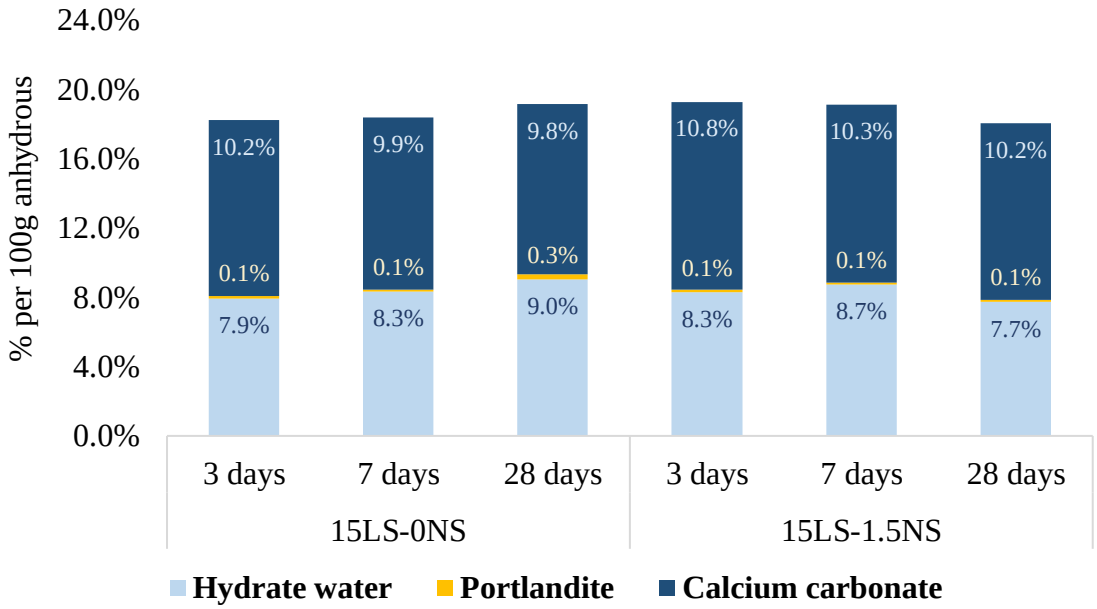

Figure 4-17 TGA quantification of phases

From *Figure 4-17*, the hydrate water content at ages 3 and 7 appears higher for the sample with 1.5% $NaSO_4$, but the amount inexplicably drops after 28 days for this mix. The higher hydrate water amounts in early ages correlate well with the accelerated kinetics of this mix compared with the 0NS mix, as shown in the early kinetics section (see section 4.5.1). It also explains the improved mechanical performance showed by this mix between 3 and 7 days. Nonetheless, it is unexpected that the hydrate water amount would decrease between two ages. It could be hypothesized that this behavior is related to hydrate products converting to non-hydrate products or to hydrates with lower water content. This could for example occur if a high-water containing hydrate such as ettringite was converting to another phase with lower water content. Further microscopic investigations are required to determine what products may be transforming and accounting for the decrease in hydrate water content. Regarding portlandite content, both 0NS and 1.5NS appear to have very little portlandite forming. This is most likely linked to the high amounts of metakaolin and sodium sulfate that will react with the portlandite at early ages.

4.5.2.2 XRD

The diffraction peaks of the water activated, and NS activated mix at 3, 7 and 28 days measured with XRD is shown in *Figure 4-18*. Similarly, as for the factorial mixes at 90 days shown in section 4.4.4.2, the main peaks are attributed to ettringite, monosulfoaluminate, gypsum, hemicarboaluminate, quartz and calcite. It is interesting to observe that both the height and distribution of the peaks are similar across different mixes and for different testing ages. It was hypothesized that the 1.5NS sample could have zeolite forming between the ages of 7 and 28 days and which could account for the conversion of the 65 °C peak into non-hydrate products. However, this was not observed in the XRD data. Furthermore, as discussed in the previous section, this 65 °C peak might correspond to monosulfoaluminate. Based on the XRD data, it does appear that monosulfoaluminate is forming in all mixes, but it is not possible to determine whether it is diminishing at 28 days. Moreover, the reduction in the hydrate water content for the 1.5NS was tentatively attributed to the possible conversion of high-water content hydrates such as ettringite into lower water content hydrates or non-hydrates. Due to the similarity between the diffraction peak profiles at various ages, it is not possible to confirm or not this hypothesis. The conduction of Rietveld refinement would be an additional step that could be used to investigate the likelihood of this explanation.

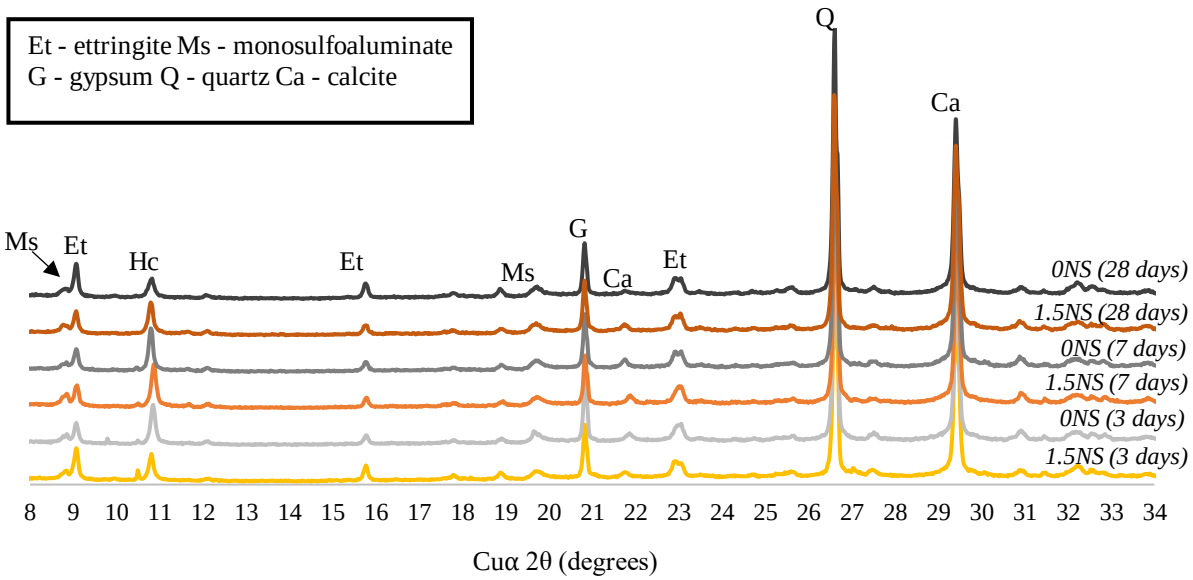

Figure 4-18 XRD of 0% Na_2SO_4 and 1.5% Na_2SO_4 binders

4.6 Proposed framework for hybrid AAMs mix-design

Based on the findings of this work, it is recommended that the design of hybrid metakaolin AAMs activated with sodium sulfate is done with the following steps:

(1) **Determine the binder composition in terms of metakaolin, limestone and Portland cement to meet later age performance requirements and sustainability goals.** The addition of alkalis will accelerate the kinetics and may lead to greater reaction from the SCMs, which may ultimately improve later age performance. However, the presence of alkalis may also hinder later age strength through its negative impact on the pore structure and through phase instability. Therefore, the addition of alkalis should not be considered at this stage.

(2) **Determine the required added sulfate to achieve sulfate balance.** Sodium sulfate will provide sulfate ions to the cementitious systems, but it might not be enough to achieve sulfate balance. In such cases, gypsum should be added as well, based on preliminary isothermal calorimetry testing.

(3) **Determine the minimum required alkali content to achieve the prescribed early age properties.** Alkalis will improve early age strength, but the added quantity should be minimized to ensure that the strength development of the binder is not hindered, and that 28-days strength is not impaired.

(4) **Re-evaluate the binder composition if the required 28-days strength is not reached.** If the minimum alkali content to achieve early age strength is too high and affects significantly later age strength, re-evaluate the binder composition. Replacing metakaolin by limestone increases the tolerance of the system to high alkali content and increasing Portland cement content may help reduce the amount of alkalis needed to reach the required early age strength.

This framework is designed for projects requiring a specific 28-days strength, and only considering this requirement (i.e., not addressing slump, setting or other fresh state needs). Nevertheless, applications in the field will greatly vary from one project to another, and the research on sodium sulfate-activated hybrid AAMs is not developed sufficiently for a precise mix-design strategy to be suggested. The guidelines presented here are intended as a first step towards the design of a more comprehensive and applicable framework for the mix-design of hybrid AAMs.

4.7 Conclusion

This study focused on understanding the evolution of macroscale and microscale properties of hybrid sodium sulfate-activated MK-PC mixes with varying limestone and sodium sulfate contents. A factorial design of experiment was used to investigate the influence of limestone and sodium sulfate by themselves and in combination with each other. The selection of one mix from the factorial design optimization experiments was also done to conduct further microscale testing on a high early strength mix and compare the measured microscale properties with those of water-activated mix of similar binder composition.

Multiscale testing between 0 and 90 days yielded the following conclusions:

- Isothermal calorimetry testing showed that the addition of up to 2.5% of Na_2SO_4 is not sufficient to achieve sulfate balance in mixes with 45 to 65% of metakaolin, 5 to 25% of limestone and 30% of Portland cement. Both sodium sulfate and metakaolin enhances aluminate reaction. At an optimal amount of sodium sulfate found around 1.5%, the cumulative heat flow is maximized, and higher 3-day and 7-day strengths are reached.
- Setting time is significantly shortened when NS is added to 15LS-30PC-55MK mixes. Isothermal calorimetry results have shown that higher heat flows and cumulative heat flow occurred for these mixes in comparison with water-activated ones. Therefore, it is shown that NS indeed contributes to both an enhancement and acceleration of the kinetics.
- Compressive strength testing revealed that an optimal combination of 15% of limestone, 65% of metakaolin and 30% of Portland cement activated with 1.5% sodium sulfate yields the best early day results with respect to strength. However, 28 days' strength was maximized when decreasing the limestone content to 5% and the sodium sulfate content to 0.5%. Furthermore, the statistical analysis performed on the strength results highlighted that there were non-negligible interactions between the levels of sodium sulfate and limestone. This correlates with the enhancement of the aluminate peak observed in isothermal calorimetry due to both MK (which LS replaces) and NS contents. The effect of sodium sulfate on strength appears to be dependent on the whole binder composition, and not only on the Portland cement fraction.

- Bulk resistivity testing showed an upward trend of values in time, but the two mixes with high NS content retained low values, even at 28 days. It is hypothesized that these mixtures had higher porosity due to the excess of alkalis causing high capillary porosity and that the kinetics acceleration induced by NS addition may be stunting further porosity refinement.
- TGA testing after 90 days revealed similar amounts of hydrate water for the different mixes, but lower amounts of calcite for mixes with low NS content. It is suggested that some calcite may have been used to form AFm phases in mixes with 0.5% of Na_2SO_4. Indeed, the XRD diffraction patterns of 5LS-0.5NS shows the presence of additional AFm phases that do not appear in 5LS-2.5NS. Based on this finding, it is hypothesized that the excess of sodium sulfate may hinder later age AFm phases formation.
- It was found through TGA and XRD testing of NS-activated versus water-activated mixes that the formation of a metastable product decomposing at a range of 65-75 ºC occurred in both mixes. However, the disappearance of this TGA peak at 28 days and the absence of increase in other hydrate peaks for the NS-activated sample suggest the conversion of this reaction product to a non-hydrate or low water content hydrate. In addition to the limited AFm product formation, this could lead to lower later ages strength for hybrid binders with high NS contents.
- Based on the findings, a framework for mix-design of hybrid metakaolin AAMs containing limestone was proposed.

4.8 References

[1] J.L. Provis, S.A. Bernal, Binder chemistry – Blended systems and intermediate Ca content, in: RILEM State-of-the-Art Reports, 2014: pp. 125–144. https://doi.org/10.1007/978-94-007-7672-2_5.

[2] C. Shi, A.F. Jiménez, A. Palomo, New cements for the 21st century: The pursuit of an alternative to Portland cement, Cem Concr Res 41 (2011) 750–763. https://doi.org/10.1016/j.cemconres.2011.03.016.

[3] L. Xue, Z. Zhang, H. Wang, Hydration mechanisms and durability of hybrid alkaline cements (HACs): A review, Constr Build Mater 266 (2021) 121039. https://doi.org/10.1016/j.conbuildmat.2020.121039.

[4] A.K. Mohapatra, B. Pradhan, Hybrid alkali activated cements (HAACs) system: A state-of-the-art review on fresh, mechanical, and durability behaviour, Constr Build Mater 361 (2022) 129636. https://doi.org/10.1016/j.conbuildmat.2022.129636.

[5] G. Habert, J.B. D'Espinose De Lacaillerie, N. Roussel, An environmental evaluation of geopolymer based concrete production: Reviewing current research trends, J Clean Prod 19 (2011) 1229–1238. https://doi.org/10.1016/j.jclepro.2011.03.012.

[6] S.A. Bernal, Advances in near-neutral salts activation of blast furnace slags, RILEM Technical Letters 1 (2016) 39. https://doi.org/10.21809/rilemtechlett.v1.8.

[7] B. Mota, T. Matschei, K. Scrivener, The influence of sodium salts and gypsum on alite hydration, Cem Concr Res 75 (2015) 53–65. https://doi.org/10.1016/J.CEMCONRES.2015.04.015.

[8] B. Mota, T. Matschei, K. Scrivener, Impact of NaOH and Na2SO4 on the kinetics and microstructural development of white cement hydration, Cem Concr Res 108 (2018) 172–185. https://doi.org/10.1016/j.cemconres.2018.03.017.

[9] A.T.M. Marsh, Z. Yue, Y. Dhandapani, K. Button, S. Adu-Amankwah, S.A. Bernal, Influence of limestone addition on sodium sulphate activated blast furnace slag cements, Constr Build Mater 360 (2022). https://doi.org/10.1016/j.conbuildmat.2022.129527.

[10] J. Fu, A.M. Jones, M.W. Bligh, C. Holt, L.M. Keyte, F. Moghaddam, S.J. Foster, T.D. Waite, Mechanisms of enhancement in early hydration by sodium sulfate in a slag-cement blend – Insights from pore solution chemistry, Cem Concr Res 135 (2020) 106110. https://doi.org/10.1016/j.cemconres.2020.106110.

[11] S. a Bernal, D. Herfort, J. SKibsted, Hybrid binders based on alkali sulfate-activated Portland clinker and metakaolin, 13th International Congress on the Chemistry of Cement. (2011) 1–7.

[12] A. Dakhane, S. Tweedley, S. Kailas, R. Marzke, N. Neithalath, Mechanical and microstructural characterization of alkali sulfate activated high volume fly ash binders, Mater Des 122 (2017) 236–246. https://doi.org/10.1016/j.matdes.2017.03.021.

[13] M.A. Nawaz, B. Ali, L.A. Qureshi, H.M. Usman Aslam, I. Hussain, B. Masood, S.S. Raza, Effect of sulfate activator on mechanical and durability properties of concrete incorporating low calcium fly ash, Case Studies in Construction Materials 13 (2020). https://doi.org/10.1016/j.cscm.2020.e00407.

[14] P. Nath, P.K. Sarker, Use of OPC to improve setting and early strength properties of low calcium fly ash geopolymer concrete cured at room temperature, Cem Concr Compos 55 (2015) 205–214. https://doi.org/10.1016/j.cemconcomp.2014.08.008.

[15] G. Millán-Corrales, J.R. González-López, A. Palomo, A. Fernandez-Jiménez, Replacing fly ash with limestone dust in hybrid cements, Constr Build Mater 243 (2020) 118169. https://doi.org/10.1016/j.conbuildmat.2020.118169.

[16] J. Fu, M.W. Bligh, I. Shikhov, A.M. Jones, C. Holt, L.M. Keyte, F. Moghaddam, C.H. Arns, S.J. Foster, T.D. Waite, A microstructural investigation of a Na2SO4 activated cement-slag blend, Cem Concr Res 150 (2021) 106609. https://doi.org/10.1016/j.cemconres.2021.106609.

[17] W.J. Zhou, S.L. Wu, H.X. Chen, Early Strength-Promoting Mechanism of Inorganic Salts on Limestone-Calcined Clay Cement, Sustainability 15 (2023). https://doi.org/10.3390/su15065286 WE - Science Citation Index Expanded (SCI-EXPANDED) WE - Social Science Citation Index (SSCI).

[18] H. Li, Z. Xue, G. Liang, K. Wu, B. Dong, W. Wang, Effect of C-S-Hs-PCE and sodium sulfate on the hydration kinetics and mechanical properties of cement paste, Constr Build Mater 266 (2021) 121096. https://doi.org/10.1016/j.conbuildmat.2020.121096.

[19] M. Zhang, L. Yang, F. Wang, Influence of C–S–H seed and sodium sulfate on the hydration and strength of limestone calcined clay cement, J Clean Prod 408 (2023) 137022. https://doi.org/10.1016/j.jclepro.2023.137022.

[20] A.T.M. Marsh, Z.L. Yue, Y. Dhandapani, K. Button, S. Adu-Amankwah, S.A. Bernal, Influence of limestone addition on sodium sulphate activated blast furnace slag cements, Constr Build Mater 360 (2022). https://doi.org/10.1016/j.conbuildmat.2022.129527.

[21] A.M. Kaja, A. Lazaro, Q.L. Yu, Effects of Portland cement on activation mechanism of class F fly ash geopolymer cured under ambient conditions, Constr Build Mater 189 (2018) 1113–1123. https://doi.org/10.1016/j.conbuildmat.2018.09.065.

[22] A. Fernández-Jiménez, I. Garcia-Lodeiro, O. Maltseva, A. Palomo, Hydration mechanisms of hybrid cements as a function of the way of addition of chemicals, Journal of the American Ceramic Society 102 (2019) 427–436. https://doi.org/10.1111/jace.15939.

[23] ASTM C1702, Standard Test Method for Measurement of Heat of Hydration of Hydraulic Cementitious Materials Using Isothermal Conduction Calorimetry, ASTM (2023). https://doi.org/10.1520/C1702-23.

[24] ASTM, ASTM C191 − 21 Standard Test Methods for Time of Setting of Hydraulic Cement by Vicat Needle, ASTM International (2021). https://doi.org/10.1520/C0191-21.

[25] ASTM, ASTM C39/C39M - 21 Standard Test Method for Compressive Strength of Cylindrical Concrete Specimens, ASTM International (2021). https://doi.org/10.1520/C0039_C0039M-21.

[26] ASTM C1876-24, Standard Test Method for Bulk Electrical Resistivity or Bulk Conductivity of Concrete 1, ASTM Committee C09.66 (2024). https://doi.org/10.1520/C1876-24.

[27] B. Lothenbach, K. Scrivener, R. Snellings, A practical guide to microstructural analysis of cementitious materials, CRC Press, Boca Raton, Florida, 2016. https://doi.org/10.1201/b19074.

[28] K. De Weerdt, M. Ben Haha, G. Le Saout, K.O. Kjellsen, H. Justnes, B. Lothenbach, Hydration mechanisms of ternary Portland cements containing limestone powder and fly ash, Cem Concr Res 41 (2011) 279–291. https://doi.org/10.1016/J.CEMCONRES.2010.11.014.

[29] F.A. Zunino Sommariva, Limestone calcined clay cements (LC3): raw material processing, sulfate balance and hydration kinetics, EPFL, 2020.

[30] R. Hay, L. Li, K. Celik, Shrinkage, hydration, and strength development of limestone calcined clay cement (LC3) with different sulfation levels, Cem Concr Compos 127 (2022) 104403. https://doi.org/10.1016/j.cemconcomp.2021.104403.

[31] F. Zunino, K. Scrivener, The reaction between metakaolin and limestone and its effect in porosity refinement and mechanical properties, Cem Concr Res 140 (2021) 106307. https://doi.org/10.1016/j.cemconres.2020.106307.

[32] Y. Dhandapani, M. Santhanam, Assessment of pore structure evolution in the limestone calcined clay cementitious system and its implications for performance, Cem Concr Compos 84 (2017) 36–47. https://doi.org/10.1016/J.CEMCONCOMP.2017.08.012.

[33] A. Rafeet, R. Vinai, M. Soutsos, W. Sha, Effects of slag substitution on physical and mechanical properties of fly ash-based alkali activated binders (AABs), Cem Concr Res 122 (2019) 118–135. https://doi.org/10.1016/j.cemconres.2019.05.003.

[34] Y. Zhao, J. Qiu, S. Zhang, Z. Guo, Z. Ma, X. Sun, J. Xing, Effect of sodium sulfate on the hydration and mechanical properties of lime-slag based eco-friendly binders, Constr Build Mater 250 (2020) 118603. https://doi.org/10.1016/j.conbuildmat.2020.118603.

[35] J.J. Zhang, H.B. Tan, M. Bao, X.H. Liu, Z.T. Luo, P.G. Wang, Low carbon cementitious materials: Sodium sulfate activated ultrafine slag/fly ash blends at ambient temperature, J Clean Prod 280 (2021). https://doi.org/10.1016/j.jclepro.2020.124363 WE - Science Citation Index Expanded (SCI-EXPANDED).

[36] Herbert Pöllmann, Die Kristallchemie der Neubildung bei Einwirkung von Schadstoffen auf hydraulische Bindelmittel, PhD thesis, University of Erlangen, 1984.

[37] H.-J. Kuzel, Initial hydration reactions and mechanisms of delayed ettringite formation in Portland cements, Cem Concr Compos 18 (1996) 195–203. https://doi.org/10.1016/0958-9465(96)00016-9.

[38] F. Zunino, Y. Dhandapani, M. Ben Haha, J. Skibsted, S. Joseph, S. Krishnan, A. Parashar, M.C.G. Juenger, T. Hanein, S.A. Bernal, K.L. Scrivener, F. Avet, Hydration and mixture design of calcined clay blended cements: review by the RILEM TC 282-CCL, Mater Struct 55 (2022). https://doi.org/10.1617/s11527-022-02060-1.

Chapter 5 Conclusions and Research Recommendations

This research focused on the optimization of hybrid alkali-activated binders as sustainable alternatives to traditional Portland cement. It also aimed at investing how early kinetics and microscopic features were affected by the presence of sodium sulfate. The background section of this thesis highlighted that there was a need to combine previous knowledge on blended and alkali-boosted Portland cements with knowledge on the chemistry of hybrid alkali-activated materials. Investigating hybrid alkali-activated binders through both of these lights can be a first step towards helping the scientific community better understand how should high volume SCMs binders be designed. This should be done with the objective to maximize Portland cement replacement, while achieving both high early age strength and meeting the requirements of later age strength. The acceleration of kinetics provided by the addition of alkalis in hybrid AAMs enable their use of high amounts of SCMs as replacement of Portland cement. However, mix-proportioning for these binders remains not fully understood, and more research is needed on how different binder components (i.e., Portland cement, limestone, metakaolin, sodium sulfate) would affect the early and later ages micro- and macroscale properties.

The first part of this work is to be found in Chapter 3. It focused on the factorial optimization of binary sodium sulfate-activated metakaolin-Portland cement blends with varying Portland cement and sodium sulfate. Early age macroscale properties such as setting time and compressive strength between 1 and 6 days were investigated first, followed by TGA and XRD at 6 days. This research found that sodium sulfate played an important role in accelerating the setting time of cement paste with 30% of Portland cement and more. Through TGA and XRD, it was apparent that sodium sulfate could help enhance the reaction and extent of product formation. It also found that the maximum Na_2SO_4 used (5%) was too high, and that a maximum of 2.5% should be chosen for the next set of experiment. Finally, based on the compressive strength results, the mix with 30% of Portland cement was the minimum optimum mix in terms of Portland cement content. Therefore, the next investigation was performed with a fixed Portland cement content of 30% and a varying sodium sulfate content of 0.5 to 2.5%.

The second part of this work is developed in Chapter 4. Based on conclusions derived from Chapter 3, this subsequent study was undertaken to further investigate sodium sulfate-activated ternary limestone-metakaolin-Portland cement blends. A factorial design of experiment was again used to

choose the mix binder compositions, varying limestone, and sodium sulfate contents. The testing program included isothermal calorimetry, compressive strength, bulk electrical resistivity, XRD and TGA testing. The use of RSM plots and other statistical plots and tools allowed to further understand the significance of the parameters' influence on the materials' strength. It was found that the improved early age performance of sodium sulfate mixes was linked to the enhancement of aluminate reaction caused by the greater dissolution of metakaolin due to the increase in sodium sulfate content, and which can occur as well when metakaolin content itself is raised. The better early age properties of hybrid AAMs with higher sodium sulfate and metakaolin contents is thus related to the acceleration of reaction kinetics, a result of the high concentrations of sodium sulfate and the presence of high amounts of metakaolin's large specific surface area particles.

Nevertheless, it was verified that the faster the reaction took place, the lower long-term age strength were. In Chapter 4, it was possible to relate this behavior to two main causes: the first was the lower porosity of the hybrid binders which had enhanced and accelerated early kinetics and the second cause was the formation of more metastable products for sodium sulfate-activated binders than water-activated binders. High sodium sulfate samples were indeed characterized with much lower bulk electrical resistivity values than their low to moderate counterparts from 3 days to 28 days. A TGA experiment run at day 3, 7 and 28 demonstrated that there was a decrease in hydrate water at 28 days for the sodium sulfate-activated sample, while the water-activated one showed an increase. From the TGA data, it appears that some of the hydrates forming in sodium sulfate-activated binders could be converting to non-hydrates or to hydrates with lower water content. The potential phases instability in these binders might lead to the creation of voids in the pore system and decrease the performance at later ages.

More research should be conducted on the hybrid AAMs studied in this work to further understand the underlying mechanisms behind the strength evolution of mixes with varying amounts of limestone, metakaolin, Portland cement and sodium sulfate. Future work on this topic should include porosity measurements to correlate the distribution of voids and the volume of capillary voids to mechanical performance. Performing Rietveld refinement on the XRD results could also benefit the analysis of results by providing semi-quantitative estimates of some of the crystalline phases forming. The use of scanning electron microscopy on pastes from 3 to 90 days would also provide additional insights into the changes in microstructure induced by sodium sulfate and

limestone addition. Moreover, since it was found that the addition of 1.5% of sodium sulphate led to optimal early strength result for a mix with 30% of Portland cement, it would be interesting to conduct additional experiments with lower amounts of Portland cement and investigate how the optimal amount of sodium sulfate might be affected by this change in composition. Future work should strive to develop experimental models correlating hybrid AAMs' binder composition and their mechanical properties. Finally, durability testing would need to be conducted to gain insight on the long-term performance of hybrid AAMs. Through the conduction of durability test, it would be possible to evaluate the financial and carbon-related life cycle costs of these binders. This is an essential step towards implementing their large-scale use.

Chapter 6 Appendix A – Factorial design rationale

6.1 Preliminary experiment

6.1.1 Design of preliminary experiment

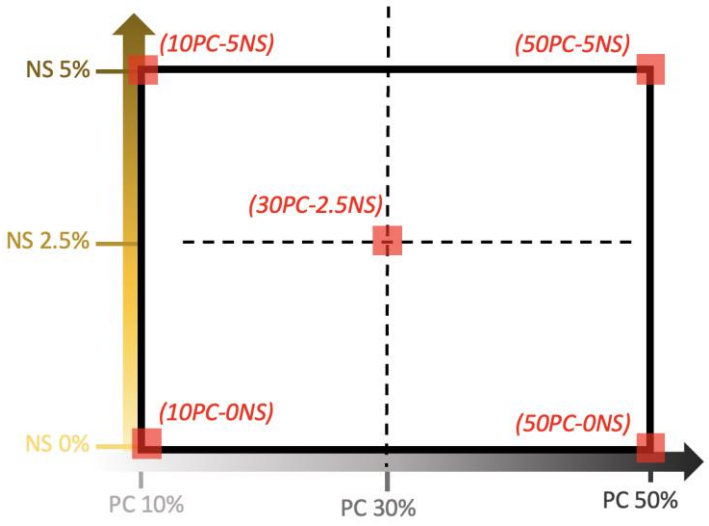

Figure 6-1 Factorial design of the preliminary investigation

In the preliminary investigation, a factorial design was used to evaluate the behavior over the range of $NaSO_4$ of 0 to 5 wt.% of total binder and over the range of Portland cement of 10 to 50 wt.% of binder fraction (*Figure 6-1*). Vicat needle testing and early age compressive strength (i.e., 1 - 6 days) was conducted to assess respectively the fresh and early mechanical performance of the mixtures. To understand better the differences between the mixes, XRD was performed on the factorial points (i.e., 10PC-0NS, 10PC-5NS, 50PC-0NS and 50PC-10NS) and TGA was performed on 50PC-10NS and 50PC-0NS. TGA was used to determine if a greater extent of product formation is associated with the addition of sodium sulfate at a fixed Portland cement content. A summary of the mixes and associated testing can be found in Table 6-1.

This first testing program was aimed at shedding light on the interaction between sodium sulfate and Portland cement, and particularly, its effect on setting, strength, as well as the distribution and relative amounts of phases forming.

Table 6-1 Summary of mixes and testing matrix for preliminary investigation

Binder families	PC (%)	MK (%)	NS[1] (%)	w/b	Vicat needle	Compressive strength	XRD	TGA
10PC-0NS	10	90	0	0.55	X	X	X	
10PC-5NS	10	90	0	0.55	X	X	X	
30PC-2.5NS	30	70	2.5	0.55	X	X		
50PC-0NS	50	50	5	0.55	X	X	X	X
50PC-5NS	50	50	5	0.55	X	X	X	X

[1]*Sodium sulfate is proportioned as w/w of total binder.*

6.1.2 Response surface methodology outcomes

This section will focus on the impact that Portland cement and $NaSO_4$ played on 1-day and 6-day strength since one of the main goals of this research is to minimize Portland cement content, as well as determine an appropriate range of sodium sulfate content to promote both early and later age strength. The analysis of the factors' impact on strength is illustrated in *Figure 6-2*. It shows that, while Portland cement content enhances strength at both ages similarly, the increase in strength provided by $NaSO_4$ almost disappears at 6 days. This is consistent with the work of numerous authors, which had shown that the addition of alkalis improved properties in the very early days (1-3 days), but that the difference no longer appeared at 7 days. It must be noted that the concentration of $NaSO_4$ used was particularly high, which also plays a significant role. To determine if a lower concentration might have been beneficial, the RSM plots of 1-day and 6-day strength are shown in *Figure 6-3*.

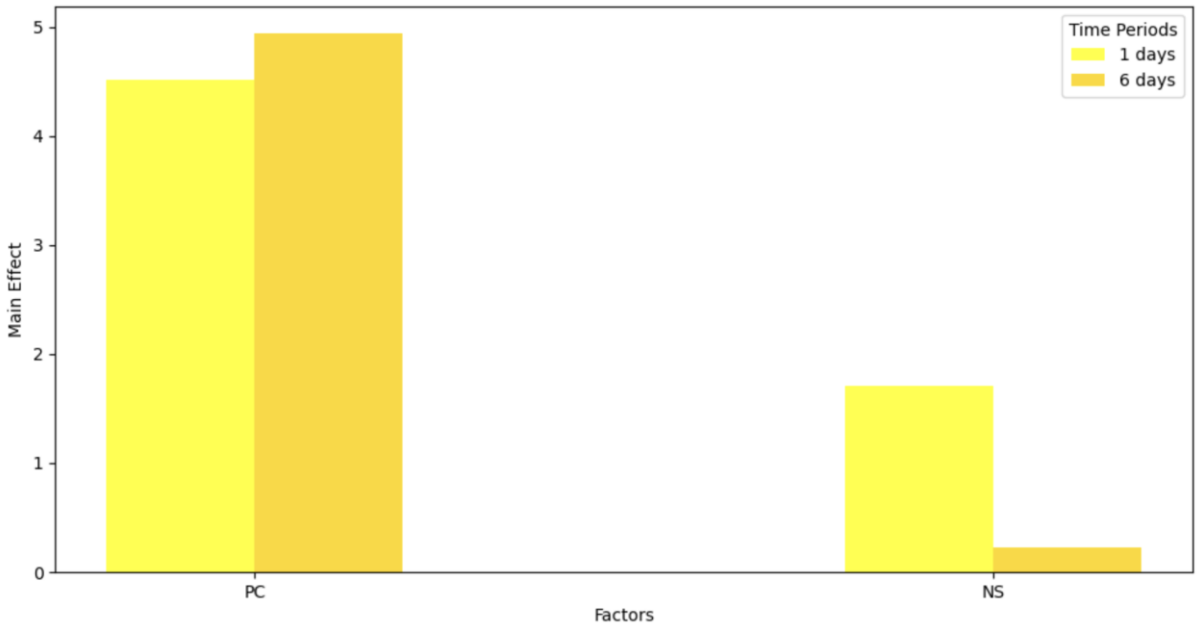

Figure 6-2 Main effect of Portland cement and sodium sulfate on strength at 1 and 6 days

The 3D RSM plots were plotted based on the modelling of strength (f'c) with the formula below:

$$f'c = aNS + bPC + c(NS * PC) + dNS^2 + ePC^2$$

Where a, b, c, d and e are constants, and NS and PC are the individual factors. This second-degree polynomial formula was used to account for the curvature in the response. However, in factorial design without axial points, and with only a central point, the curvature can only be accounted by the data around the central point. This is important in the analysis of the plots in *Figure 6-3*, since it is possible to observe that the upward trend in strength values along the y-axis (NS-axis) was not effectively captured. On the other hand, the increase in strength due to PC content is easy to observe on the graphs. Also, even though 50% of PC yields the highest strength, the observation of a yellow-colored area from 30 to 50% of PC indicates that almost as desirable strengths are attained with 30% of PC inclusion. Based on this result, 30% is the minimum optimum chosen for Portland cement for the ternary hybrid pastes optimization.

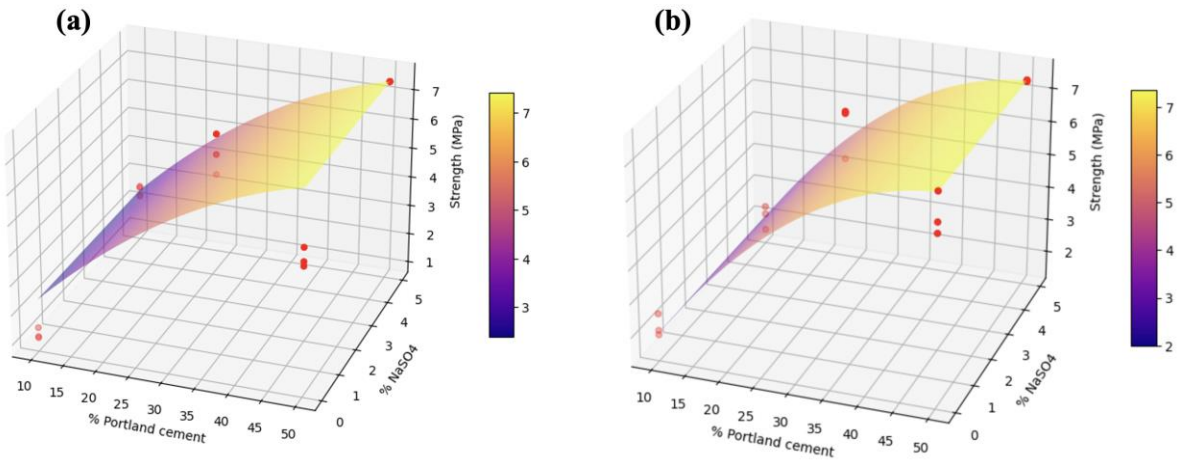

Figure 6-3 RSM of the (a) 1-day and (b) 6-day compressive strength of investigation samples

Regarding sodium sulfate content, since the RSM was not able to effectively capture the behavior, another strategy is adopted. In the case of optimal range of NS content, it is not only strength at a certain age that matters, but that the increase in strength between two ages remains as high as possible. Since it is known that sodium sulfate may negatively impact later ages strength, this factor will play a large role in the ternary hybrid optimization trial where the pastes will be cured for up to 28 days. In *Figure 6-4*, the difference in strength between 1 and 6 days is therefore plotted.

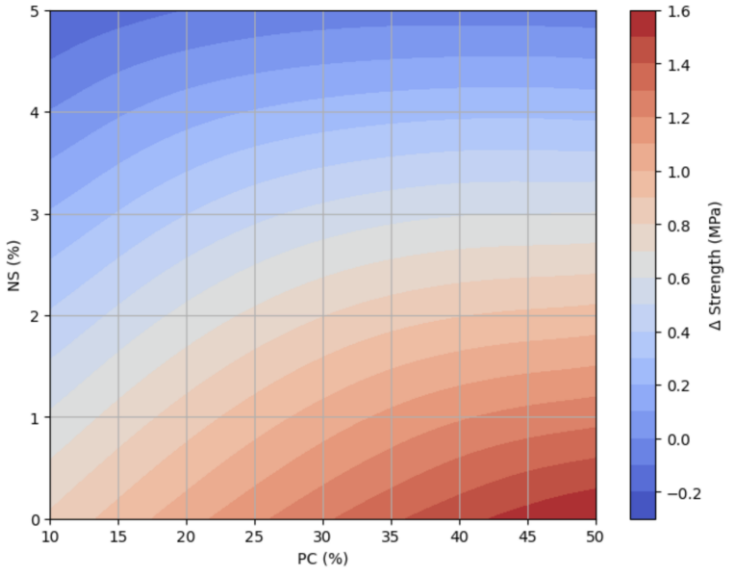

Figure 6-4 Contour plot of the difference in strength between 1 and 6 days

It is interesting to observe that to achieve at least 1 MPa of strength increase, the maximum amount of $NaSO_4$ is around 2% for a PC of 50% but falls to 1.5% at a PC level of 30%. This shows that the optimal level of NS in the system is first governed by PC content.

6.1.3 Design of "Multiscale statistical investigation of hybrid metakaolin alkali-activated binders"

Based on the findings of the preliminary trial, for a ternary blend of varying (limestone + metakaolin) blend with a fixed Portland cement (PC) content, there could be an optimum amount of sodium sulfate, regardless of the percentages of metakaolin and limestone. To investigate this hypothesis, the factorial experiment discussed in Chapter 4will be designed around the optimum PC-NS combination, 30PC-1.5NS.

In this ternary optimization trial, all mixes will have a Portland cement content of 30%, but sodium sulfate (NS) content will vary between a low end at 0.5% (below the found maximum NS content for 30PC) and a high end at 2.5% (higher than the found maximum NS for 30PC). Limestone (LS) will be added to the mixes, in the range of 5 to 25% of binder weight. The detailed schematic can be found in *Figure 6-5*.

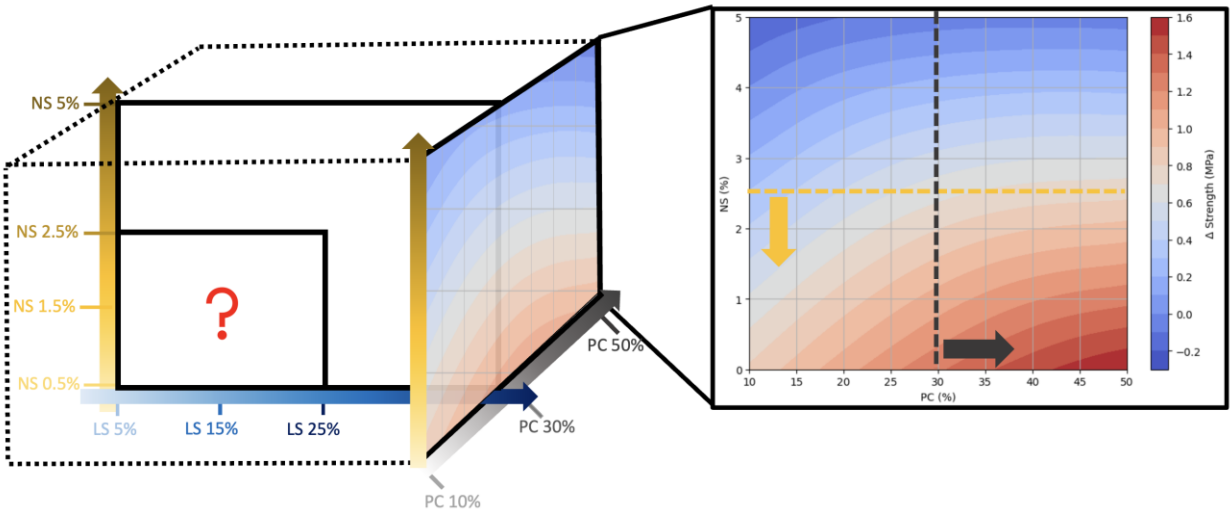

Figure 6-5 RSM outcomes - boundaries for ternary optimization experiment

Chapter 7 Appendix B – Residual plots

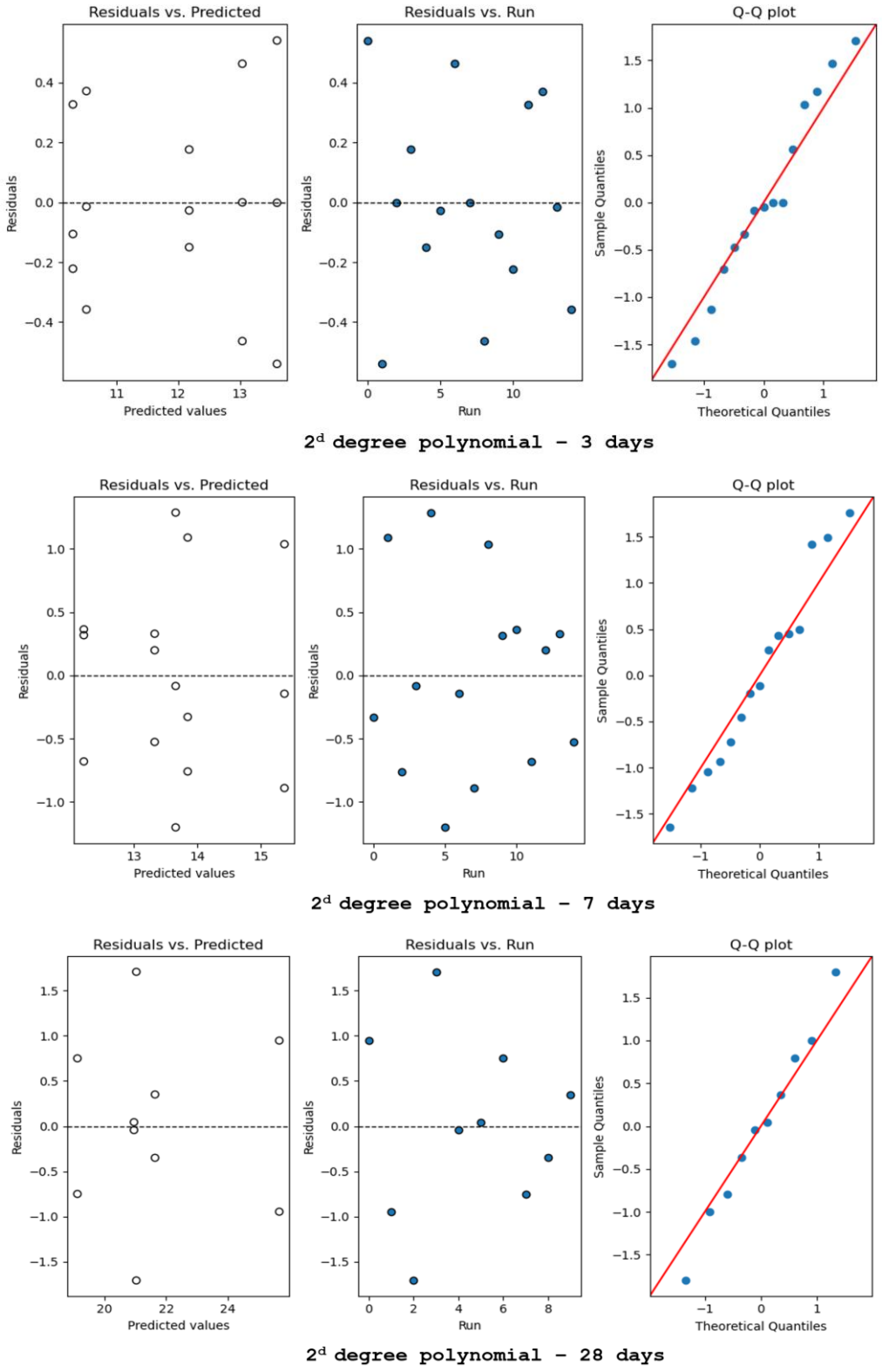

Figure 7-1 Residual plots for factorial model